

Syracuse University

SURFACE

Theses - ALL

1-1-2017

AN EVALUATION OF CAPILLARY FLOW TEST FOR DETERMINING THE PORE SIZE DISTRIBUTION OF GEOTEXTILES AND ESTABLISHING CORRELATIONS

Nuzhath Fatema
Syracuse University

Follow this and additional works at: <https://surface.syr.edu/thesis>



Part of the [Engineering Commons](#)

Recommended Citation

Fatema, Nuzhath, "AN EVALUATION OF CAPILLARY FLOW TEST FOR DETERMINING THE PORE SIZE DISTRIBUTION OF GEOTEXTILES AND ESTABLISHING CORRELATIONS" (2017). *Theses - ALL*. 155.
<https://surface.syr.edu/thesis/155>

This Thesis is brought to you for free and open access by SURFACE. It has been accepted for inclusion in Theses - ALL by an authorized administrator of SURFACE. For more information, please contact surface@syr.edu.

Abstract

For the last four decades, geotextiles have been used extensively for the purpose of separation, filtration, drainage and soil reinforcement. The basic criteria that impact the behavior of a geotextile filter are soil retention, permeability, and clogging potential. The ability of a geotextile filter to fulfill these requirements depends on the pore sizes and pore size distribution. There are numerous techniques to measure the pore sizes of a geotextile, but not all of them are widely accepted. In the USA, two standard methods of measuring the largest pore size of a geotextile have been accepted, the Dry sieving test (ASTM D4751) and the Capillary flow test (ASTM D6767). Despite of the several drawbacks of the dry sieving test, including trapping of glass beads inside the geotextiles and electrostatic effects, many filtration criteria are designed based on the apparent opening size (AOS, O_{95}). On the other hand, the capillary flow test provides a complete pore size distribution along with the largest pore size (bubble point, O_{98}) of a geotextile, but this method is not typically used in design.

The main objectives of this study are to: 1) perform calibration of the Capillary flow test device (Geo Pore Pro, GPP-1001A) to assess the accuracy of the test; 2) establish correlations between bubble point (O_{98}) and AOS (O_{95}) for woven and non-woven geotextiles; and 3) evaluate the role of pore size distribution in the performance of geotextiles using 1-D filtration tests (Falling-head test) and Pressurized 2-D tests.

To achieve these objectives, more than 700 capillary flow tests were performed using Geo Pore Pro (GPP-1001A) manufactured by Porous Materials, Inc. 20 woven geotextiles, 29 non-woven, and 2 composite geotextiles were used in the study. From Capillary flow test, O_{10} , O_{15} , O_{50} , O_{85} , O_{90} , O_{95} and O_{98} were measured. From the calibration test, it was found that for some thin metallic plates and membranes Capillary flow test provides 16% - 23% larger pore size than the

actual pore size. To establish a correlation between Bubble point (O_{98}) and AOS (O_{95}), the outliers were removed and a good correlation ($R^2 = 78\%$) was established for all geotextiles. A decreasing trend of Bubble point (O_{98}) was found with the increasing mass per unit area for both needle punched and heat bonded non-woven geotextiles. However, no such trend was found for woven geotextiles. 1-D filtration tests were performed with 3 different water contents (232.56%, 400% and 882.35%) and it was found that piping rate increases with the decreasing water content in slurry (232.56% - 882.35%) and degree of clogging decreases with the increasing pore sizes (both O_{50} and O_{98}). In the Pressurized 2-D tests, since flocculated slurry was used, instead of soil retention and piping rate, flow rate was the main issue. Therefore, flow ratio (a ratio of radial flow and axial flow) was calculated for all geotextiles and it was found that needle punched non-woven geotextiles showed some decreasing trend of flow ratio with the increasing permeability of clean geotextiles.

**AN EVALUATION OF CAPILLARY FLOW TEST FOR DETERMINING THE PORE
SIZE DISTRIBUTION OF GEOTEXTILES AND ESTABLISHING CORRELATIONS**

By

Nuzhath Fatema

BSc., Bangladesh University of Engineering and Technology, Bangladesh, 2013

Thesis

Submitted in partial fulfillment of the requirements for the degree of

Master of Science in Civil Engineering

Syracuse University

June 2017

Copyright © Nuzhath Fatema 2017

All Rights Reserved

Acknowledgement

I would like to convey my sincere gratefulness to several people who helped me throughout the journey of this research to be accomplished successfully.

First and foremost, I would like to extend my wholehearted gratitude to my advisor, Dr. Shobha K. Bhatia. Without her continuous support, inspiration, and precious suggestions, it was undoubtedly impossible to complete this thesis successfully.

I would like to thank my committee members: Dr. Shobha K. Bhatia, Dr. Dawit Negussey, Dr. Ashok S. Sangani and Dr. Jennifer Smith, for their encouragement and support.

I would like to express my gratitude to Mr. Dick Chave, who helped me fix the pressure and leakage problem of the Capillary flow test device. Special thanks are to Ms. Elizabeth Buchanan, Ms. Heather Flaherty and Ms. Morgan Narkiewicz for their constant help and kindness. I would like to express thankfulness to the Department of Civil and Environmental Engineering for providing me with teaching assistantship.

My sincere appreciation goes to Dr. Krishna Gupta of Porous Materials, Inc. for providing the equipment to perform Capillary flow test.

I would like to express my gratitude to Mr. Robert Smith and Mr. Michael Richard Norman to help me with SEM pictures in SUNY ESF.

There are some people who supported and encouraged me in every feasible way throughout my Masters. I would like to convey my special thanks to Mr. Ratnayesuraj C.R for his endless inspiration and assistance, during his stay. I would like to thank Mr. Zeru Kiffle, Mr. Prabesh Rupakheti, and Mr. Mahmoud Khachan for their help and valuable suggestions.

My immense gratefulness goes to my parents who encouraged and guided me every single day throughout my life. The credit of my any accomplishment throughout my entire life goes to my parents indeed. I am very much grateful to my lovely siblings, Kaniz and Shafkat for their understanding and advice.

I cannot extend my enough gratefulness to my dearest friend Ms. Mahmuda Rahman, who, in the absence of my parents and family, being an elder sister, gave me a shelter of love and care. I am very much thankful to my friends, Tamanna, Samia and Engda for their persistent motivation.

Finally, all praises and gratefulness are to the Almighty Allah, who gave me enough patience and courage to face all difficulties and surrounded me with wonderful people.

Contents

Abstract.....	i
Table of Figures	x
List of Tables	xiv
Chapter 1 Introduction	1
Chapter 2 Literature Review and Calibration	4
2.1 Introduction:	4
2.2 Capillary Flow Test: Principles.....	7
2.3 Wetting liquid:.....	8
2.3.1 Contact Angle and Viscosity of Wetting Liquid.....	10
2.4 Shape Factor	11
2.5 Previous Studies	13
2.6 Calibration Performed in the Previous Studies:	18
2.7 Capillary Flow Test Apparatus	19
2.8 Calibration.....	23
2.8.1 Method	27
2.8.1.2 Wetting Liquid.....	27
2.8.1.3 Contact Angle Test Results.....	27
2.9 Summary	37
2.10 References	37

Chapter 3 Capillary Flow Test Results	41
3.1 Introduction:	41
3.2 Test Procedures	50
3.2.1 Specimens' Preparation	50
3.2.2 Wetting Liquid.....	51
3.2.3 Shape Factor.....	51
3.2.4 Testing Procedure	51
3.2.5 Factors Influencing the Results.....	53
3.3 Test Results	54
3.3.1 Box Plot and Whisker Diagram	64
3.4 Relationships between O_{98} , O_{50} and O_{10} , and Mass per Unit Area of Geotextiles.....	72
3.5 Dry Sieving Test.....	76
3.6 Previous studies.....	83
3.7 Summary	86
3.8 References	87
Chapter 4 Bubble Point Results: Correlations	93
4.1 Introduction	93
4.2 Correlation between Capillary Flow and Dry Sieving Test	94
4.2.1 Current study.....	94
4.2.2 Previous studies	100

4.3	Comparison of Filtration Opening Size and Bubble Point.....	103
4.4	Performance Tests	107
4.4.1	1-D Filtration Test (Falling Head Test)	109
4.4.2	Pressurized 2-D Test.....	122
4.5	Summary:	131
4.6	References:	132
Chapter 5 Conclusion.....		138
5.1	Major Conclusion	138
5.2	Future Work	142

Table of Figures

Figure 2.1: Contact Angle (Jena et al. 1999)	10
Figure 2.2: Elliptical Cross-Section of Pore (Cap.Fl.5-12- 09)	12
Figure 2.3: Schematic of the Capillary Flow Device Used in University of Maryland by Aydielk, et al. (2006)	14
Figure 2.4: Schematic of the Capillary Flow Device used in Auburn University by Elton, et al. (2007).....	14
Figure 2.5: Geo Pore Pro GPP-1001A at Syracuse University.....	20
Figure 2.6: Schematic of the Capillary Flow Device Geo Pore Pro (GPP 1001A), used in Syracuse University (2017).....	22
Figure 2.7: Accessories of Geo Pore Pro; (a) Adapter Plate; (b) Adapter Plate Built-in Screen, Support Screen, and O-Ring; (c) Wedge Plate;(d) Sample Chamber and Cap.....	23
Figure 2.8: SEM Images of Calibration Materials: Thin Metal Plate (A1, A2, A3, and A4); and Membrane (C1, C2)	26
Figure 2.9: Test Setup for Calibrating Materials with Mineral Oil	29
Figure 2.10: Pore Size Distribution of Thin Metal Plate, A1 (a) before Cleaning and (b) after Cleaning the Equipment.....	31
Figure 2.11: Pore Size Distribution of Thin Metal Plate, A3 (a) before Cleaning and (b) after Cleaning the Equipment.....	32
Figure 2.12: Measured O_{100} vs. SEM Measurements for Thin Metallic Plates and Membranes .	35
Figure 2.13: Measured O_{100} vs. Manufacturing Pore Sizes for Thin Metallic Plates and Membranes.....	36

Figure 3.1: SEM Images of Woven Geotextiles (a) Monofilament, (b) Monofilament (Slit Film in Cross Direction), (c) Slit Film, (d) Multifilament.....	42
Figure 3.2: SEM Images of Needle Punched Non-Woven Geotextiles.....	44
Figure 3.3: SEM Image of Heat Bonded Non-Woven Geotextile (Smith, 1996).....	45
Figure 3.4: SEM Image of a Geo-Composite	45
Figure 3.5: Step by Step Procedure of Placing a Geotextile (a) Placing Gasket, (b) Placing Geotextile Over Gasket, (c) Adapter Plate Over the Geotextile, (d) Placing Chamber Cap	52
Figure 3.6: Typical Pore Size Distribution Results of a Non-Woven Geotextile.....	53
Figure 3.7: Pore Size Distribution of a Monofilament Woven Geotextile (A-7)	55
Figure 3.8: Pore Size Distribution of a Slit Film Woven Geotextile (B-2)	56
Figure 3.9: Pore Size Distribution of a Multifilament Woven Geotextile (C-2)	57
Figure 3.10: Pore Size Distribution of a Heat Bonded Non-Woven Geotextile (D-3)	58
Figure 3.11: Pore Size Distribution of a Needle Punched Non-Woven Geotextile (E-2)	59
Figure 3.12: Pore Size Distribution of a Geo-Composite (F-1).....	60
Figure 3.13: Pore Size Distribution of a Monofilament Woven Geotextile (A-4)	62
Figure 3.14: Pore Size Distribution of a Needle Punched Non-Woven Geotextile (E-10)	63
Figure 3.15: Pore Size Distribution of a Needle Punched Non-Woven Geotextile (E-1)	63
Figure 3.16: Box Plot and Whisker Diagram.....	65
Figure 3.17: Box Plot and Whisker Diagram for a Set Of 7 Monofilament Woven Geotextiles .	66
Figure 3.18: Box Plot and Whisker Diagram for a Set Of 11 Slit Film Woven Geotextiles.....	67
Figure 3.19: Box Plot and Whisker Diagram for a Set Of 2 Multifilament Woven Geotextiles..	68
Figure 3.20: Box Plot and Whisker Diagram for a Set Of 8 Heat Bonded Non- Woven Geotextiles	69

Figure 3.21: Box Plot and Whisker Diagram for a Set Of 21 Needle Punched Non- Woven Geotextiles	70
Figure 3.22: Box Plot and Whisker Diagram for a Set of 2 Geo-Composites.....	71
Figure 3.23: Bubble Point vs. Mass per Unit Area of Monofilament and Slit-film Woven Geotextiles	73
Figure 3.24: O_{10} , O_{50} , and O_{98} vs. Mass per Unit Area of Needle Punched Non-Woven Geotextiles	74
Figure 3.25: Bubble Point vs. Mass per Unit Area of Heat Bonded Non-Woven Geotextiles.....	75
Figure 3.26: Dry sieving equipment and sieve shaker.....	77
Figure 3.27: Geotextile with glass beads secured in the frame.....	77
Figure 3.28: AOS vs. Mass per Unit Area for Needle Punched Non-Woven Geotextiles	78
Figure 3.29: AOS vs. Mass per Unit Area for Heat Bonded Non-Woven Geotextiles	79
Figure 3.30: Bubble point vs. mass/unit area (a) needle-punched, (b) heat-bonded nonwoven geotextiles	84
Figure 4.1: Correlation between Bubble Point and AOS of Woven Geotextiles.....	96
Figure 4.2: Correlation between Bubble Point and AOS of Non- Woven Geotextiles	98
Figure 4.3: Correlation between Bubble Point, O_{98} and AOS, O_{95} of All Geotextiles.....	99
Figure 4.4: Correlation between Bubble Point, O_{98} and AOS, O_{95} of All Geotextiles (Bhatia et al. (1996), Aydilek et al. (2006), Elton eta al. (2007) and TENCATE (2014)).....	102
Figure 4.5: Theoretical and Measured Pore Openings vs. Mass Per Unit Area of Needle Punched Non-Woven Geotextiles.....	106
Figure 4.6: Bubble Point vs. Theoretical Pore Openings of Needle Punched Non-Woven Geotextiles	107

Figure 4.7: Pore Size Distribution of Six Pairs of Geotextiles used for 1-D Filtration Test	113
Figure 4.8: 1-D Filtration Test Setup.....	115
Figure 4.9: Filter Cake Obtained from the Test with E-19	115
Figure 4.10: 1-D Filtration Test Piping Rate Results Against O_{98}/d_{85} for the Soil-Geotextile Systems	118
Figure 4.11: Clogged and Wet Non-Woven Geotextiles (E-19) after 1-D Filtration Test	120
Figure 4.12: Relationship of Clogging to O_{95}/d_{85} and O_{50}/d_{50}	121
Figure 4.13: Pore Size Distribution of Geotextiles used in the P2DT	124
Figure 4.14: Pressurized 2-D Test Setup (Ratnayesuraj (2017))	125
Figure 4.15: Filter Cake Formed for GC-1 (Ratnayesuraj (2017)).....	127
Figure 4.16: Pressurized 2-D Test Results of Geotextiles (a) Woven Geotextiles and Geo-composites (b) Non-Woven Geotextiles	128
Figure 4.17: Flow ratio vs. Permeability	130

List of Tables

Table 2.1: Summary of Results with Dynamic Contact Angles (Elton et al. (2007))	11
Table 2.2: Pore Cross-Section and Shape Factors, Jena et al., 2003	12
Table 2.3: Details of Capillary Flow Test Devices Used by Different Researchers.....	15
Table 2.4: Calibration Results by Previous Studies.....	18
Table 2.5: Physical Properties of Calibration Materials	23
Table 2.6: Capillary Flow Test Results for Thin Metallic Plates and Membranes.....	33
Table 3.1: Physical and Hydraulic Properties of Geotextiles	47
Table 3.2: Minimum and Maximum Outliers of Monofilament Woven Geotextiles.	67
Table 3.3: Minimum and Maximum Outliers of Slit Film Woven Geotextiles.....	67
Table 3.4: Minimum and Maximum Outliers of Multifilament Woven Geotextiles.....	68
Table 3.5: Minimum and Maximum Outliers of Needle Punched Non-Woven Geotextiles.....	70
Table 3.6: Capillary Flow and Dry Sieving Test Results of Geotextiles.....	80
Table 4.1: Previous Studies (Bhatia and Smith (1996), Elton et al. (2006), Aydilek et al. (2006), TENCATE (2015))	100
Table 4.2: Physical Properties of Non-Woven Geotextiles	105
Table 4.3: Geotextile Filter Selection Criteria with High-Water Content Slurry	111
Table 4.4: Physical properties of geotextiles used in the test	112
Table 4.5: Properties of Slurry (50% Standard Silica and 50% Tully Silt)	114
Table 4.6: 1-D Filtration (Falling-Head Test) Test Results	116
Table 4.7: Applicability of the Existing Criteria	119
Table 4.8: Impregnation Level of Clogged Geotextiles Obtained from the Test	121
Table 4.9: Properties of Tully Sand Used in the Test, Ratnayesuraj (2017)	123

Table 4.10: Physical Properties of Geotextiles Used in the Pressurized 2-D Test	124
Table 4.11: Pressurized 2-D Test Results (Ratnayesuraj (2017)).....	129

Chapter 1 Introduction

For the last four decades, geotextiles have been used extensively for the purpose of soil retention, filtration, and reinforcement. Both woven and non-woven geotextiles have been used as filters in many civil and environmental applications, such as geotextile tube dewatering technology. Over the past two decades, geotextile tube dewatering has been predominantly used for dewatering high water content slurries. A variety of methods are available to successfully assess the geotextile tube dewatering technology. A properly designed geotextile tube should have the following properties: ability to support a steady flow without clogging, a high dewatering rate, and retention of soil. In order to ensure good retention for erodible materials and provide adequate discharge capacity for the safety of a structure, there are several factors that need to be addressed. The three basic criteria that impact the behavior of a geotextile filter are soil retention, permeability, and clogging potential. Numerous criteria have been developed for geotextile retention and to clogging prevention, which depend on the pore openings of geotextiles (O_n : O_{98} , O_{95} , O_{90} , O_{85} , O_{50} , and O_{15}) and diameter of soil particles (d_n). Despite of the importance of pore openings and pore size distribution of geotextiles, these properties are difficult to measure and the results might be different for different methods. In the USA, two standards are used to measure the pore size of geotextiles, including, the dry sieving test (ASTM D 4751) and the capillary flow test (ASTM D 6767). There are other standards available in other countries, such as: Hydrodynamic sieving (standard in Canada), and Wet sieving (used in Europe).

In the USA, most of the filtration and soil retention criteria are based on the apparent opening size (AOS, O_{95}) obtained by the dry sieving test. The dry sieving test is based on the concept that glass beads of a specific diameter are sieved through a geotextile to determine whether the percentage of beads passing through the geotextile equals 5% or less. Based on this percentage,

the immediate larger beads would be selected and the same technique is followed to measure the percentage of glass beads that pass through the pores. The repetition of the process provides apparent opening size (AOS, O_{95}) of a geotextile. The details of the Dry sieving test are explained in Chapter 3. However, the dry sieving test has several disadvantages, including electrostatic effects, trapping of glass beads, etc., which make it difficult to obtain accurate pore size of a geotextile (Bhatia and Smith 1996, Giroud 1996, Koerner 1990).

Another method for measuring the pore sizes of geotextiles is the capillary flow test (ASTM D 6767). In contrast to the dry sieving test, the capillary flow test has the advantage of not only providing the largest pore (bubble point, O_{98}) of a geotextile, but also providing a complete pore size distribution. Therefore, O_{85} , O_{50} , and O_{15} can be calculated. Previous studies established that, along with the largest pore sizes (O_{90} and O_{95}), smaller pores including O_{50} and O_{15} significantly control the soil retention (Giroud 1982, Christopher and Holtz 1985). Therefore, the capillary flow test establishes a common method that can provide both the largest pore size of a geotextile along with a complete pore size distribution. There are other techniques, such as Image Analysis (Rollin et al. 1977) and Mercury Intrusion Porosimetry (Prapaharan et al. 1989), but these have not been widely adopted. Researchers and practitioners have been trying for the last 20 years to develop the capillary flow test, rather than the dry sieving test, as a common standard to measure the pore sizes of a geotextile.

Since 1996, very few capillary flow test studies (Vermeersch, et al. (1996), Bhatia et al. (1996), Lydon, et al. (2004), Aydilek, et al. (2006), Elton, et al. (2007), Przybylo (2007), and TENCATE (2015)) have used a capillary flow porometer in their analysis, in contradiction to the current ASTM standard. The first goal of this study is to use the capillary flow test ASTM D6767 to produce results on a range of geotextiles (woven, non-woven and composite geotextiles) and

evaluate the quality of the results (including calibration). The second goal is to compare data from the capillary flow test in regard to applications such as soil retention, filtration and soil reinforcement, to those produced by the dry sieving test. The capillary flow test was conducted with 51 geotextiles for this study following the ASTM D6767 and using the latest version of capillary flow porometry, Geo Pore Pro (GPP-1001A) manufactured by the Porous Materials, Inc. (PMI).

The main objectives of this study are to:

- 1) Perform calibration of the Geo Pore Pro (GPP-1001A) with several materials of known sizes and compare the capillary flow test devices used by others with different ASTM standards and limitations.
- 2) Compare the results obtained by the capillary flow test with the dry sieving test results.
- 3) Establish correlations between bubble point, O_{98} and AOS, O_{95} for woven and non-woven geotextiles. Evaluate the influence of pore size distribution on the performance of geotextiles using 1-D filtration test and Pressurized 2-D test.

The thesis is divided into 4 chapters;

Chapter 2: The calibration of Geo Pore Pro (GPP-1001A) was performed using four thin metallic plates with uniform holes and two membranes with irregular holes.

Chapter 3: Capillary flow tests were conducted for 51 geotextiles following ASTM D6767. Geo Pore Pro (GPP-1001A) was used to perform all the tests.

Chapter 4: A correlation between bubble point, O_{98} obtained by capillary flow test and AOS, O_{95} obtained by the dry sieving test, was established for all geotextiles. The role of pore size distribution in the performance of geotextiles were evaluated.

Chapter 5: Conclusion and Future work.

Chapter 2 Literature Review and Calibration

2.1 Introduction:

In terms of the performance of geotextiles as a filter, pore size distribution is an important property of geotextiles. The geotextile filter design criteria include permeability, soil retention and resistance to clogging. During the last 25 years, extensive research has been conducted to establish two of the primary design criteria, permeability and soil retention criteria. Many of the soil retention criteria require the largest pore openings (O_{98} and O_{95}) and some criteria need O_{50} and O_{15} (Rankilior 1981, Giroud 1982, Christopher and Holtz 1985, Fannin, J., 2006). Filtration within soil/ geotextile system includes soil and geotextile interaction with each other. The continuous rearrangement of soil particles at the geotextile interface zone influence the long-term performance of the filtration system. The largest pore openings and the pore size distribution of geotextile filters are directly related to the degree of rearrangement of soil particles. When the opening of the geotextile filter is too small or too large, the geotextile filter is ineffective. Although larger pore openings and pore size distribution are the key property of a geotextile, these properties are very difficult to measure. The commonly used techniques to evaluate the largest pore openings and pore size distribution of geotextiles are: Dry Sieving (ASTM D 4751), Hydrodynamic Sieving (CGSB 148.1 n°10), Wet Sieving (SW-640550-83), and Capillary flow test (ASTM D 6767). Dry sieving, Hydrodynamic sieving, and Wet sieving tests are used to measure the largest pore opening only. Dry sieving test is used in US, Hydrodynamic test is used in Canada and Wet sieving in Europe. Only Capillary flow test provides the largest pore opening as well as O_{50} and O_{15} . There are other techniques such as Image analysis (Rollin et al. 1977) and Mercury Intrusion Porosimetry (Prapaharan et al. 1989, and Bhatia and Smith, 1994) have been used to measure pore size distribution but not widely adopted. It is possible to achieve different

pore size distribution results of a geotextile within and between different test methods (Rollin 1986, Bhatia et al. 1994). The larger pore openings of a geotextile that predominantly influence soil retention includes O_{95} , O_{90} , and O_{50} . Many of the established soil retention criteria of geotextiles depend upon the larger O_{95} , O_{90} , O_{50} and O_{15} pore openings of geotextiles (Giroud 1982, Christopher and Holtz 1985, Fannin, J., 2006); and it is believed that the finer pore openings of a geotextile, O_{15} also controls soil retention (Rankilior 1981).

In the USA, Dry sieving (ASTM D 4751), an approved and commonly used method to measure the apparent opening size, O_{95} (AOS) of geotextiles, is used for many soil retention criteria. The Canadian standard, Hydrodynamic Sieving is a method where a mixture of glass beads is sieved through geotextiles by altering water to determine the O_{95} of a geotextile. Wet sieving is standardized in Europe to measure the O_{95} of a geotextile, where a particle mixture is used instead of fractions and a continuous water spray is used in the method to reduce the electrostatic effect occupied with the glass beads. Due to several disadvantages of dry sieving test such as electrostatic effects and clogging of glass beads within the geotextiles, this method does not provide the accurate AOS values (Bhatia and Smith 1996, Giroud 1996, Koerner 1990).

Capillary flow test (ASTM D 6767) was approved in 2002 which can provide the largest pore size (O_{98}) and a complete pore size distribution. However, there is no standard device to perform capillary flow test. For this test, mineral oil is recommended as a wetting liquid, however in ASTM standard it is also mentioned that other liquids could be used with proper judgement. Due to variation in the test devices and wetting liquids, different capillary flow devices and wetting liquids have been used by researchers and geosynthetic industries.

In the summer of May 4th, 2015, a meeting was held at Syracuse University to discuss round robin test results of ASTM D 6767. The meeting participants include the executive director of

North American Geosynthetics Society (L. David Suits); representatives from Ten Cate (geosynthetic manufacturing company), representatives from two testing labs: Texas Research International, Inc. (TRI) and State-of-the-art Geosynthetics Laboratory (SAGEOS); representatives from Porous Materials, Inc. (PMI); Dr. Shobha Bhatia and her few graduate students. TRI uses their own Capillary flow device, PMI makes several versions of Capillary flow devices, SAGEOS and Ten Cate use different versions of PMI devices. The group discussed a need to come up with a correlation factor between O_{95} (AOS) obtained by dry sieving test and O_{98} obtained by capillary flow test. This would encourage more manufacturers, researchers and practitioners to use Capillary flow test to measure O_{98} of geotextiles. Moreover, since most of the geotextile filter design criteria use results (O_{95}) from dry sieving test, a correlation factor is needed to use O_{98} from Capillary flow test. It was concluded that the practitioners and manufacturers need a correlation factor between dry sieving (O_{95}) and capillary flow (O_{98}) test results. These relationships have not been established till now due to the limited number of geotextiles used for studies and lack of proper calibration of the Capillary flow test. Hence, a study has been taken to perform the capillary flow test using ASTM D 6767 to calibrate the test equipment with a wide range of materials including thin (0.003-inch thickness) metal plate with circular holes (made of 300 series Alloy stainless steel), and membranes with irregular holes. A state of the art capillary flow porometer Geo Pore Pro (GPP 1001A) is used to evaluate pore opening of these calibrating materials and ASTM D6767 is used to conduct the tests.

2.2 Capillary Flow Test: Principles

Capillary flow test is a standardized test which is used to determine pore size distribution of both woven and non-woven geotextiles with pore sizes ranging from 1 to 1000 microns. This test is delineated in ASTM D 6767-16, “Standardized Test Method for Pore Size Characteristics of Geotextiles by Capillary Flow Test”. The capillary flow test is based on the principle that the continuous pores in a geotextile hold a wetting liquid by capillary attraction and surface tension, and they will only allow the liquid to pass when the pressure applied exceeds the capillary attraction of the liquid in the largest pore. Consequently, smaller pores demand higher pressure to discharge liquid, since they have larger solid-liquid attraction. In order to originate the air flow through a saturated sample, it needs a gateway pressure or minimum pressure, which is related to the largest pore size, or bubble point, and the type of wetting liquid being used. The ASTM D6767 uses the following equation based on the equilibrium of forces:

$$\pi * d * \tau * \cos \theta = \frac{\pi}{4} * d^2 * P \quad 2.1$$

Where,

d = pore diameter, microns (microns),

τ = surface tension of the liquid saturating the porous material, mN/m, (dynes/cm),

θ = contact angle in degrees between the wetting liquid and the porous material ($\cos \theta = 1$ for a wetted sample with $\theta = 0^\circ$), and

P = Pressure measured, Pa (N/m^2).

If the test liquid used in testing is assumed to be “wetting”, or contact angle, $\theta = 0$, the equation is simplified even further:

$$d = \frac{4\tau}{p} \quad 2.2$$

The capillary flow test can be used to measure the complete pore size distribution of a porous material by gradually increasing the pressure and approving steadily smaller pores to be vacant of liquid. The extended method is based on: (a) air is passed through the pores of a dry specimen during the period when any amount of air pressure will be imposed to one side of the specimen; and (b) air will be passed through the pores of a saturated specimen when the capillary attraction of the fluid is exceeded by the air pressure, (c) smaller and smaller pores will pass the air with the increase in air pressure. A complete pore size distribution of a geotextile can be determined using the following equation (ASTM D 6767).

$$\%Finer = \left[1 - \frac{(\text{wet flow rate})}{(\text{dry flow rate})} \right] \times 100\% \quad 2.3$$

2.3 Wetting liquid:

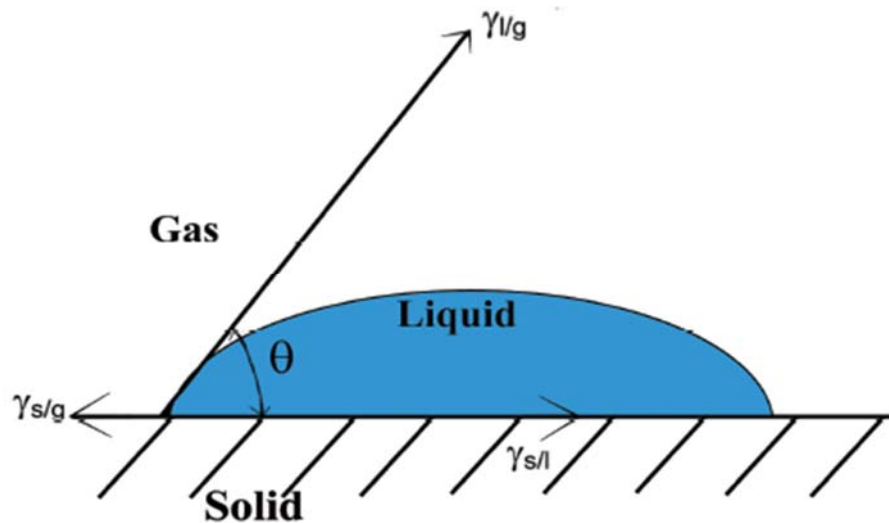
Wetting liquid is a liquid which is used to saturate the geotextile specimen for the “wet” portion of the capillary flow test. The word “wet” stands for saturating the specimen completely throughout its entire thickness without entrapping any air bubble. According to ASTM D 6767, mineral oil, with surface tension of 34.7 dynes/cm at 25° C (USP liquid petrolatum heavy), is a standard wetting liquid recommended for the capillary flow test. However, according to ASTM D6767-16, other liquids can be used with a proper verification of consistency of the resulting pore size distribution of geotextiles with the results obtained with mineral oil as a wetting liquid. In the past twenty years, researchers have used different types of wetting liquids in the capillary flow test. Vermeersch and Mlynarek (1996) used Coulter Porometer II® in the capillary flow test to determine the pore size distribution of needle punched and heat bonded, polypropylene continuous filament non-woven geotextiles with Porofil as a wetting liquid (16 dynes/cm).

Lydon, et al. (2004) tested several multi-layered woven filter media using Coulter Porometer I, with 1100AEX Capillary Flow Porometer. Lydon et al. (2004) used both Porofil and Galwick (surface tension was not mentioned) in Coulter Porometer I and only Galwick in 1100AEX Capillary Flow Porometer. Aydilek, et al. (2006) used deionized water as a wetting liquid for 11 non-woven and 18 woven geotextiles in the capillary flow test. They used a capillary flow device which was made at the University of Washington. Elton and Hayes (2007) conducted tests on a polypropylene non-woven geotextile with six different liquids (water, porewick, mineral oil, 2-ethyl-hexanol, drakeol 600, and glycerin). The device used in their tests was designed at Auburn University. Przybylo (2007) used CFP-1500 AEDLS-2C manufactured by PMI, to test 12 heat bonded non-woven geotextiles with Galwick as a wetting liquid (15.9 dynes/cm). TENCATE (2015) used 3 different types of woven monofilament geotextiles (woven monofilament, woven monofilament with tape filling, and high strength woven monofilament with tape filling) to perform capillary flow test using PMI porometer. No further information about the device and liquid was reported. Zeru, et al. (2014) used two woven, one non-woven and one geo-composite in the analysis using PMI automated Capillary flow porometer (CFP- 1003A) with mineral oil as a wetting liquid (34.7 dynes/cm).

In addition to mineral oil, researchers have used Porofil, Galwick, Porewick, 2-ethyl-hexanol, Drakeol 600, glycerin, water as wetting liquid and very few of them verified the consistency with mineral oil. In ASTM D 6767, it is mentioned that mineral oil with a surface tension of 34.7 dynes/cm at 25°C should be used as a wetting liquid. Use of different liquids may produce different results, since the contact angle between test specimen and wetting liquid is different.

2.3.1 Contact Angle and Viscosity of Wetting Liquid

The contact angle is the angle, conventionally measured through the liquid, where a liquid interface meets a solid surface (see Figure 2.1). Generally, liquids generating an angle with solid surface less than 90 degrees are called ‘hydrophilic’ and greater than 90 degrees are called ‘hydrophobic’. A wetting situation is called when a hydrophilic liquid runs over a fibrous matrix or a given surface. Elton et al. (2007) stated that the hydrophobic liquids demand an external energy to propagate. According to the studies, surface roughness (Bikerman 1958, Adamson 1976, Good 1984, Berg 1989) and surface chemistry (Berg 1989) can influence the contact angle. Since, contact angle is a function of solid –liquid interactions (Van de Velde and Kickens 1999), any discrepancy in the properties of either liquid or solid may change the result of the contact angle. Chemical properties of a liquid such as pH, ionic strength, and concentration can also change the contact angle (Byron et al 2000, Mohammed and Kibbey 2005).



θ = Contact angle

Figure 2.1: Contact Angle (Jena et al. 1999)

Since, ASTM D 6767-16 does not provide any instruction about the measurement of contact angle, generally it is assumed that the contact angle is zero. However, Elton et al. (2007) showed that different liquids generate different contact angles with the same geotextile, which results in the change of bubble point (O_{98}). Elton et al. (2007) measured bubble point, O_{98} of a polypropylene non-woven geotextile using the capillary flow testing with six different liquids having distinct surface tension and viscosity. The wetting liquids, used included water, Porewick, mineral oil, 2-ethyl-hexanol, drakeol 600, glycerin etc. Cahn Dynamic Contact Angle (DCA) Analyzer was used to measure the contact angle of different liquids. Table 2.1 shows the results of the capillary flow test performed with different liquids.

Table 2.1: Summary of Results with Dynamic Contact Angles (Elton et al. (2007))

Geotextiles	Wetting liquid	Bubble point (microns), with θ contact angle	Dynamic contact angle (Cahn Dynamic contact angle, θ)	Bubble point (microns) with dynamic contact angle
Polypropylene non-woven geotextile	Water	390	67.53	160
	Porewick	190	0	190
	Mineral oil	300	0	300
	2-ethyl-hexanol	180	0	180
	Drakeol	290	0	290
	Glycerin	300	34.51	240

Table 2.1 shows that the dynamic contact angle of water and glycerin with geotextile is not zero but 67.53° and 34.51° respectively. Using the correct contact angle, the bubble point of geotextile changed significantly. Mineral oil and Porewick, the most widely used wetting liquid, have zero contact angle with the polypropylene nonwoven geotextiles.

2.4 Shape Factor

The relation between the measured pore size by the capillary flow test and the actual pore size depends on the ratio of the diameter of the largest particle passing through the pore (d) and the

measured pore diameter (D), which is called pore shape factor, λ . The shape factor can be defined by the following equation (Jena et al., 2003):

$$\lambda = \frac{d}{D} = [(1 + n^2) / 2n^2]^{1/2} \quad 2.4$$

n = axial ratio of elliptical cross – section of pore

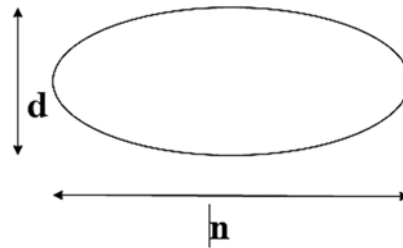
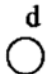
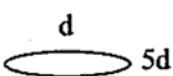
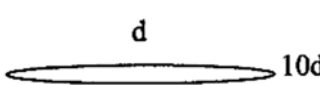
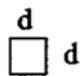
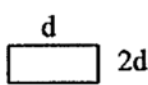


Figure 2.2: Elliptical Cross-Section of Pore (Cap.Fl.5-12- 09)

In Table 2.2 shape factors are given for pores of different shapes (Jena et al., 2003). Based on the pore cross-section, the measured diameter of a pore is computed by multiplying the shape factor, λ with the diameter measured by equation 2.4.

Table 2.2: Pore Cross-Section and Shape Factors, Jena et al., 2003

Pore cross-section		Shape factor λ ($d = \lambda D$)
Circular: $n=1$		1
Elliptical: $n = 5$.		0.72
Slit: $n = 10$		0.71
Square:		1
Rectangular		0.75

2.5 Previous Studies

Different researchers have used different devices based on the capillary flow test principles. Some of the devices were made by the researchers themselves and others were made of by the commercial companies like Coulter Corporation and Porous Materials, Inc (PMI). Different versions of PMI manufactured devices have been using to perform capillary flow test. The capillary flow device used by Aydilek, et al. (2006) at University of Maryland and Elton, et al (2007) at Auburn University were constructed based on the schematic sketch given in Figure 2.3 and Figure 2.4 respectively. Two versions of Porometer manufactured by Coulter, Coulter Porometer I and Coulter Porometer II, were used by Vermeersch, et al. (1996) and Lydon, et al. (2004). The Coulter Porometer II, controlled by microprocessor, is associated with a compressor, since the supplied pressure is used for the capillary flow test. However, no detailed information is available about the Coulter Porometer I, which was used by Lydon, et al. (2004). Different generations of PMI devices have been using at Syracuse University for the capillary flow tests. These devices included PMI Automated Perm-Porometer (Model No. APP-200) by Bhatia, et al. (1996); PMI automated device CFP-1500 AEDLS-2C by Przybylo (2007); Capillary Flow Porometer (CFP-1003A) by Kiffle, et al. (2014); and Geo Pore Pro (GPP-101A). For the current study, the Geo Pore Pro (GP-1001A) is used. Lydon, et al. (2004) also tested several multi-layered woven filter media using 1100AEX Capillary Flow Porometer manufactured Porous Materials, Inc. (PMI). In Table 2.3, details of all different Capillary Flow Porometers used by researchers are provided.

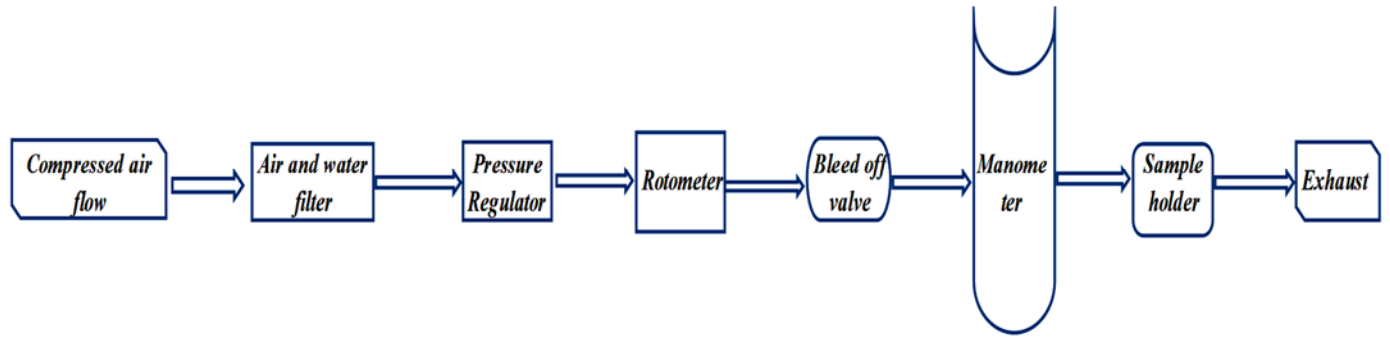
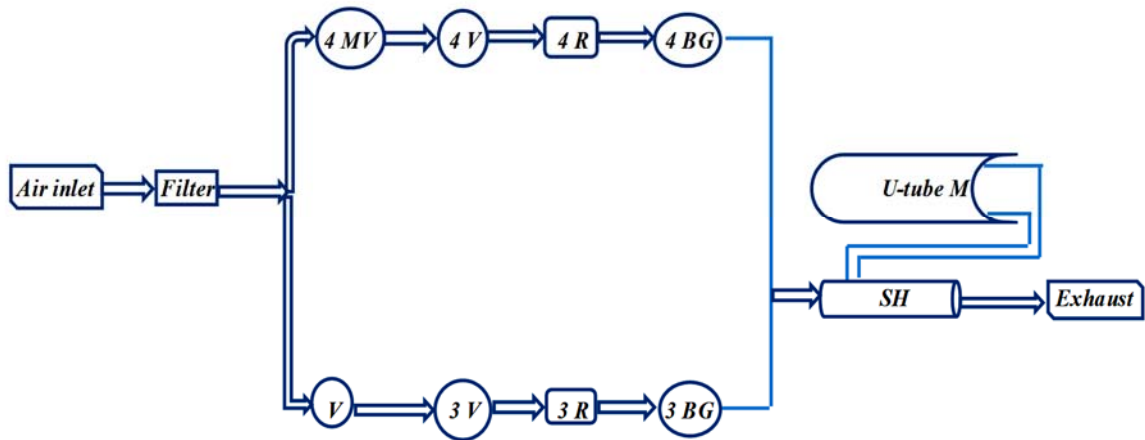


Figure 2.3: Schematic of the Capillary Flow Device Used in University of Maryland by Aydielk, et al. (2006)



MV = Metering valve, V = Valve, R = Rotometer, BG = Backpressure Gauges, SH = Sample Holder, M = Manometer

Figure 2.4: Schematic of the Capillary Flow Device used in Auburn University by Elton, et al.

(2007)

Table 2.3: Details of Capillary Flow Test Devices Used by Different Researchers

Device	Vermeersch, et al. (1996)	Lydon, et al. (2004)	Aydilek, et al. (2006)	Elton, et al. (2007)	Przybylo (2007)	Current study
Standard	ASTM E 1294-89 was followed.	ASTM F316-80 and SAE ARP901 were followed.	ASTM D6767 was followed	ASTM D6767 was followed	ASTM D6767-02 was followed	ASTM D6767-16 was followed
Testing device	Coulter Porometer II®	Coulter Porometer I, and 1100AEX Capillary Flow Porometer.	No information was available.	No information was available.	CFP-1500 AEDLS-2C	Geo Pore Pro (GPP-1001A)
Research institution	No information was available.	No information was available.	University of Washington	Auburn University	Syracuse University	Syracuse University
Manufacturing company	Coulter	Coulter and Porous Materials Inc.	Designed by the research institution	Designed by the research institution	Porous Materials Inc.	Porous Materials Inc.
Mechanization	No information was available.	No information was available.	No information was available.	No information was available.	Fully automated	Fully automated
Dynamic range of operation	202 Pa (0.002 bar) to 1418 Pa (14 bar)	No information was available.	No information was available.	No information was available.	No information was available.	No information was available.
Features	Compressor as the pressure supplier, RS232C microprocessor, data acquisition system to collect 256 data points.	No information was available.	No information was available.	No information was available.	No information was available.	No information was available.
Rotometers	No information was available.	No information was available.	Rotometer (flow meter) is installed between the pressure regulator and the bleed-off valve. According to Aydilek, et al. (2006), the rotometer/flow meter does not have sufficient capacity to measure the airflow in the system through the 25 mm diameter geotextile specimens.	The rotometers measure the flow rate of air ranging from 0.00838 to 3400 L/min. A hose running from the filter is divided into two parts, one leading to the larger rotometers, which measure the higher flows and involve higher air velocities, and the other one leading to the smaller ones. Therefore, the larger rotometers have a more direct link	A set of rotometers record air flows. No more information was available.	Flow transducer is installed between V1 (controls the flow to the low flow controller) and pressure transducer (P1).

				to the air source, reducing head losses.		
Washers and O rings	No information was available.	No information was available.	Due to the problem in measuring airflow and reduce the airflow, nylon flat washers having a 12 mm center hole were installed on each side of the geotextile specimen. O- rings were inserted between the washers and specimen holder to prevent air loss around the perimeters of the washers.	No information was available.	A thin metal disc with multiple circular holes arranged in a grid pattern each with an approximate diameter of 40 microns was used as a support screen. The samples are located on the supporting screen inside the depression. 14 mm O-ring was used to seal the sample.	The sample is sealed by the O-rings. The sample perimeter must be enclosed by the O- ring to prevent gas flow between the O- ring and sample.
Metering and cutoff valves	No information was available.	No information was available.	No information was available.	Metering valves with variable sizes were used to control the airflow to the open rotometer.	No information was available.	Motorized metering valve opens in increments. The numbers indicate how many increments (displayed in counts) the valve has been opened or closed. This valve, located in the conjunction with the regulator, is used to control pressure flow.
Sample holder	No information was available.	No information was available.	A sample holder is installed next to the manometer. No more information was available.	Sample holder has four parts: the inlet pipe, a wire screen, a washer, and an exhaust pipe.	CFP-1500 AEDLS-2C has two sample chambers for high and low flow rates capable of analyzing materials with a wide range of bubble points. Each chamber is equipped with a computer- controlled pneumatic piston which seals the samples being tested.	The sample is inserted inside the sample chamber which is connected to a tube of 1.0-inch diameter.
Testing mode	Wet and dry test respectively.	Wet and dry test respectively.	No information was available.	Dry run and wet run accordingly.	Dry up/wet up: It consists a sequence	Wet up/Calc. Dry: the wet curve is run with

					which includes a dry and wet run with sample saturation accordingly.	the pressure increasing; a linear dry plot is extrapolated from the wet phase data.
Reference	Vermeersch, et al., 1996	Lydon, et al., 2004	Aydilek, et al. (2006)	Elton, et al. (2007)	Przybyło (2007)	Fatema (2017)

Due to the use of different types of capillary flow devices, the pore size distribution results of a geotextile could be different. Hence, it was necessary to validate the accuracy of the test results by calibrating the equipment.

2.6 Calibration Performed in the Previous Studies:

The calibration of the individual capillary flow equipment was performed by testing meshes of known pore openings at both Auburn University (Elton et al., 2007), and Syracuse University (Przybylo, 2007 and Kiffle, 2014). To evaluate the accuracy of the capillary flow test, Elton et al. (2007) performed calibration test with US Sieve no. 100 (0.150 mm) and no. 200 (0.075 mm) squared-holed screens, and a round-holed screen with a diameter of 0.140 mm. The result of the calibration tests (see Table 2.4) shows that O_{100} obtained from the test is larger (11% - 28%) than the actual hole size of squared holed screens, while for round-holed screen it is 34% larger than the actual size. No information of wetting liquid was found.

Table 2.4: Calibration Results by Previous Studies

Reference	Materials	Hole size	Wetting liquid	Theoretical measurement (microns)	Bubble point, O_{100} (microns)	% difference
Elton et al. (2007)	#100	Square	Not mentioned	150	175 – 210	28.3
	#200	Square	Not mentioned	75	80 – 86	10.67
	Round holed screen	Round	Not mentioned	140	175 – 200	33.92
Przybylo (2007)	Thin metal plate	Cylindrical	Galwick	166	207	20
	Wire mesh	Square	Galwick	58	77	24
	Membrane 1	Cylindrical	Galwick	20	32	37
	Membrane 2	Cylindrical	Galwick	5	8.4	40
Kiffle (2014)	Thin metal plate	Round	Mineral oil	180	244.71 – 254.44	38.65

Przybylo (2007) used a thin metal plate with cylindrical holes, wire mesh with square holes, and two polycarbonate tracts etch membranes for calibration and he used galwick (surface tension of 15.9 dynes/cm) as a wetting liquid. The metal plate and wire mesh were examined using a Scanning Electron Microscope (SEM). The average bubble point (O_{100}) measured for metal plate and wire mesh were 166 and 58 microns respectively. In Table 2.4, the results of calibration for 4 materials are provided. The measured bubble points were larger by 20% - 40% than the real pore openings. The difference decreases as the pore size increases.

Kiffle, 2014 used a metallic screen with round holes (180 microns) of known size to validate the accuracy of the equipment (PMI automated porometer, CFP 1003A) using mineral oil as a wetting liquid (34.76 dynes/cm). The measured bubble point, O_{98} reported differs 38.65% from the actual value measured by microscopic image (see Table 2.4).

2.7 Capillary Flow Test Apparatus

A state of the art capillary flow porometer, Geo Pore Pro (GPP 1001A) (see Figure 2.5) was used in this study for the calibration tests. This device is fully automated and manufactured by the Porous Materials Inc. (Ithaca, NY). It is consolidated by PMI with the evolution of improved rotometer, manometer, pressure transducer and electronic system, new sample chamber design etc. The equipment consists of an electronically controlled pressure regulator (0 to 4000 counts), an absolute pressure transducer (usually 100 psi) and a differential pressure transducer (5 psi), 1 part in 20000 resolution, 0.15% accuracy in readings, two mass flow transducers (0 to 10 cc/min, 0 to 500 L/min), and a sample chamber. The sample chamber is connected to a tube of 1.0-inch diameter. The PMI porometer's APP CPCS is directed by a computer connected to the device, which controls valves opening and closing.

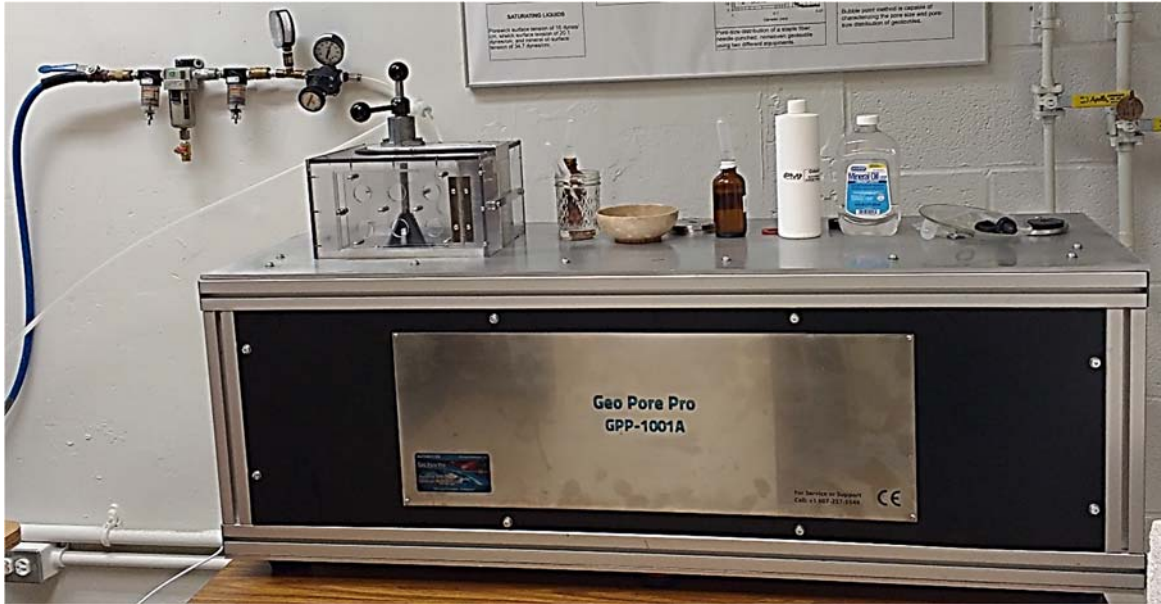


Figure 2.5: Geo Pore Pro GPP-1001A at Syracuse University

- Software Consideration:

A software “CapWin” is used to analyze the results obtained from capillary flow test and produce a complete pore size distribution.

- Wetting Liquid:

ASTM D 6767-16 suggests mineral oil as a standard wetting liquid. However, it does not restrict use of other wetting liquids in the testing. Based on the properties of wetting liquid such as surface tension and contact angle, the software automatically modifies the bubble point and pore size distribution results.

- Shape Factor:

A shape factor of 1 is used for round and square holes. However, for rectangular and irregular holes 0.75 and 0.715 are used as a shape factor respectively.

- Type of test:

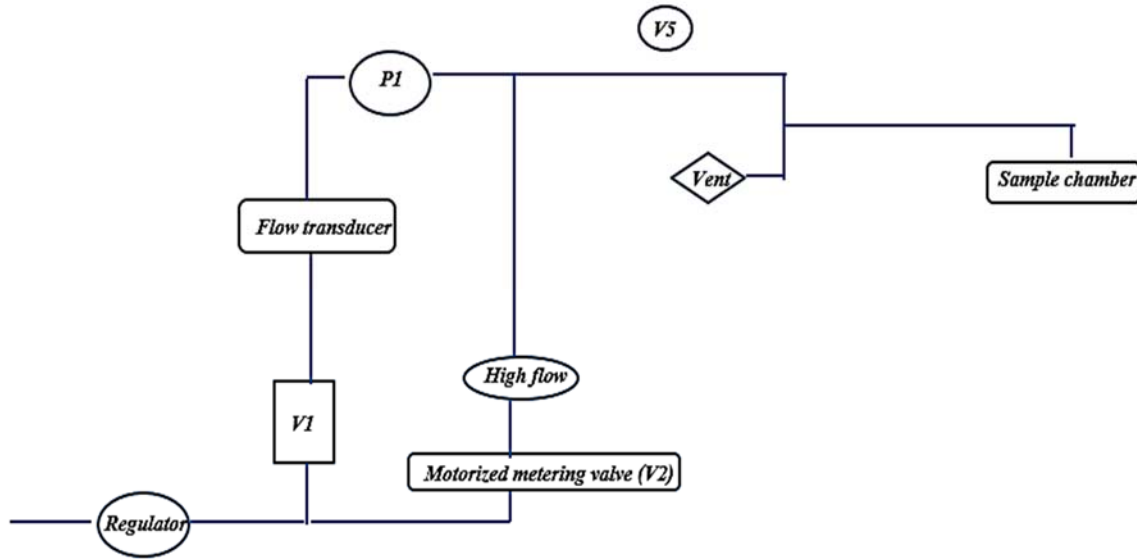
Based on the sequence of the dry and wet phase during testing, the software can function the testing phase. The operator can change the category of the test based on the order of the test phases. Geo Pore Pro can perform four functions as follows: Wet up/ Dry down, Wet up/ Dry up, Dry up/ Wet up, Wet up/ Calc. Dry. For this study, Wet up/ Calc. Dry was used to perform capillary flow test, which stands for the wet curve is run with the pressure increasing; a linear dry plot is extrapolated from the wet phase data. Therefore, the operator does not need to interrupt during the test and the software will compose the dry curve itself. However, the results do not get affected by the type of function. The operator can select for bubble point test only, in that case the specimen will be saturated and tested only to obtain the largest pore opening and no pore size distribution will be generated.

- Max/Min. Pressure:

The selection of pressure lets the operator to determine the starting and terminating pressure. Usually the starting pressure is assigned as 0 psi. The maximum or ending pressure is assigned in a way so that the pressure can force the fluid to come out of the smaller pores and allow the data to be collected to make a complete ‘S’ shaped pore size distribution. The highest maximum pressure recorded during testing stage was 0.5 psi. With 0.5 psi pressure, the test usually takes 40 minutes to complete. However, one can choose higher pressure than 0.5 psi, which will take a long time to complete one test.

- Regulator:

The pressure entering the system is controlled by the regulator (see Figure 2.6), which is defined as counts (0 to 4000), referring to the maximum regulator setting. The amount of pressure incremented with each count depends on the air pressure going into the machine, and regulator range.



V1 = Valve1, P1 = Pressure transducer, V5 = Valve5

Figure 2.6: Schematic of the Capillary Flow Device Geo Pore Pro (GPP 1001A), used in Syracuse University (2017)

- Internal tubing size:

The device used in capillary flow test at Syracuse University has a sample chamber which is connected to a tube of 2.54 cm diameter.

- Accessories:

The accessories of the Geo Pore Pro (GPP-1001A) include adapter plates, support screen, O-ring, wedge plate, sample chamber, chamber cap, etc. (see Figure 2.7).

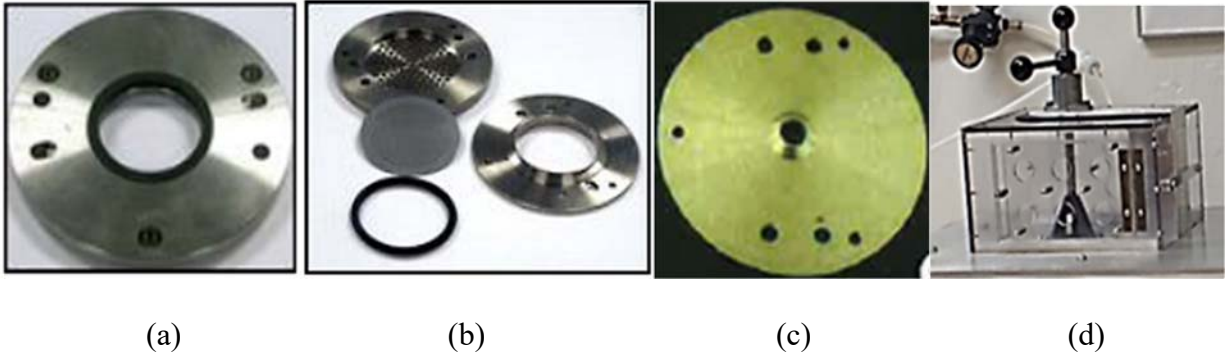


Figure 2.7: Accessories of Geo Pore Pro; (a) Adapter Plate; (b) Adapter Plate Built-in Screen, Support Screen, and O-Ring; (c) Wedge Plate;(d) Sample Chamber and Cap

2.8 Calibration

To assess the accuracy of the capillary flow test results, calibration of the latest version of PMI equipment, Geo Pore Pro (GPP-1001A) was performed. The GeoPore at Syracuse University was calibrated using six different materials. The materials used in calibration included thin metal plate with circular holes (made of 300 series Alloy stainless steel, 0.003-inch thickness), and membranes. Table 2.5 shows the physical properties of the materials used in calibration.

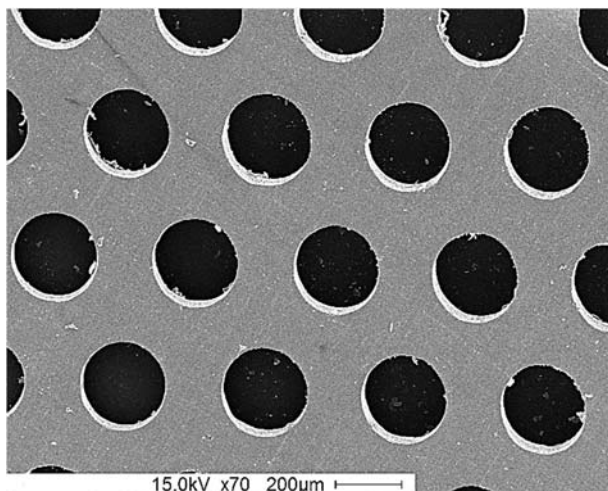
Table 2.5: Physical Properties of Calibration Materials

Calibration material	Type	Type of pore	Manufacturing company	Material type	Thickness, mm	Manufacturing pore opening, mcirons
A1	Thin metal plate	Circular holes	E-FAB Photo Chemical Machining, Engineering, & Fabrication	300 series Alloy stainless steel	0.076	244
A2	Thin metal plate	Circular holes	E-FAB Photo Chemical Machining, Engineering, & Fabrication	300 series Alloy stainless steel	0.076	165
A3	Thin metal plate	Circular holes	E-FAB Photo Chemical Machining, Engineering, & Fabrication	300 series Alloy stainless steel	0.076	150

A4	Thin metal plate	Circular holes	E-FAB Photo Chemical Machining, Engineering, & Fabrication	300 series Alloy stainless steel	0.13	169
C1	Membrane	Non-uniform	Collected from Porous Materials, Inc.	N/A	0.7	120
C2	Membrane	Non-uniform	Collected from Porous Materials, Inc.	N/A	0.22	40

* E-FAB Photo Chemical Machining, Engineering, & Fabrication (1075 Richard Ave. Santa Clara, California 95050, USA)

The metal plate and membraes were examined using Scanning Electron Microscope in the departement of Paper and Bioprocess Engineering at State University of New York College of Environmental Science and Forestry (SEM, JSM-5800LV, manufactured by JEOL, Solutions for Innovation). The SEM images of the calibration materials are provided below.



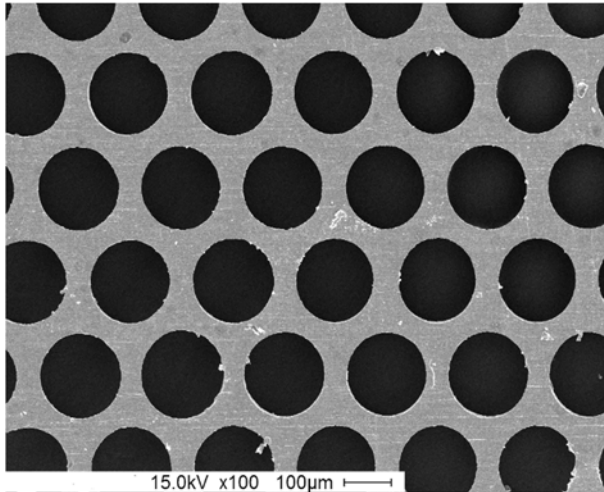
Specimen: Thin metal plate, A-1

Manufacturing company: E-FAB Photo
Chemical Machining, Engineering, &
Fabrication

Manufacturing pore size: 244 mcirons

Shape of pores: ○

Thickness: 0.076 mm



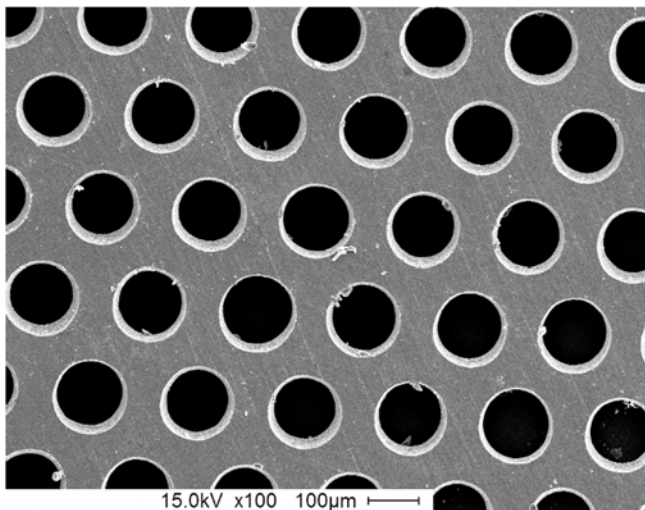
Specimen: Thin metal plate, A-2

Manufacturing company: E-FAB Photo
Chemical Machining, Engineering, &
Fabrication

Manufacturing pore size: 165 mcirons

Shape of pores: ○


Thickness: 0.076 mm



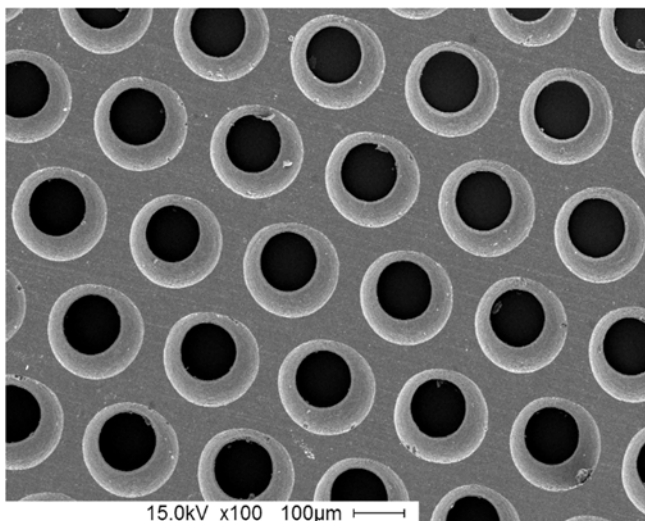
Specimen: Thin metal plate, A-3

Manufacturing company: E-FAB Photo
Chemical Machining, Engineering, &
Fabrication

Manufacturing pore size: 150 mcirons

Shape of pores: 


Thickness: 0.076 mm



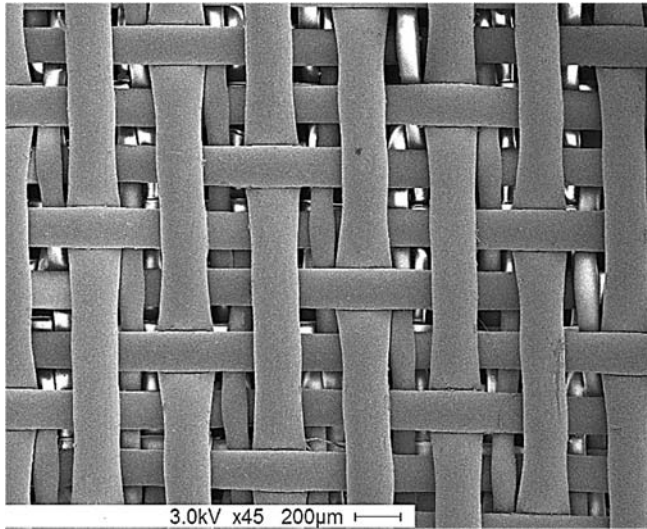
Specimen: Thin metal plate, A-4

Manufacturing company: E-FAB Photo
Chemical Machining, Engineering, &
Fabrication

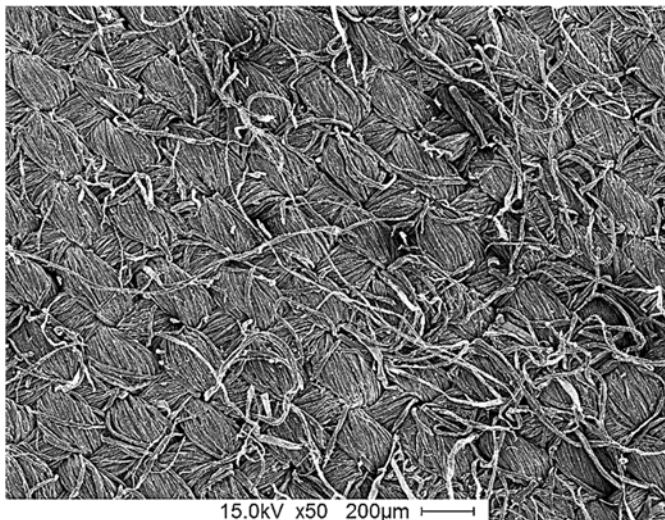
Manufacturing pore size: 169 mcirons

Shape of pores: 

Thickness: 0.13 mm



Specimen: Membrane, C-1
 Manufacturing company: Collected from
 Porous Materials, Inc.
 Manufacturing pore size: 120 mcirons
 Shape of pores: irregular
 Thickness: 0.7 mm



Specimen: Membrane, C-2
 Manufacturing company: Collected from
 Porous Materials, Inc.
 Manufacturing pore size: 40 mcirons
 Shape of pores: irregular
 Thickness: 0.22 mm

Figure 2.8: SEM Images of Calibration Materials: Thin Metal Plate (A1, A2, A3, and A4); and
 Membrane (C1, C2)

In

Figure 2.8, A1 and A2 are thin metal plates with circular holes, A3 and A4 are thin metal plates with 3D shaped circular holes; and C1 and C2 have irregular holes. Capillary flow device

measured the constriction size of pores, which means for meshes A3 and A4, it would measure the smallest size of the hole.

2.8.1 Method

For the Capillary Flow test, the following sample preparation and testing procedures were used.

2.8.1.1 Sample Preparation

- Five to eight samples were cut with a measurement of 2-inch x 2-inch to fit in the sample holder. The samples were selected randomly from the swatch/sheet of the sample.
- ASTM D6767-16 suggests submerging the specimens into tap water for an hour and allow to dry in the standard atmosphere for 24 hours. However, the metal plates were not submerged into water, to avoid corrosion.

2.8.1.2 Wetting Liquid

Mineral oil was used to saturate the materials. Mineral oil was purchased from Walmart with a batch number of NDC 49035-035-16 (equate™). Its surface tension was measured by KRUSS USA (1020 Crews Road, Suite K Matthews, NC 28105, USA). They used the Wilhelmy Plate method to measure the surface tension of the mineral oil. Three tests were performed to achieve the accuracy and 30 ml aliquots were used for each testing. Surface tension of each aliquot were monitored for 180 secs using the Wilhelmy plate method. In addition, the surface tension of water was measured as a reference. The surface tension of mineral oil was reported as 31.67 – 31.71 dynes/cm.

2.8.1.3 Contact Angle Test Results

The dynamic contact angle between mineral oil and thin metallic plate was tested measured by KRUSS USA (1020 Crews Road, Suite K Matthews, NC 28105, USA). They used the Wilhelmy

Plate method to measure the dynamic contact angle and five tests were performed to achieve the accuracy. The receding contact angle between mineral oil and thin metallic plate was reported as zero degree.

2.8.1.4 Cleaning Materials

The cleaning of the test specimens plays an important role in the calibration. Four thin metal plates and two membranes were selected to use in the cleaning process prior to calibration. The calibration materials were cleaned with Methanol (from PHARMCO-AAPER, Batch no: 12214-03). The following procedure was used:

- A 2-inch x 2-inch specimen was soaked in Methanol for 1/2 hour in a shaker and removed.
- Then the specimen was dried thoroughly for 24 hours and transferred into the Porometer for testing.
- Cleaning is very important for calibration materials and it can affect the result significantly. The results of cleaned and uncleaned samples are produced later.

2.8.1.5 Testing Procedure

The common procedure used in the calibration test either with or without cleaning process is as follows:

- The specimens were submerged in mineral oil for a period of 1 hour.
- Test was conducted with Wet up/ Calc. dry and a linear dry curve. The tests were performed in the wet state first and then the sample was pressurized to calculate the dry curve by the software.
- The following set up was made for the test with mineral oil as a wetting liquid; a gasket of 0.5-inch diameter at the bottom – specimen – a 0.5-inch adapter plate – clamp (see Figure

2.9). Then the chamber cap was placed above the adapter plate to secure the system provided a tight seal around the sample to ensure that no air escaped during the test.

- During testing 0.5 psi was kept as maximum pressure. For metallic screen with circular holes, a shape factor of 1.0 was used; for membranes with irregular holes a shape factor of 0.715 was used (Jena, 2014).

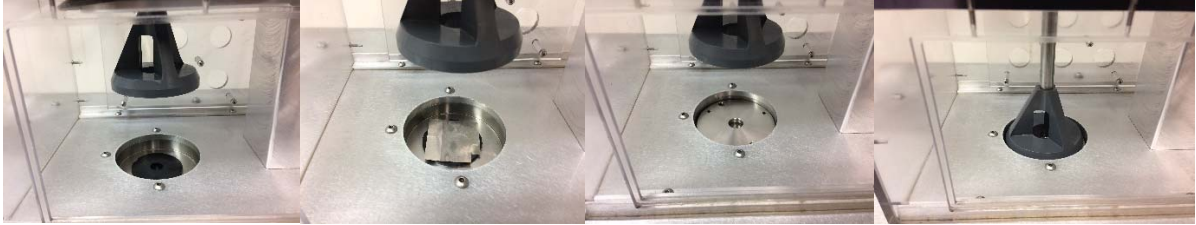


Figure 2.9: Test Setup for Calibrating Materials with Mineral Oil

- The test was started and the pressure was increased at a constant rate. The pressure and flow rate were recorded by the software.
- Each test took approximately 30-35 minutes to complete.
- After the test the pressure was reduced itself, the holder and adapter plate were removed and holder was cleaned for the next test.

2.8.1.6 Factors Affecting the Results

- During testing with mineral oil as a liquid, the hole of the adapter plate should be large enough for mineral oil to get enough pressure to be pushed out from the pores. Otherwise, the results obtained would be 2-3 times larger than the actual size.
- It was noticed that the maximum pressure (0.5 psi) setup for one test fluctuated frequently, even it became zero at some points. Sometimes the pressure dropped down to negative and the test stopped itself without any results. There is a regulator inside the test equipment (Geo Pore Pro - 1001 A) which controls the pressure, which was beyond the

capacity of the operator to manage. When the pores are pressurized to drain out the liquid, there might be a little drop in the regulator which affects the test. To increase the pressure, the regulator of the equipment needed to increase up to 1200 – 1800 counts. It takes 45 – 50 minutes to finish the test rather than 30 - 35 minutes (usual time). However, it does not affect the test results.

- Sometimes it happened that the specimen could not hold the liquid in the pores and the flow was not 100% in the test. Therefore, the smaller pores did not get enough pressure to discharge the liquid and the software could not measure the smaller pores in the specimen
- During the test, it was ensured that the plate and gasket were dry completely. The gasket, metal plates, clamp should be cleaned with alcohol if the fluid needs to be changed.
- It should be kept in mind that Geo Pore is measuring the complete pore size distribution. Therefore, in the case of materials that have 3-D shaped holes, the smallest pore size is measured as the largest pore, O_{100} or bubble point diameter (See A4 in
- Figure 2.8).

2.8.1.7 Cleaning of the Equipment during Test

ASTM D6767 suggests cleaning the geosynthetics with water for an hour before testing. Since, the metallic screens may get corroded, Methanol was used to clean the calibration materials instead. However, with several tests performed in the current study, it was noticed that only cleaning the test specimens is not enough to get accurate calibration results. Along with the test specimens, the test chamber, gasket, and adapter plate needed to be cleaned properly after each test. Otherwise, mineral oil would not get pressurized enough to discharge from the pores. Cleaning plays a very important role on the calibration test results. A broad deviation in the test results was noticed with and without the cleaning process. Without cleaning the test specimens and equipment, the O_{100} measured with mineral oil was two times larger than the actual pore size

measured by SEM. In order to allow the pores to get enough pressure to drain out the liquid from the pores, the testing chamber, gasket, adapter plate and clamp were cleaned with Methanol after each test. Figure 2.10 shows that the pore size distribution of a thin metal plate with circular holes (A1, SEM pore size = 237.28 – 251.72 microns) using mineral oil as a wetting liquid (31.69 dynes/cm surface tension), before and after cleaning the specimen with equipment. The range of O_{100} obtained by before cleaning is approximately 2 times larger than the range of O_{100} obtained by after cleaning technique.

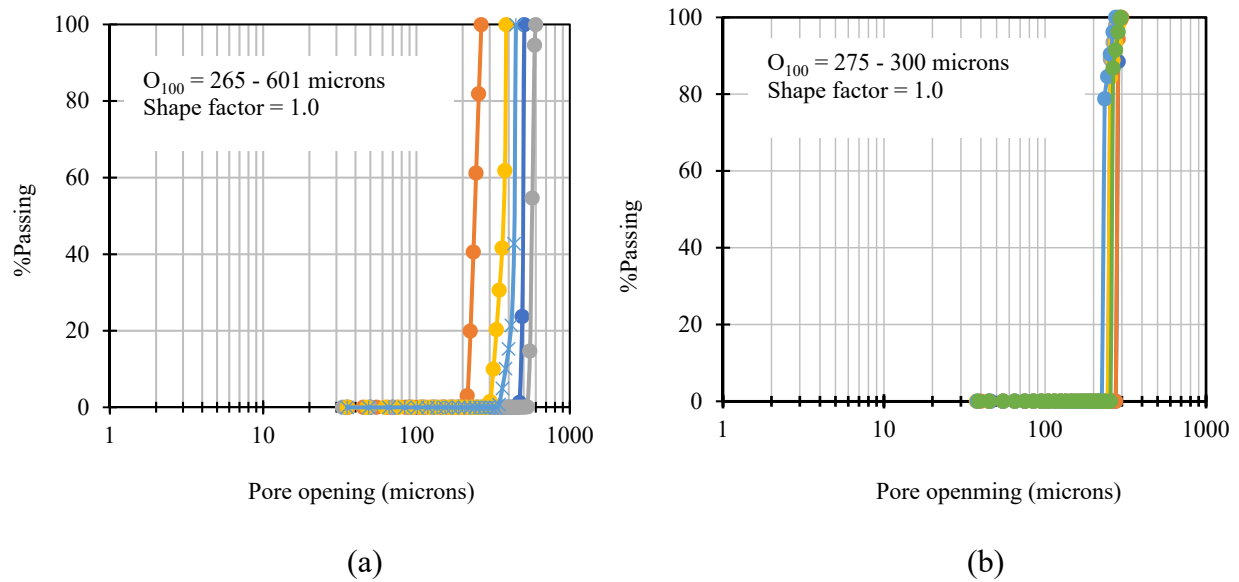


Figure 2.10: Pore Size Distribution of Thin Metal Plate, A1 (a) before Cleaning and (b) after Cleaning the Equipment

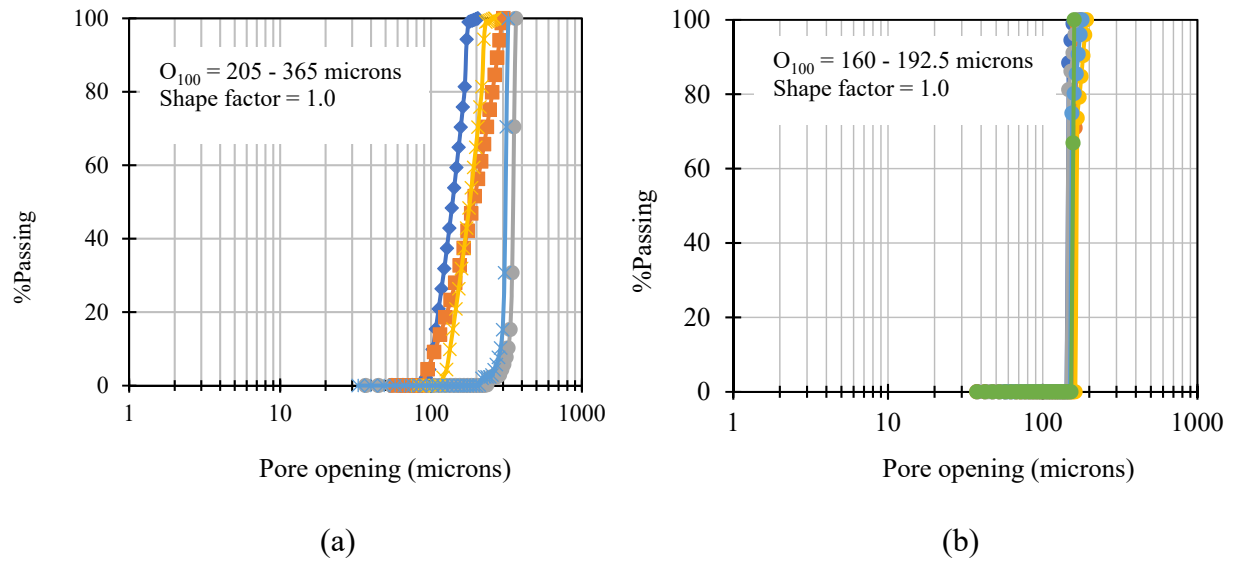


Figure 2.11: Pore Size Distribution of Thin Metal Plate, A3 (a) before Cleaning and (b) after Cleaning the Equipment

Figure 2.11 shows the capillary flow test results of A3 (SEM pore size = 120 – 130.91 microns), a thin metal plate of circular holes using mineral oil as a wetting liquid (31.69 dynes/cm surface tension), before and after cleaning. The difference in the range of pore sizes before and after cleaning process is 45 – 175 microns. The pore size distribution of both thin metal plates after cleaning process provided more reproducible results. The cleaning of testing device made a notable change in the result of bubble point, O_{100} for both thin metal plates. However, the range is still 40 – 50 microns larger than the actual pore size obtained by SEM analyzer.

2.8.1.8 Results

The largest pore size (O_{100}) was measured by the Capillary flow test for 4 metallic screens with circular and cylindrical holes and 2 membranes with irregular holes. Mineral oil (31.69 dynes/cm surface tension) was used for all tests and a shape factor of 1 was used for uniform holes and 0.715 was used for irregular holes. In Table 2.6, manufacturing pore sizes, SEM image measured pore sizes and O_{100} from the Capillary Flow test for six thin metal plates and membranes are

shown. For A1 and A2, the manufacturing pore sizes fall in the range of SEM pore sizes, whereas, for A3 and A4, the manufacturing pore sizes are higher than the range of SEM pore sizes. Metal sheets, A3 and A4 have not cylindrical holes, one side smaller than other (see Figure 2.8). Since, the manufacturing values are larger than the SEM sizes for A3 and A4, which means the manufacturing values were reported as the largest sizes and SEM values were reported as the constriction sizes.

Table 2.6: Capillary Flow Test Results for Thin Metallic Plates and Membranes

Wetting liquid: Mineral oil							
Type	Manufacturing process	Pore opening	Shape factor	Manufacturing Pore size, microns	SEM pore size, microns	Measured O_{100} , microns	Difference in pore opening, microns (SEM $\sim O_{100}$)
A1	Thin metal plate	Circular	1	244	Range = 237.28 – 251.72	Range = 275 – 300	Range = 37.72 – 48.28
					Mean = 244.5	Mean = 289.5	
					Standard deviation = 10.21	Standard deviation = 9.29	
A2	Thin metal plate	Circular	1	165	Range = 160 – 169.09	Range = 181 – 214.5	Range = 21 – 45.41
					Mean = 164.55	Mean = 202.07	
					Standard deviation = 6.43	Standard deviation = 11.83	
A3	Thin metal plate	Cylindrical	1	150	Range = 120 – 130.91	Range = 160 – 192.5	Range = 40 – 61.59
					Mean = 125.45	Mean = 174.83	
					Standard deviation = 7.71	Standard deviation = 11.14	
A4	Thin metal plate	Cylindrical	1	169	Range = 106– 112	Range = 161 – 182.5	Range = 55 – 70.5

					Mean = 109	Mean = 169.43	
					Standard deviation = 4.24	Standard deviation = 7.41	
C1	Membrane	Irregular	0.715	120	N/A	Range = 135 - 189.5	N/A
						Mean = 170.42	
						Standard deviation = 19.50	
C2	Membrane	Irregular	0.715	40	N/A	Range = 46.5 - 53	N/A
						Mean = 49.35	
						Standard deviation = 2.66	

The pore sizes obtained by SEM images and Capillary flow test were reported in range rather than a single number. The membranes have complex pore sizes, which made it difficult to have any measurements from SEM images. The computed mean and standard deviation of the pore sizes obtained by SEM image and Capillary flow test are given in Table 2.6. The difference between SEM measurements and test results was provided in Table 2.6 for 4 metallic screens. It was found that the test results were 15.89% - 62.94% larger than the pore sizes measured by SEM images. It was noticed that the %difference increases with the decreasing actual pore sizes. The test results reported were higher than the manufacturing values as well. Based on the comparison made in Table 2.6, it could be stated that the Capillary flow test measured the largest opening sizes of the metallic screens and membranes rather than the constriction sizes. Figure 2.12 shows the range of O_{100} (obtained from the test) plotted against the SEM pore sizes. The measured pore sizes were showed in the plot as a range rather than a single number, because the measured pore sizes for A1 to A4 by the Capillary flow test were 20 – 70 microns larger than

the SEM measurements and it was found that not all the holes were accurately identical. It was also noticed that the SEM pore sizes were equally smaller than manufacturing values (See Table 2.6).

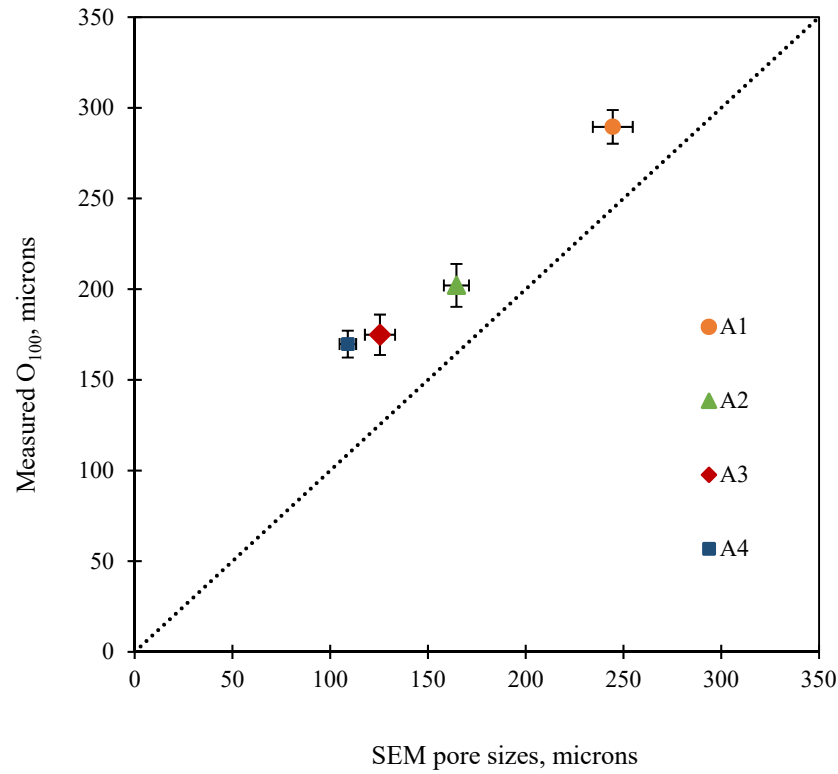


Figure 2.12: Measured O_{100} vs. SEM Measurements for Thin Metallic Plates and Membranes

It is clearly noticed from Figure 2.12 that the ranges of measured O_{100} by the Capillary flow test were larger than the ranges of pore sizes obtained by SEM images. The dotted line plotted Figure 2.12 provided the SEM measurements of 4 metallic screens. Due to the complex and irregular pore sizes, SEM images could not measure the pore sizes of 2 membranes (C1 and C2).

Therefore, to evaluate the difference between O_{100} (obtained by Capillary flow test) and manufacturing values, O_{100} were plotted as a function of manufacturing pore sizes in Figure 2.13.

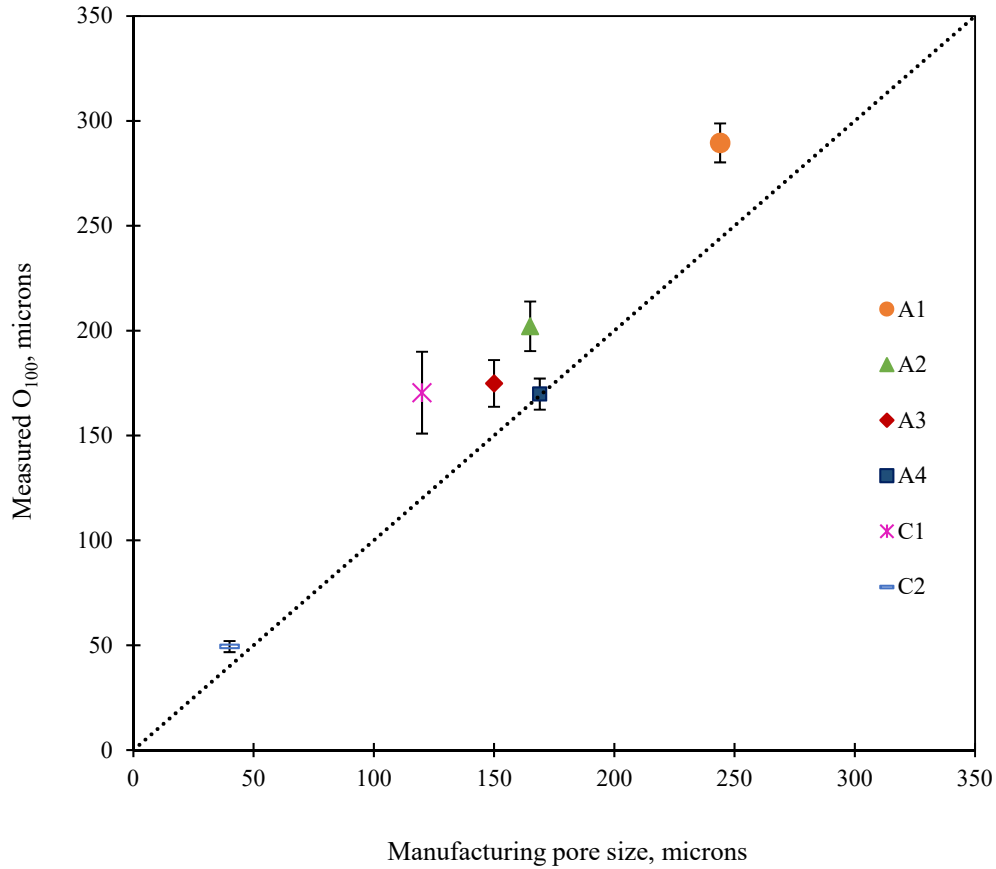


Figure 2.13: Measured O_{100} vs. Manufacturing Pore Sizes for Thin Metallic Plates and Membranes

Figure 2.13 showed the values of pore openings obtained by the test as a range, however, the manufacturing values were reported as a single number. It was noticed that the range of measured pore size is larger than the manufacturing values as well.

Based on the results obtained from the capillary flow test, larger pore values were compared to SEM measurements and manufacturing values and the percent increase in pore size is inversely proportional to the actual size of a specimen.

To validate the accuracy of the calibration test, two thin metal plates with circular holes (A1 and A3) and known pore sizes were sent to an industry, SAGEOS (CTT Group) to perform capillary flow test. The device used in the test was Geo Pore Pro (GPP 1001A) manufactured by PMI.

Mineral oil (32.51 dynes/cm surface tension) was used in the test as a wetting liquid. The results obtained by SAGEOS were reported as 335.38 microns for A1 and 189.09 microns for A3.

2.9 Summary

Four thin metallic plates and two membranes were used in the calibration of the Geo Pore Pro (GPP-1001A), following the ASTM D 6767. Mineral oil (31.69 dynes/cm surface tension) was used as a wetting liquid for the calibration tests. The surface tension of the wetting liquid and dynamic contact angle between wetting liquid and thin metallic plate were measured tested as well. It was found that cleaning of the specimens and equipment made a significant difference in the test results, which was not mentioned in the ASTM D6767. The results (O_{100}) obtained by the Capillary flow test were larger than pore sizes obtained by SEM measurements and manufacturers. The calibration results obtained in the current study were compared with the results obtained by Przybylo (2007) and a similar trend of larger test results was found. However, ASTM D 6767 was not followed in the test performed by Przybylo (2007).

2.10 References

- ASTM D6767-16 Standard Test Method for Pore Size Characteristics of Geotextiles by Capillary Flow Test, ASTM International, West Conshohocken, PA, 2014.
- ASTM F316, “Standard Test Method for Pore Size Characteristics of Membrane Filters by Bubble Point and Mean Flow Pore Test”, American Society for Testing and Materials, West Conshohocken, Pennsylvania, USA.
- Akshaya Jena, 'Wetting Liquid Extrusion Techniques: Part I-Capillary Flow Porometry', PMI Short Course May 2009, 2.0-2.30.
- Akshaya Jena and Krishna Gupta, 'Characterization of Pore Structure of Filtration Media', Fluid/Particle Separation Journal, Vol. 14, No. 3, 2002, 227-241.

- Aydilek, A. H., D'Hondt, D., & Holtz, R. D. (2006). Comparative evaluation of geotextile pore sizes using bubble point test and image analysis. (2006): 1-9.
- Bhatia, S. K., & Smith, J. L. (1996). Geotextile characterization and pore-size distribution: Part II. A review of test methods and results. *Geosynthetics International*, 3(2), 155-180.
- Bhatia, S. K., & Smith, J. L. (1994). Comparative study of bubble point method and mercury intrusion porosimetry techniques for characterizing the pore-size distribution of geotextiles. *Geotextiles and Geomembranes*, 13(10), 679-702.
- Cap.Fl.5-12- 09 Capillary Flow Porometer 7.0, Porous Materials Inc.
- Christopher, B.R. and Holtz, R.D., 1985, “Geotextile Engineering Manual”, U.S. Department of Transportation, Federal Highway Administration, Washington, DC, USA, Report No. FHWA-TS-86/203, March 1985, 1044.
- Elton, D. J., Hayes, D. W., & Adanur, S. (2006). Bubble point testing of geotextiles: apparatus and operation. (2006): 1-8.
- Elton, D. J., & Hayes, D. W. (2007). The Bubble point Method for Characterizing Geotextile Pore Size. In *Geosynthetics in Reinforcement and Hydraulic Applications* (1-10). ASCE.
- Fannin, J. (2006). The use of geosynthetics as filters in civil engineering. *Geosynthetics in Civil Engineering*, Sarsby, R. W., Editor, Woodhead Publishing, Cambridge, UK, 127–147.
- Fischer, G. R., 1994, “The Influence of Fabric Pore Structure on the Behavior of Geotextile Filters,” Ph.D. Dissertation, University of Washington, Seattle, WA, 501.
- Fischer, G.R., Holtz, R.D. and Christopher, B.R., 1996, “Characteristics of Geotextile Pore Structure”, *Recent Developments in Geotextile Filters and Prefabricated Drainage*

Geocomposites, Bhatia, S.K. and Suits, L.D., Editors, ASTM Special Technical Publication 1281, proceedings of a symposium held in Denver, Colorado, USA, June 1995, in press.

- Giroud, J.P., 1982, “Filter Criteria for Geotextiles”, Proceedings of the Second International Conference on Geotextiles, IFAI, Vol. 1, Las Vegas, Nevada, USA, August 1982, 103-108.
- Giroud, J.P. (1996). “Granular Filters and Geotextile Filters.” Proceedings of Geofilters ‘96, Montreal, Canada, 565-680.
- Gupta, K. (2014). Wetting Liquid Extrusion Techniques: Part I- Capillary Flow Porometry.
- Jena, A. K., & Gupta, K. M. (1999). In-plane compression porometry of battery separators. *Journal of Power Sources*, 80(1), 46-52.
- Jena, A., & Gupta, K. (2003). Liquid extrusion techniques for pore structure evaluation of nonwovens. *International Nonwovens Journal*, 12(3), 45-53.
- Kiffle, Z. B., Bhatia, S. K., Khachan, M. M. & Jackson, E. K. (2014). Effect of pore size distribution on sediment retention and passing.
- Koerner, R.M., *Designing with Geosynthetics*, 2nd edition, Prentice Hall, Englewood Cliffs, N.J., 1990.
- Koerner, R. M., & Koerner, G. R. (2014). On the Need for a Better Test Method Than Dry or Wet Sieving to Obtain the Characteristic Opening Size for Geotextile Filter Design Purposes. *Geosynthetic Institute’s White Paper*, 31.
- Lydon, R., Mayer, E., & Rideal, G. R. (2004, April). Comparative methods for the pore size distribution of woven and metal filter media. In *Ninth world filtration congress*, New Orleans, LA, USA (1-6).

- Przybylo, Lukasz (2007). An investigation of the Bubble Point method and Capillary flow porometry for geotextiles characterization. MS Thesis. Syracuse University, Syracuse, NY, USA.
- Rankilior, P.R., 1981, “Membranes in Ground Engineering”, John Wiley, Chichester, United Kingdom, 377.
- Smith, J. L., & Bhatia, S. K. (1995). Application of the bubble point method to the characterization of the pore-size distribution of geotextiles. (1995): 94-105.
- Vermeersch, O. G., & Mlynarek, J. (1996). Determination of the pore size distribution of nonwoven geotextiles by a modified capillary flow porometry technique. In Recent developments in geotextile filters and prefabricated drainage geocomposites. ASTM International.
- Washburn, E.W. (1921). Proceedings of the National Academy of Science, Vol. 7, No. 115.

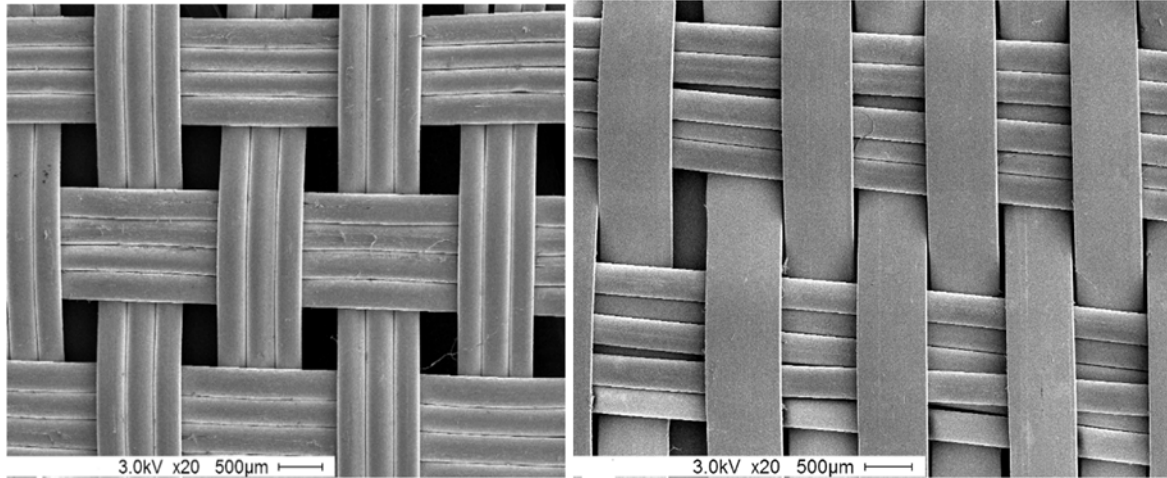
Chapter 3 Capillary Flow Test Results

3.1 Introduction:

A research study was undertaken at Syracuse University with 51 different types of geotextiles to measure the largest pore size O_{98} , bubble point and pore size distribution of geotextiles using the Capillary flow test (ASTM D 6767). This study included 7 monofilament woven, 10 slit-film woven, 1 fibrillated fiber woven, 2 multifilament, 8 heat-bonded non-woven, 21 needle-punched non-woven and 2 geo-composites (a combination of woven and non-woven geotextiles). The geotextiles were selected based on the difference in manufacturing process from 4 US, 1 Canadian and 1 UK geotextile manufacturers. These manufacturers produce diverse kinds of geotextiles to fulfill the multi-purpose requirements of industries and research institutions. Based on the capillary flow technique stated in the ASTM D 6767 – 16, pore size distribution of each geotextile was measured. From the pore size distribution, O_{98} (bubble point according to ASTM) is calculated. O_{50} and O_{15} are also calculated. Dry sieving tests (ASTM D 4751) were also performed for selected geotextiles. Physical properties including mass per unit area and thickness were measured. Relationships between O_{98} and mass per unit area, permeability and O_{98} , O_{50} , O_{10} were investigated.

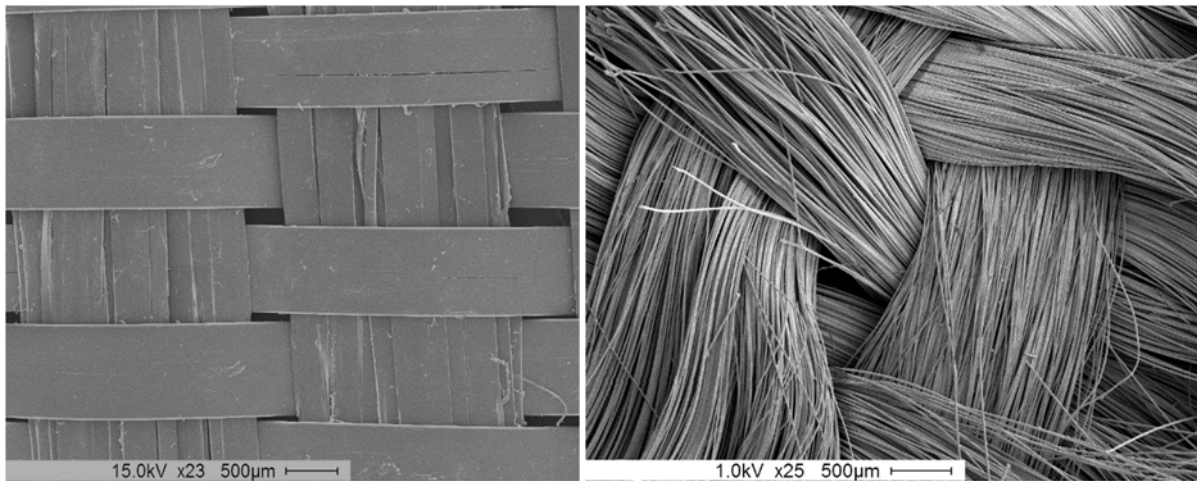
Woven geotextiles of high tensile strength and low elongation are produced on a loom from monofilament, multifilament or slit-film fibers, to provide dimensional stability, and these geotextiles are used for soil reinforcement, separation, and filtration. For woven geotextiles, Warp threads (longitudinal thread in a roll held in tension on a frame), run along the length of the loom are interrupted by weft threads (transverse thread). Four approaches are used in the weaving process including shedding, picking, battening and taking up and letting off (Joseph 1981). Based on the fiber types, woven geotextiles are classified as monofilament, multifilament,

slit – film, and fibrillated fibers geotextiles. In this study, 7 monofilaments made of single strand nylon with semi shiny appearance with a range of mass/area of 191 – 330 g/m² and a thickness of 0.39 – 0.89 mm were selected from two US companies (see Figure 3.1a). The monofilaments used in the study were made of polypropylene and tended to be less resilient in nature. Few woven geotextiles were made of as a combination of slit film yarns in the cross direction and monofilaments in the machine direction (see Figure 3.1 b).



(a) A-4

(b) A-5



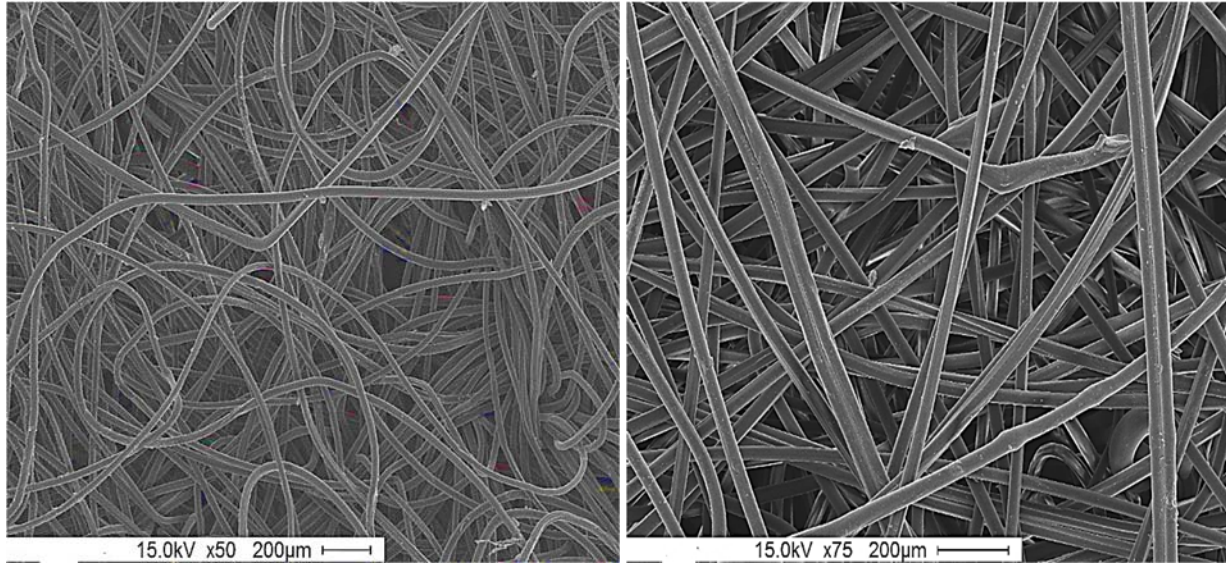
(c) B-11

(d) C-1

Figure 3.1: SEM Images of Woven Geotextiles (a) Monofilament, (b) Monofilament (Slit Film in Cross Direction), (c) Slit Film, (d) Multifilament

10 high strength slit-films ($229 - 571 \text{ g/m}^2$ and $0.59 - 1.89 \text{ mm}$) made of polypropylene and polyethylene were also used in the study. Individual flat yarns slit from extruded polypropylene film were used to weave the slit-film geotextiles (see Figure 3.1 c). 2 multifilament geotextiles with a mass/area of $805 - 1100 \text{ g/m}^2$ and a thickness of $1.04 - 1.78 \text{ mm}$ were used. Multifilament fibers (see Figure 3.1 d) are manufactured from the yarns consisting of many continuous filaments or strands. The number of monofilament fibers used and their combination to form a yarn, both together determine the diameter of fibers. Many continuous monofilaments are used to manufacture the multifilament making a multifilament geotextile more resilient than a monofilament geotextile.

Non-woven geotextile manufactured by either bonding or interlocking of fibers, or both together by mechanical or thermal, as a combination of the techniques mentioned, are generally used for filtration, separation, stabilization and reinforcement. Needle punched geotextiles are manufactured mechanically where thousands of irregular needles of about 76 mm length are operated into the web at a rate up to 2200 strokes per minute, or according to the needle density or lone speed the rate of operating needles could be 500 penetrations per minute (Bhatia and Smith, 1996). In this study, 21 needle punched geotextiles (see Figure 3.2) made of polypropylene with a range of mass/area of $132 - 1075 \text{ g/m}^2$ and thickness of $0.64 - 6.2 \text{ mm}$, were used to perform the capillary flow tests. The needle punched geotextiles were selected from 2 US and 1 Canadian manufacturers.



(a) E-19

(b) E-16

Figure 3.2: SEM Images of Needle Punched Non-Woven Geotextiles

Eight heat-bonded geotextiles ($90 - 290 \text{ g/m}^2$ and $0.39 - 0.73 \text{ mm}$) from a European manufacturer were also used. Heat bonded geotextiles are produced by melt bonding thermal bonding where the web is passed through extreme heat or pressurized enough with steam or hot air to result in fusion at cross over points. The grey colored continuous filaments with a diameter of $40 - 60 \text{ microns}$ were melted in 165°C to produce the heat bonded geotextiles (see Figure 3.3).

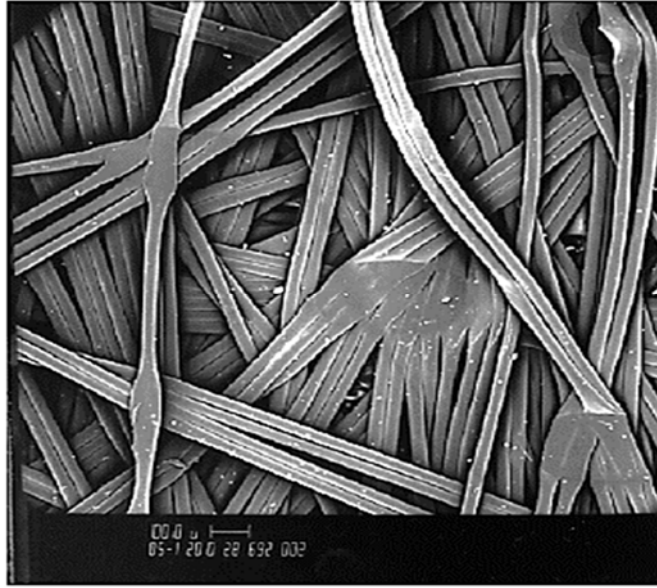


Figure 3.3: SEM Image of Heat Bonded Non-Woven Geotextile (Smith, 1996)

Geo-composites are basically combinations of two or more different types of woven and non-woven geotextiles (see Figure 3.4). As most of the individual components are thermoplastic they can be thermally laminated, but adhesive bonding and needle punching are also used. 2 geo-composites ($534 - 879 \text{ g/m}^2$ and $2.04 - 3.37 \text{ mm}$) were used in the study collected from 2 US manufacturers.

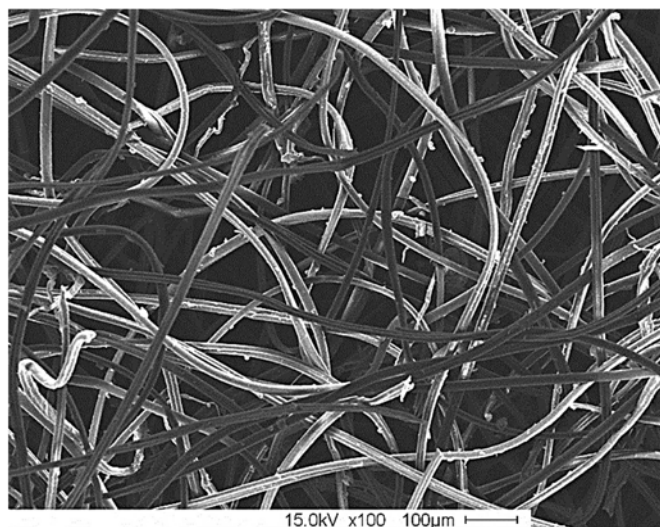


Figure 3.4: SEM Image of a Geo-Composite

The physical properties of these geotextiles, selected from different manufacturing companies, are provided in Table 3.1. The mass per unit area for each geotextile was measured following ASTM D 5261 and the thickness was measured using a slide calipers. Table 3.1 shows that majority of the geotextiles are made of polypropylene (PP) and only 3 out of 51 geotextiles are made of polyethylene (PET). All geotextiles are divided into 6 categories: Type A is monofilament woven geotextiles, Type B is slit film woven geotextiles, Type C is multifilament woven geotextiles, Type D is heat – bonded non-woven geotextiles, type E is needle – punched non-woven geotextiles, and type F is geo – composite (a combination of woven and non-woven geotextile). The mass per unit area and thickness given by the manufacturers are also provided in the Table 3.1. A difference (0.44% – 44%) could be noticed in the measured mass per unit area and thickness with manufacturing's values. Even after using the same standard ASTM D5261, few geotextiles showed a large variation in the mass per unit area. For an example: B-11 has a manufacturing mass per unit area of 585 g/m² and a range of measured mass per unit area of 388 – 408 g/m².

Table 3.1: Physical and Hydraulic Properties of Geotextiles

Geotextiles	Polymer type	Weave type	Manufacturing process	Mass/Area* (g/m ²)	Measured mass/Area (g/m ²)	Standard Deviation, σ	Thickness* (mm)	Measured thickness (mm)	Standard Deviation, σ	Permittivity (sec ⁻¹)	Manufacturing Company
A-1	PP	Monofilament	Woven	N/A	191 - 210	N/A	N/A	0.50 - 0.79	N/A	N/A	M
A-2	PP	Monofilament	Woven	212.51	208 - 214	1.07	0.70	0.59 - 0.63	0.06	2.1	N
A-3	PP	Monofilament	Woven	218.31	264 - 287	40.44	0.39	0.39 - 0.40	0.01	0.28	N
A-4	PP	Monofilament	Woven	292.40	273 - 285	9.48	0.73	0.74 - 0.82	0.04	1.5	N
A-5	PP	Monofilament	Woven	295.36	282 - 304	1.67	0.89	0.82 - 0.89	0.02	0.9	N
A-6	PP	Monofilament	Woven	307.88	288 - 313	5.22	0.76	0.72 - 0.77	0.01	0.2	N
A-7	PP	Monofilament	Woven	294.54	289 - 330	10.58	0.51	0.48 - 0.49	0.01	0.96	N
B-1	PET	Slit film	Woven	N/A	210 - 216	N/A	N/A	0.58 - 0.67	N/A	0.2	M
B-2	PP	Slit film	Woven	237.13	229 - 234	3.98	0.66	0.59 - 0.68	0.02	0.6	N
B-3	PP	Slit film	Woven	293.80	287 - 298	0.92	0.89	0.83 - 0.88	0.02	0.9	N
B-4	PP	Slit film	Woven	296.17	295 - 308	3.77	0.90	0.80 - 0.89	0.04	0.9	N
B-5	PP	Slit film	Woven	358.23	355 - 382	7.27	0.41	1.1 - 1.15	0.51	0.9	N
B-6	PP	Slit film	Woven	585.00	388 - 408	132.23	1.04	1.04 - 1.24	0.07	0.37	N
B-7	PP	Slit film	Woven	419.77	381 - 419	13.98	1.58	1.30 - 1.40	0.16	1.0	N
B-8	PP	Slit film	Woven	405.02	403 - 439	11.30	1.34	1.04 - 1.25	0.14	0.4	N
B-9	PP	Slit film	Woven	373.27	530 - 547	116.84	1.40	1.34 - 1.48	0.01	0.26	O
B-10	PET	Slit film	Woven	565.00	537 - 560	11.67	1.03	1.72 - 1.85	0.53	N/A	N
B-11	PP	Slit film	Woven	558.84	541 - 571	2.01	1.83	1.20 - 1.44	0.36	0.26	N

Geotextiles	Polymer type	Weave type	Manufacturing process	Mass/Area* (g/m ²)	Measured mass/Area (g/m ²)	Standard Deviation, σ	Thickness* (mm)	Measured thickness (mm)	Standard Deviation, σ	Permittivity (sec ⁻¹)	Manufacturing Company
C-1	PET	Multifilament	Woven	813.00	805 - 912	32.17	1.08	1.04 - 1.25	0.05	0.37	N
C-2	PP	Multifilament	Woven	1117.00	1078 - 1100	19.80	1.76	1.62 – 1.78	0.04	0.35	N
D-1	PP	Heat bonded	Non-woven	90	90 - 100	3.54	0.39	0.3 – 0.38	0.04	1	P
D-2	PP	Heat bonded	Non-woven	N/A	88 - 108	N/A	N/A	0.27 - 0.34	N/A	N/A	P
D-3	PP	Heat bonded	Non-woven	110	104 – 118	0.71	0.43	0.33 – 0.4	0.05	0.89	P
D-4	PP	Heat bonded	Non-woven	125	120 – 139	3.18	0.45	0.38 – 0.45	0.02	0.486	P
D-5	PP	Heat bonded	Non-woven	136	140 – 148	5.66	0.47	0.33 – 0.43	0.06	0.51	P
D-6	PP	Heat bonded	Non-woven	150	144 – 182	9.19	0.48	0.4 – 0.5	0.02	0.45	P
D-7	PP	Heat bonded	Non-woven	190	194 – 210	8.49	0.57	0.48 – 0.54	0.04	0.29	P
D-8	PP	Heat bonded	Non-woven	290	279 - 340	13.79	0.73	0.54 – 0.64	0.10	0.17	P
E-1	PP	Needle - punched	Non-woven	N/A	132 - 162	N/A	N/A	0.7 - 0.83	N/A	N/A	Q
E-2	PP	Needle - punched	Non-woven	N/A	146 - 163	N/A	N/A	0.64 - 0.89	N/A	1.7	N
E-3	PP	Needle - punched	Non-woven	185	226 – 235	1.3	1.3	0.99 – 1.2	0.14	0.61	Q
E-4	PP	Needle - punched	Non-woven	203	158 – 169	1.7	1.7	0.83 – 0.88	0.60	1.6	Q
E-5	PP	Needle - punched	Non-woven	N/A	223 – 256	N/A	N/A	1.02 - 1.32	N/A	1.5	N
E-6	PP	Needle - punched	Non-woven	N/A	251 – 258	N/A	N/A	0.80 - 1.09	N/A	1.4	N
E-7	PP	Needle - punched	Non-woven	271	212 - 228	2.3	2.3	1.00 – 1.19	0.85	1.26	Q
E-8	PP	Needle - punched	Non-woven	285	270 – 287	1.8	1.8	1.29 – 1.44	0.31	0.3	Q
E-9	PP	Needle - punched	Non-woven	N/A	268 - 306	N/A	N/A	1.48 - 2.0	N/A	1.5	N
E-10	PP	Needle - punched	Non-woven	N/A	268 - 325	N/A	N/A	1.14 - 1.34	N/A	1.4	N

Geotextiles	Polymer type	Weave type	Manufacturing process	Mass/Area* (g/m ²)	Measured mass/Area (g/m ²)	Standard Deviation, σ	Thickness* (mm)	Measured thickness (mm)	Standard Deviation, σ	Permittivity (sec ⁻¹)	Manufacturing Company
E-11	PP	Needle - punched	Non-woven	N/A	265 - 330	N/A	N/A	0.83 - 1.02	N/A	1.4	M
E-12	PP	Needle - punched	Non-woven	N/A	289 - 365	N/A	N/A	1.18 - 1.5	N/A	0.8	N
E-13	PP	Needle - punched	Non-woven	N/A	319 - 346	N/A	N/A	1.53 - 1.98	N/A	1.36	N
E-14	PP	Needle - punched	Non-woven	N/A	367 - 407	N/A	N/A	2.2 - 2.88	N/A	1	N
E-15	PP	Needle - punched	Non-woven	N/A	372 - 400	N/A	N/A	1.62 - 1.72	N/A	1	M
E-16	PP	Needle - punched	Non-woven	N/A	384 - 539	N/A	N/A	1.93 - 2.13	N/A	0.7	N
E-17	PP	Needle - punched	Non-woven	N/A	432 - 462	N/A	N/A	1.87 - 2.14	N/A	0.8	N
E-18	PP	Needle - punched	Non-woven	490	531 - 587	2.9	2.9	2.48 - 2.89	0.15	0.15	Q
E-19	PP	Needle - punched	Non-woven	N/A	518 - 563	N/A	N/A	3.47 - 4.12	N/A	0.9	N
E-20	PP	Needle - punched	Non-woven	N/A	545 - 648	N/A	N/A	3.49 - 4.0	N/A	0.7	N
E-21	PP	Needle - punched	Non-woven	930	937 - 1075	53.74	5.8	5.5 - 6.2	0.035	0.27	Q
F-1	PP	Geo -composite	Combination of woven and non-woven	N/A	534 - 601	N/A	N/A	2.84 - 3.37	N/A	0.45	M
F-2	PP	Geo -composite	Combination of woven and non-woven	945.6	857 - 879	54.87	2.23	2.04 - 2.40	0.01	0.39	R

PP = Polypropylene, PET = Polyester, N/A = not available, M = US Manufacturer- 1, N = US Manufacturer- 2, O = US Manufacturer- 3, P = UK Manufacturer, Q = Canadian Manufacturer, R = US Manufacturer- 4.

3.2 Test Procedures

Two methods were used to determine the largest pore size of geotextiles; Capillary flow test and Dry sieving test. The ASTM D 6767 standard was followed and the PMI Automated Geo Pore Pro (Model No. GPP-1001A) was used for Capillary flow test. For Dry sieving test, the “Standard test method for determining the apparent opening size of a geotextile” (ASTM D4751) was used.

For Capillary flow test, in total, approximately 700 tests were performed with different specimen for 51 varied materials to validate the repeatability of the test results. The capillary flow test follows the following sample preparation and testing procedure.

3.2.1 Specimens’ Preparation

- A full width swatch of 1 m long from the end of each roll geotextile was taken.
- Nine to ten samples were cut from each swatch with a measurement of 2-inch x 2-inch to fit in the sample holder. Five samples were cut regularly spaced along a diagonal line on the swatch. The rest of the four – five samples were cut randomly from the swatch of the sample.
- The specimens were weighed at the standard atmosphere. A balance Voyager Pro (accuracy up to 0.001gm) was used to weigh the specimens.
- The specimens were submerged in tap water for 1 hour.
- After that the specimens dried in the standard atmosphere with a fan for 24 hours.
- The specimens were weighed again to 0.001g after air drying until a constant weight equal or less than the initial weight of the specimen was achieved. After 24 hours, all specimens were dry.

3.2.2 Wetting Liquid

Mineral oil was used to saturate the materials. The surface tension of mineral oil used in the test was 31.69 dynes/cm and it was measured in a company called KRUSS USA.

3.2.3 Shape Factor

Shape factor is a number which is related to the measured pore size and actual pore size of the geotextile. According to PMI (Porous Materials, Inc.) operating system, a shape factor of 0.715 was used for irregular pores of a geotextile. However, for rectangular pores, 0.75 was used as a shape factor in the analysis.

3.2.4 Testing Procedure

- The specimens were submerged in the mineral oil for a period of 1 hour.
- For each type of geotextile nine/ten tests were conducted.
- Test was conducted with Wet up/ Calc. dry and a linear dry curve. The tests were performed in the wet state first and then the sample was pressurized to calculate the dry curve by the software.
- The wetted specimen was placed on the 1.5-inch gasket (see Figure 3.5 (b)) and an adapter plate with a 1.375-inch O-ring was placed over the specimen (see Figure 3.5 c). Then the chamber cap was placed above the adapter plate to secure the system provided a tight seal around the sample to ensure that no air escaped during the test (see Figure 3.5 (d)).

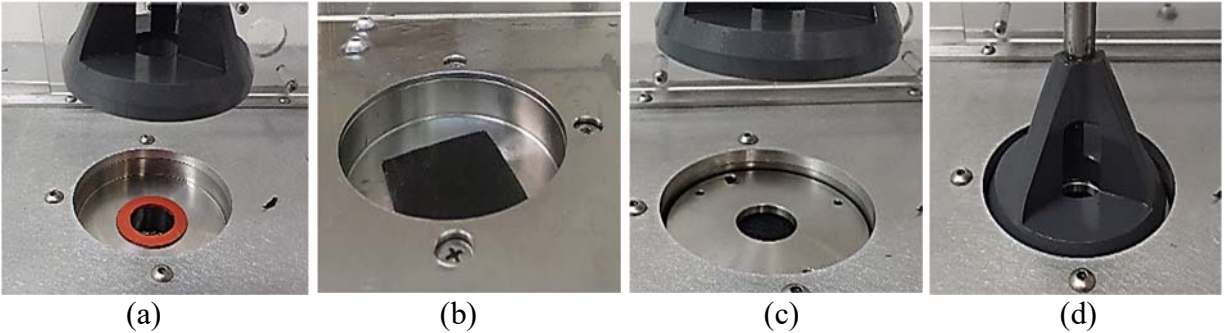


Figure 3.5: Step by Step Procedure of Placing a Geotextile (a) Placing Gasket, (b) Placing Geotextile Over Gasket, (c) Adapter Plate Over the Geotextile, (d) Placing Chamber Cap

- During testing 0.5 psi (3.45 kPa) was kept as maximum pressure. For both woven and non-woven geotextiles, the shape factor was taken 0.715 for irregular pores and 0.75 for rectangular pores.
- During the test, the pressure gradually increased in step, and for each step, pressure increased by 0.001psi. Each test took approximately 30-40 minutes to complete.
- A Typical result for a non-woven geotextile is shown in Figure 3.6. O_{98} , O_{50} and O_{10} were calculated from the pore size distribution plotted in Figure 3.6.
- Then the pressure was reduced itself, the holder and adapter plate were moved to take out the sample and the holder was cleaned for the next test.

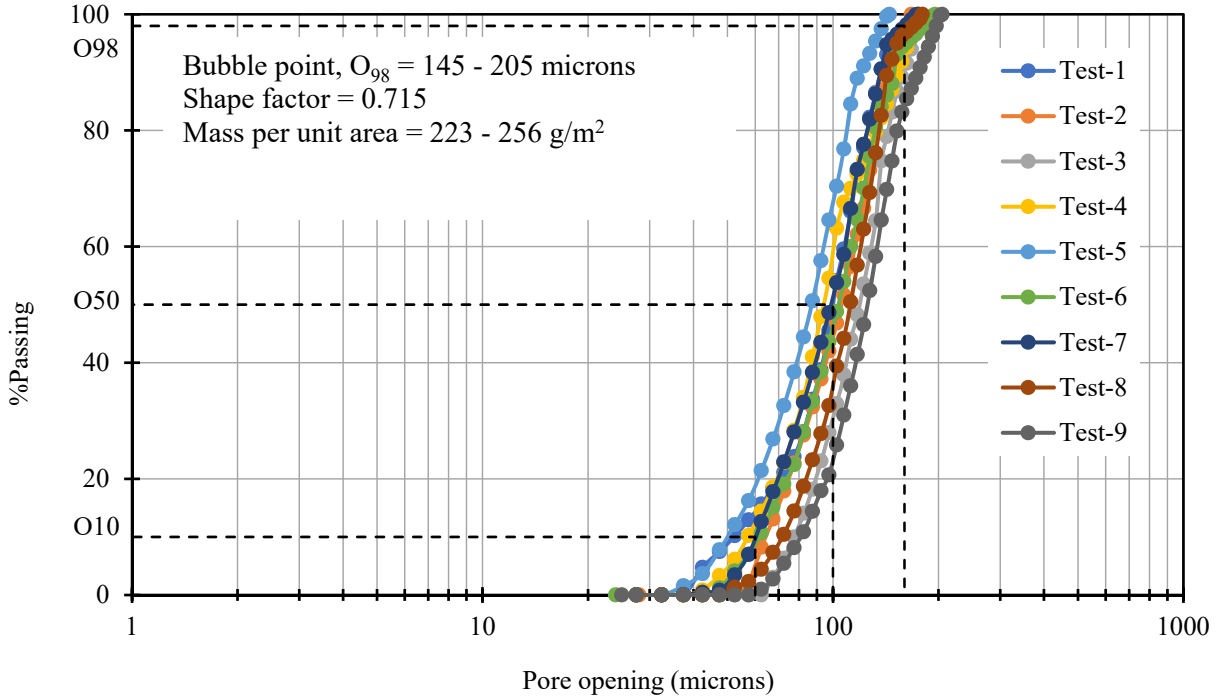


Figure 3.6: Typical Pore Size Distribution Results of a Non-Woven Geotextile

3.2.5 Factors Influencing the Results

- During the testing, periodically the pressure became zero or negative and test stopped without any results. To start the test, the regulator connected inside the device was adjusted to 1200 - 1800 counts in CapWin software, which resulted into the increase in step pressure. In this case, it took 1-1.5 hours to complete one single test. However, it did not affect the bubble point, O_{98} of a geotextile.
- For thick needle-punched non-woven geotextiles, because of lack of fully saturation, the smaller pores in the thick non-woven geotextiles did not get enough pressurized to drain out the liquid, and therefore, the smaller pores may not be measured.
- For thin non-woven and open woven geotextile, mineral oil did not stay in the large pores and the capillary flow test did not reach 100% total flow. As a result, the test might finish earlier without a complete pore size distribution.

3.3 Test Results

Capillary flow tests were performed to evaluate the pore size distribution and the largest pore size, bubble point (O_{98}) of individual geotextile specimen (51 types of geotextiles). Typical pore size distribution results for a monofilament, a slit film, and a multifilament woven geotextiles, a heat – bonded, and a needle – punched non – woven geotextiles, and a geo – composite geotextiles are provided in Figure 3.7 to Figure 3.12.

As it can be seen that good repeatability was found for majority of test results, the contact angle of mineral oil with geotextiles was taken zero in the equation $d = \frac{4\tau\cos\theta}{P}$, to calculate the bubble point, O_{98} . The maximum pressure used in all tests to conclude the test with a complete pore size distribution and persuade the smaller pores to evacuate the liquid was 0.5 psi. From the pore size distribution results, O_{95} , O_{50} and O_{10} were measured; which are the pore openings used in soil retention criterion.

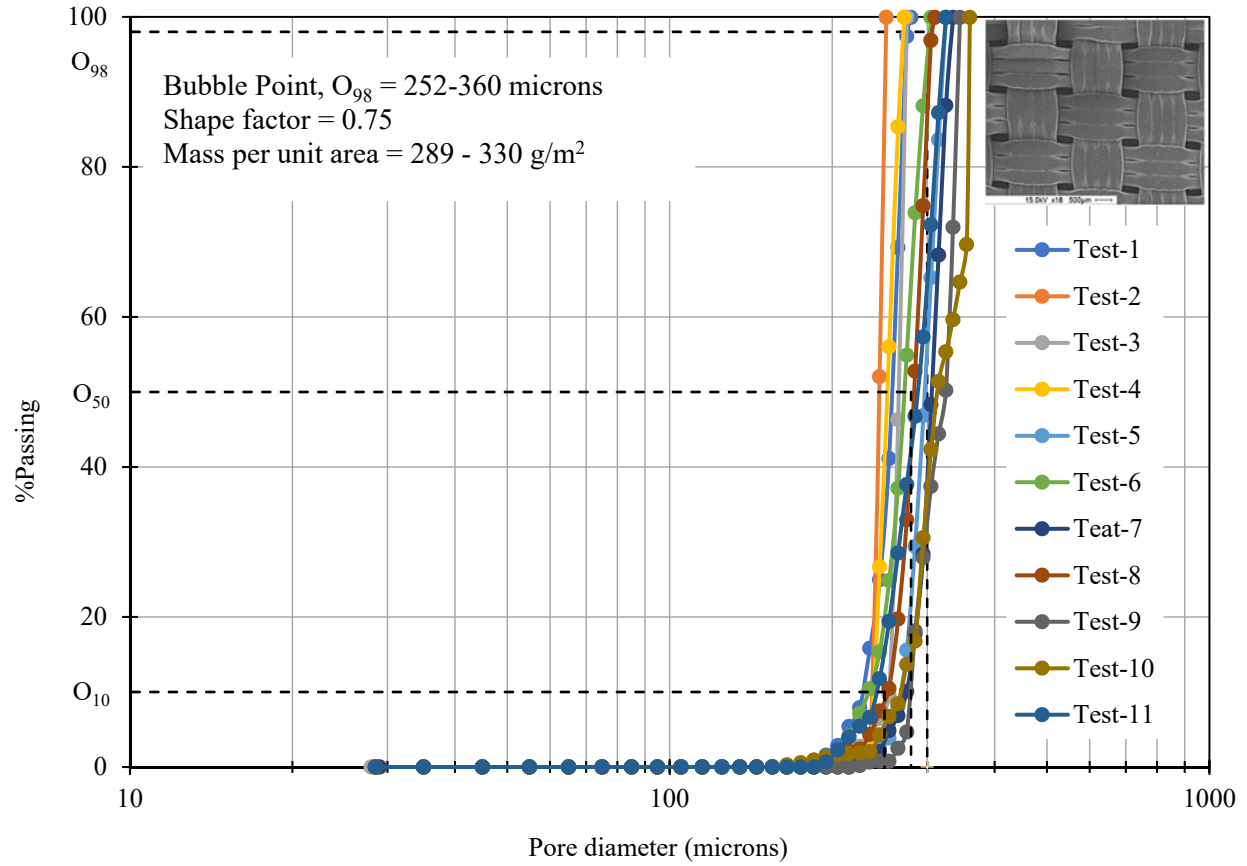


Figure 3.7: Pore Size Distribution of a Monofilament Woven Geotextile (A-7)

Figure 3.7 shows a complete pore size distribution of a monofilament woven geotextile (A-7) with a mass per unit area of 289 – 330 g/m² and a thickness of 0.48 – 0.49 mm thickness, representing 7 monofilament woven geotextiles. 11 different specimens were selected to perform the tests and produce a range of compatible results. The range of the bubble point, O_{98} obtained from the test ranged between 252 – 360 microns. The SEM image of A-7 geotextile revealed that the pores are of rectangular shape. Therefore, a shape factor of 0.75 was selected for the test. From the pore size distribution, the average O_{50} and O_{10} measured were 280 microns and 250 microns respectively. Monofilament geotextile is manufactured in a way that every single fiber passes over another single fiber and making almost uniform pore diameter similar to the pore

diameter of the holes in the spinneret. It could be noticed that the average O_{50} and O_{10} are in same ranges as of O_{98} , which indicates that the pores are almost uniform sizes for the monofilament geotextiles.

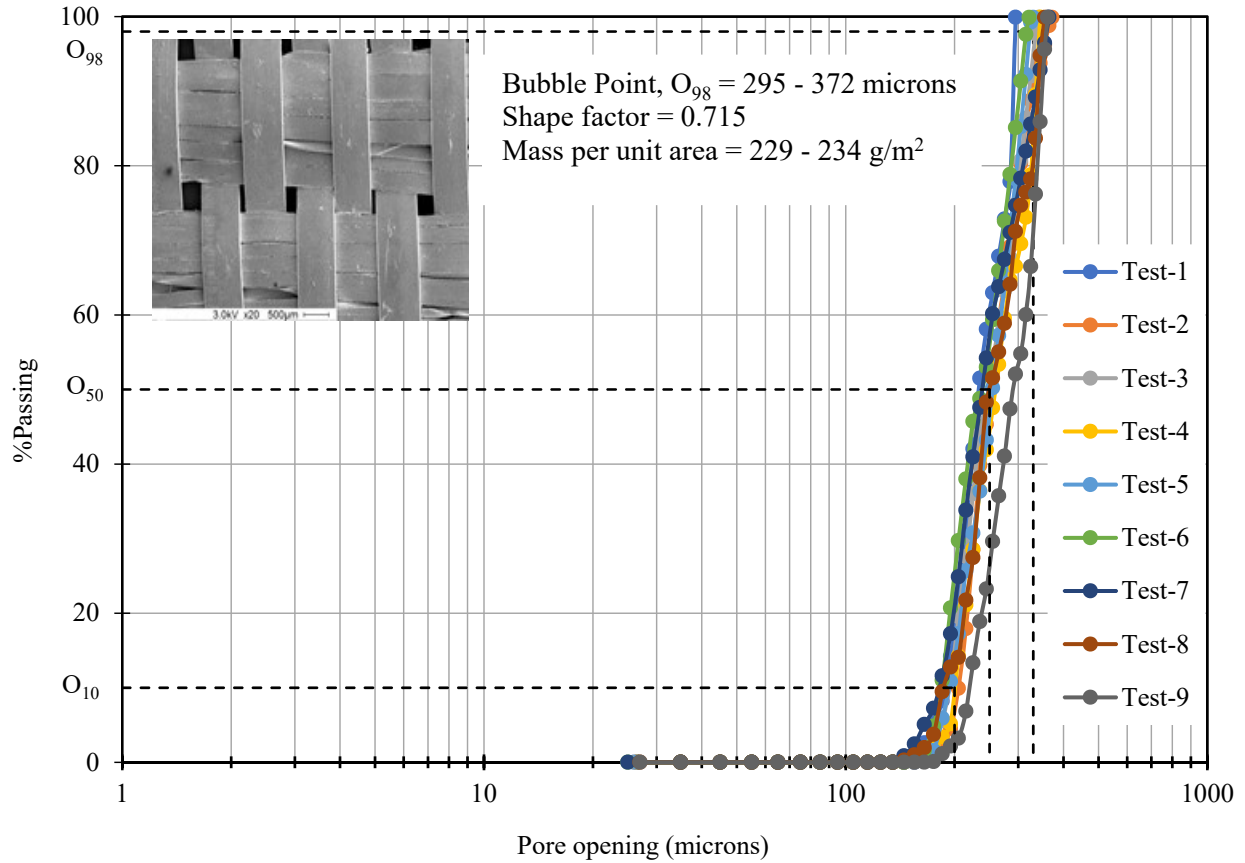


Figure 3.8: Pore Size Distribution of a Slit Film Woven Geotextile (B-2)

For the slit film woven geotextile (B-2), 9 samples were selected to perform the capillary flow tests. As a representative, the results of 1 slit film geotextile, B-2 ($229 - 234 \text{ g/m}^2$ mass/area and $0.59 - 0.68 \text{ mm}$ thickness) are showed in Figure 3.8. The SEM image shows that the pores in the geotextile are a combination of rectangular and square shapes. Unlike monofilaments, the pores in a slit film woven geotextile are not uniform. Therefore, a shape factor of 0.715 was used for the test. The range of bubble point, O_{98} obtained ranged between $295 - 372$ microns. The

average O_{50} and O_{10} measured from the pore size distribution were 250 microns and 200 microns. Therefore, in a slit film geotextile, the pores are not uniform and small pores exist in the geotextile, which resulted in smaller O_{50} and O_{10} values as compared to O_{98} .

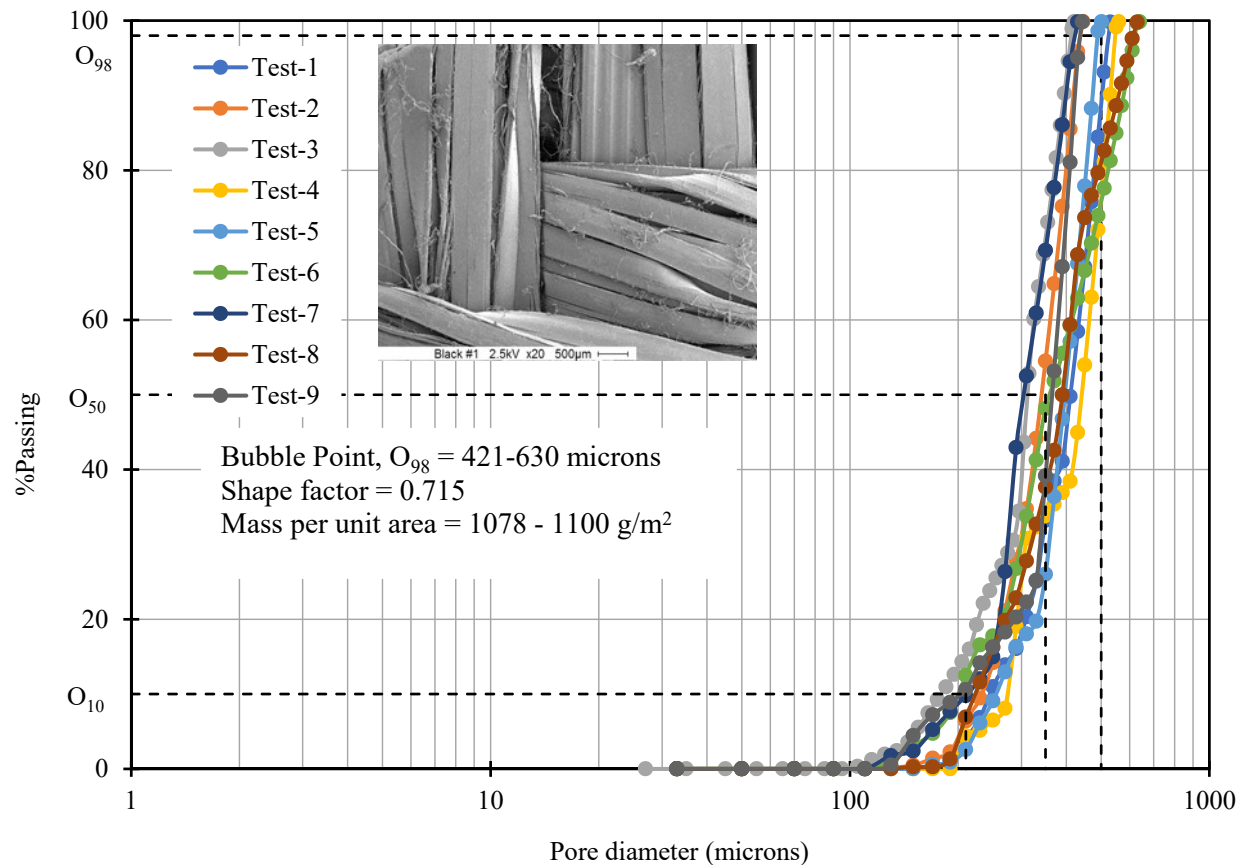


Figure 3.9: Pore Size Distribution of a Multifilament Woven Geotextile (C-2)

Figure 3.9 shows the pore size distribution of a multifilament geotextile (C-2) with a mass per unit area of 1078 - 1100 g/m² and a thickness of 1.62 – 1.78 mm. A shape factor of 0.715 was used in the test, due to the non-uniform pores in the multifilament geotextile. A range of bubble points, O_{98} (421 – 630 microns) were obtained from 9 tests using individual specimens. In a multifilament, many monofilament fibers run over each other or twisted along each other, form irregular pores. The SEM image attached shows the irregular pores of the multifilament

geotextile. A shape factor of 0.715 was used in the test for irregular pores. The smaller pores within the multifilament fiber, the average O_{50} (350 microns) and O_{10} (210 microns) obtained from the pore size distribution were 175 - 315 microns smaller than the average largest pore size (525.5 microns).

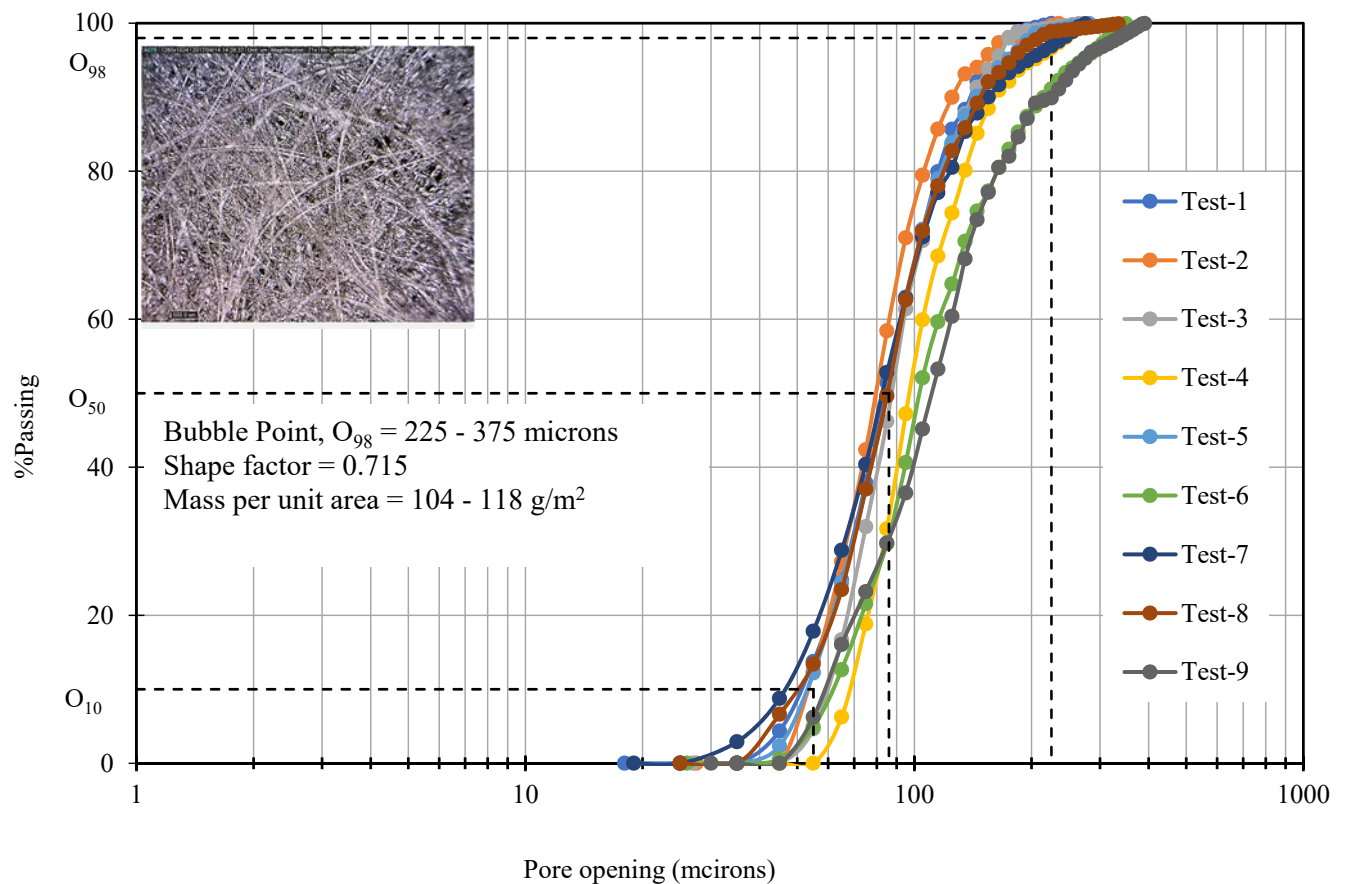


Figure 3.10: Pore Size Distribution of a Heat Bonded Non-Woven Geotextile (D-3)

Figure 3.10 shows the pore size distribution of a heat bonded non-woven geotextile (D-3) with a mass per unit area of 104 - 118 g/m² and a thickness of 0.33 – 0.4 mm. 9 heat bonded geotextiles were used to perform the capillary flow tests. The tests were conducted with 9 individual specimens providing a range of bubble point, O_{98} (225 – 375 microns). Heat bonded geotextile is manufactured by an orientation of continuous filaments or staple fibers bonded with heat or

pressurized steam either by an area or point process. The fibers run along over one another spontaneously making nonuniform pores with a range of bubble point of 225 – 375 microns. Since the fiber orientation is not uniform, a significant difference exists between O_{50} and O_{10} with O_{98} . The average O_{50} and O_{10} measured were 210 – 240 microns smaller than the bubble point, O_{98} .

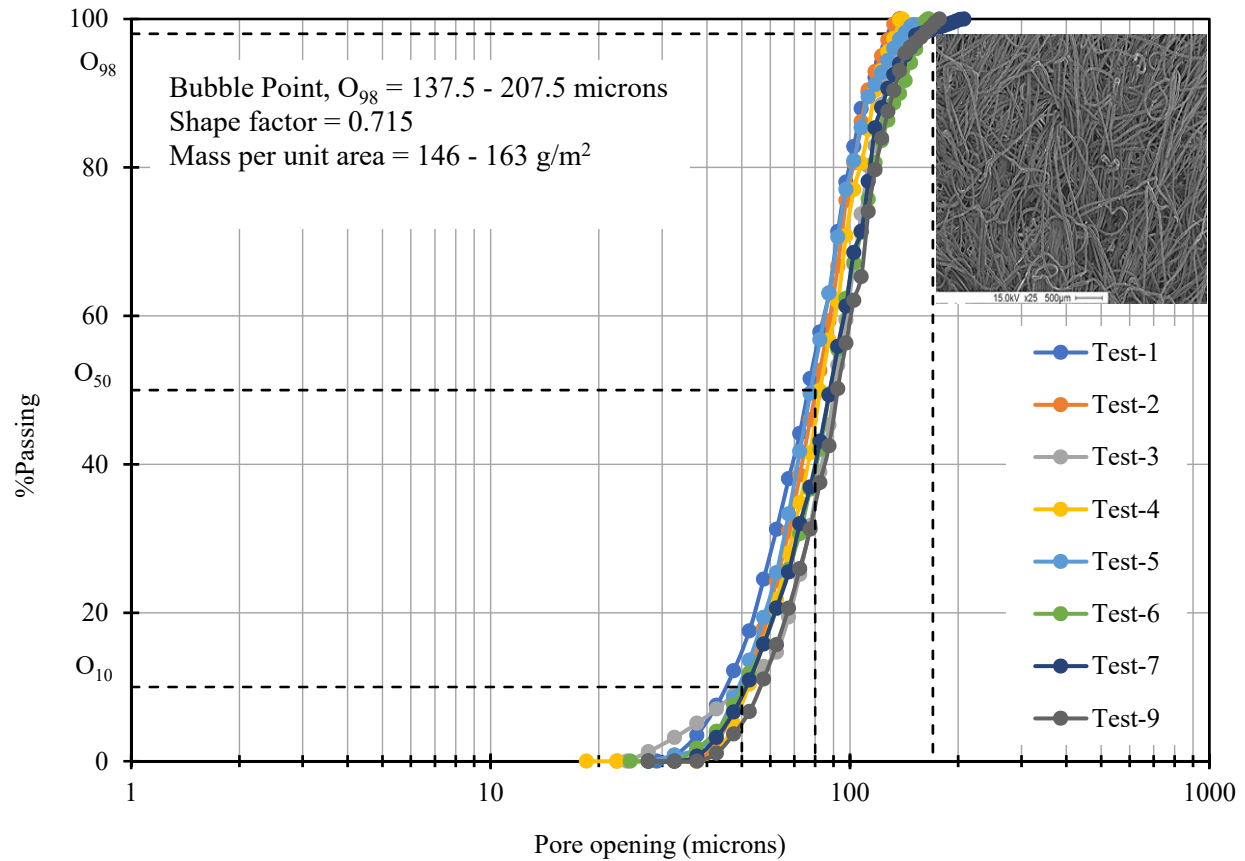


Figure 3.11: Pore Size Distribution of a Needle Punched Non-Woven Geotextile (E-2)

A total of 21 needle punched non-woven geotextiles were. Pore size distribution results of 1 out of 21 needle punched geotextiles (E-2) of a mass per unit area of 146 - 163 g/m² and a thickness of 0.64 – 0.89 mm are shown in Figure 3.11, which provides a range of bubble point, O_{98} (137.5 – 207.5 microns). The average O_{50} (80 microns) and O_{10} (50 microns) were also measured from

the pore size distribution as well. The free moving of fibers under needles makes the rough surface of geotextile with nonuniform pores in each side. The fibers running spontaneously leave random spaces in between the fibers. The pore size may vary depending on the side to be tested. The average O_{50} and O_{10} measured from the pore size distribution were 90 – 120 microns smaller than the average bubble point, O_{98} .

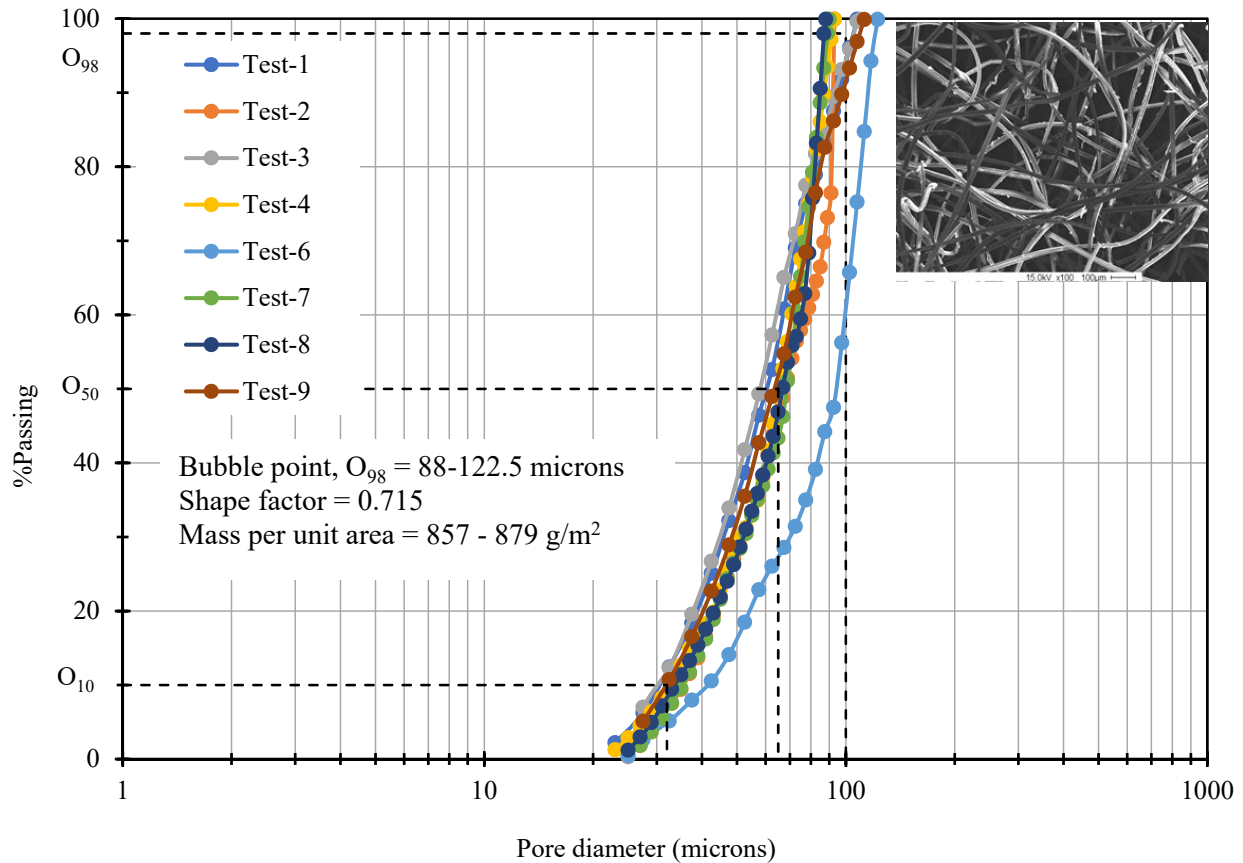


Figure 3.12: Pore Size Distribution of a Geo-Composite (F-1)

Two geo-composites (a combination of woven and non-woven geotextiles) selected from 2 US companies were used in the study. Pore size distribution results of a geo-composite, F-1 (857 – 879 g/m² mass/area and 2.04 – 2.40 mm thickness) which is a combination of a thin non-woven on top of a woven geotextile, are shown in Figure 3.12. Results showed that the average O_{50} (65

microns) and O_{10} (32 microns) were 40 – 73 microns smaller than the average bubble point, O_{98} (105.25 microns). Nine tests were conducted with individual specimens to obtain a range of bubble point, O_{98} (88 – 122.5 microns). In a geo-composite, the pore size results depended on the side either woven or non-woven, to be tested. For this geo-composite, the non-woven was placed at the bottom in the Capillary flow test device to obtain the bubble point, O_{98} . The random movement of fibers causes irregular pores between fibers. Therefore, a shape factor of 0.715 was used for the non-woven geotextiles.

Capillary flow test measures the smallest pores through a pore channel. Therefore, the test can easily differentiate between woven and non – woven geotextiles. It can be easily identified from the results mentioned above. Non-woven geotextiles have small to larger pores which provides “S” shaped pore size distribution. On the other hand, woven geotextiles have similar sized fibers moving over one another which results into almost uniform pore sizes. Therefore, the pore size distribution of woven geotextiles does not look like “S” shaped (see Figure 3.7, Figure 3.8 and Figure 3.9).

Overall, all the results shown were mostly consistent in the pore size distribution. However, there are some woven geotextiles with large openings (see Figure 3.13) and some needle – punched non – woven geotextile (see Figure 3.15) with complex structure showed the large variations in pore size distribution results. The possible variation in the Capillary flow test results are as follows:

- Pressure discrepancy: The fluctuation in maximum set up pressure (0.5 psi) caused a sudden drop in the regulator, which as a result, stopped the test without any results. To start the test, the regulator of the equipment was forced to increase up to 1200 – 1800 counts. This phenomenon does not affect the largest pore opening (bubble point, O_{98}).

However, it influenced the smaller pore openings (see Figure 3.13). It can be seen in Figure 3.13 that 7 out of 9 tests provided uniform results and only two tests showed deviation in the results. Only 1 out of 51 geotextiles showed this kind of discrepancy in the results.

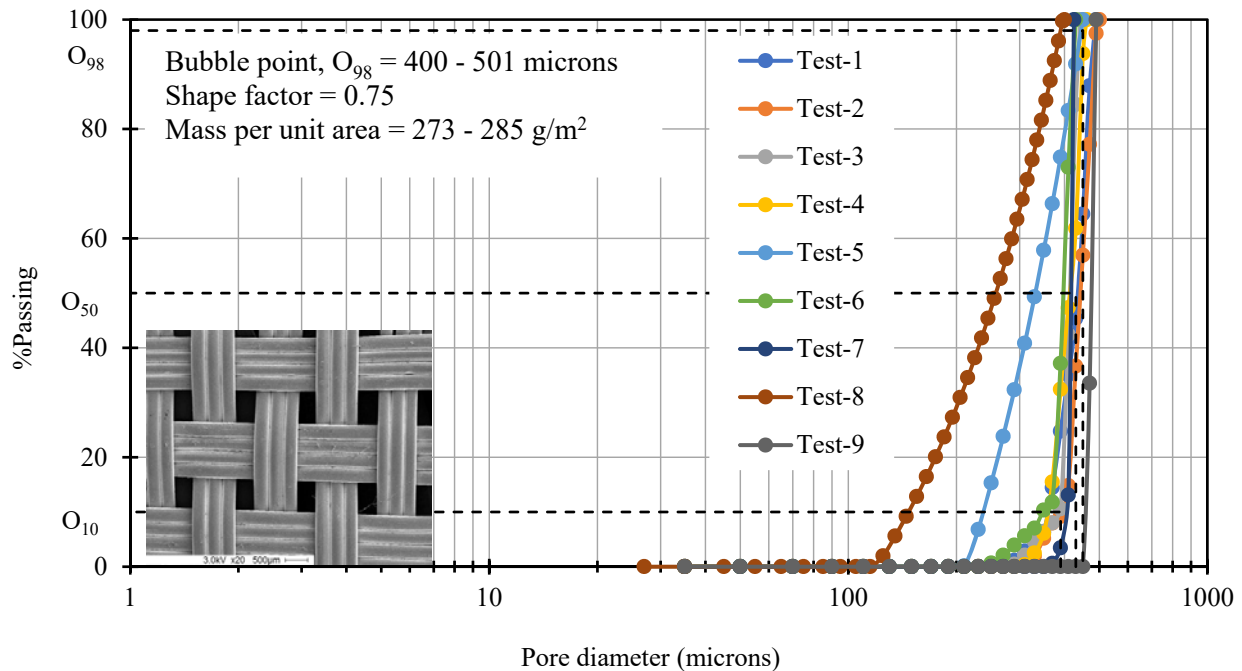


Figure 3.13: Pore Size Distribution of a Monofilament Woven Geotextile (A-4)

- Incomplete pore size distribution: When the specimens are not fully saturated enough due to either thickness or larger pores, the test cannot provide a complete pore size distribution. Figure 3.14 shows incomplete pore size distribution, the test could not measure the values of smaller pores. Another reason behind this error could be not getting enough pressure to drain out the liquid and measure the pore size. The test could not reach 100% flow during the wet test and the software could not provide the smaller pores and a complete pore size distribution. Only 1 out of 51 geotextiles provided incomplete pore size distribution result.

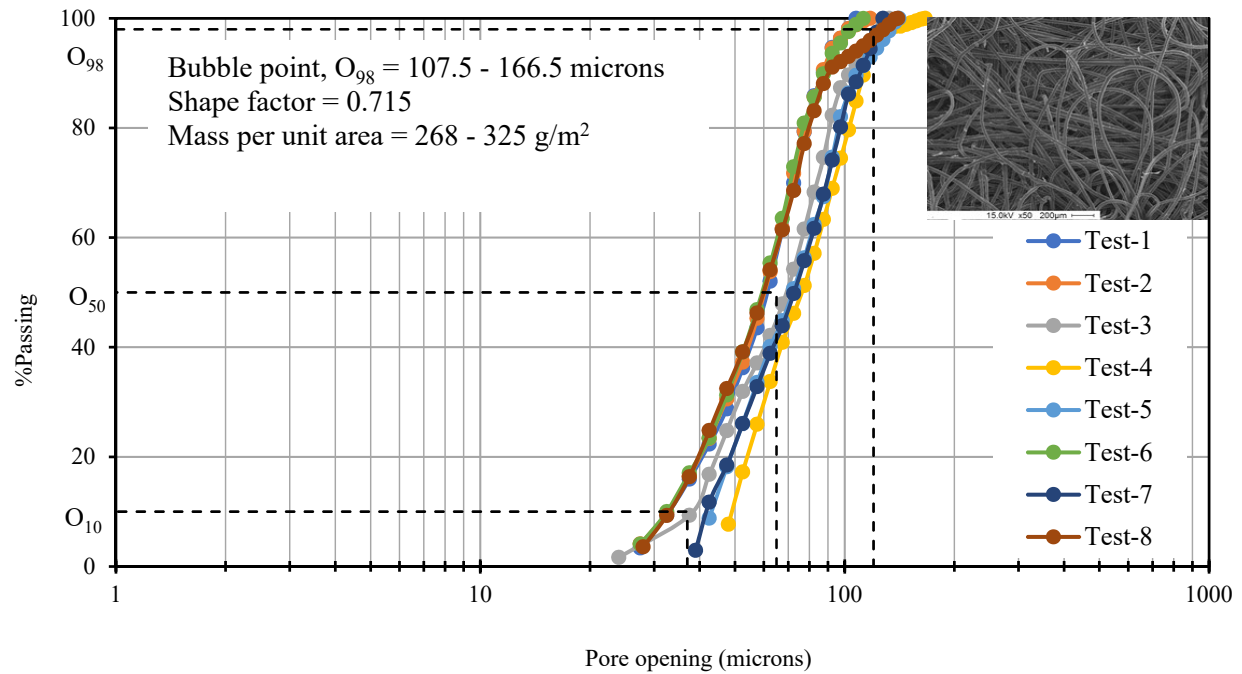


Figure 3.14: Pore Size Distribution of a Needle Punched Non-Woven Geotextile (E-10)

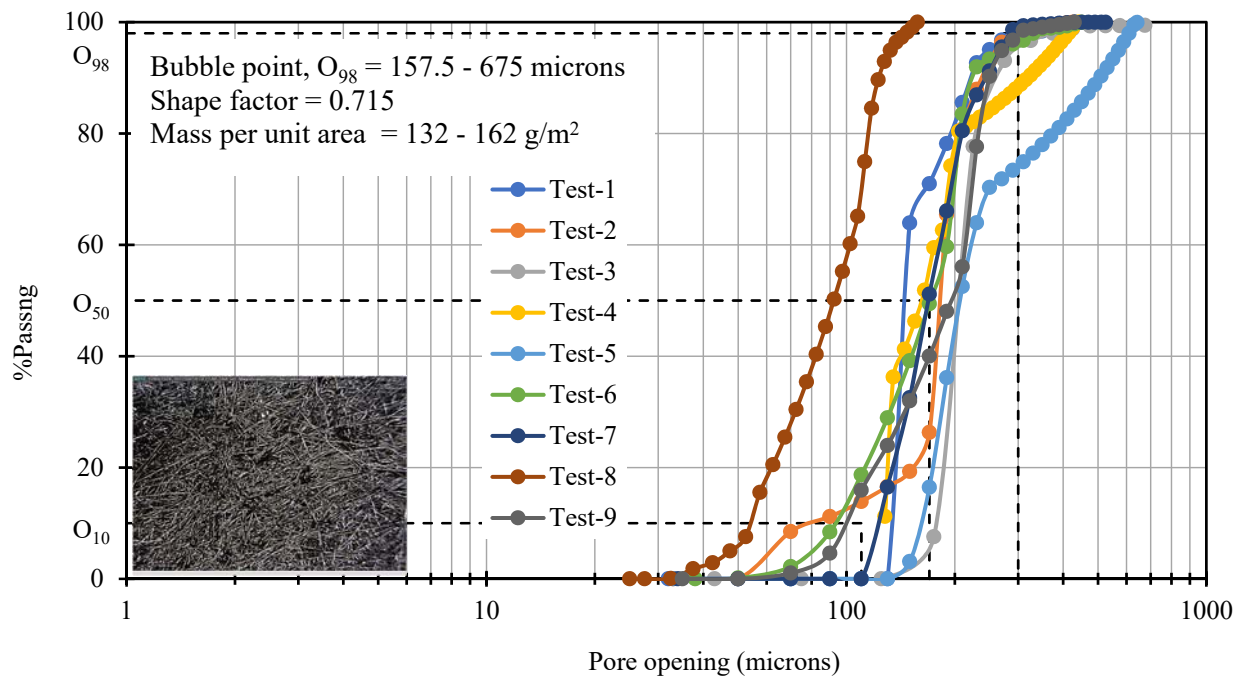


Figure 3.15: Pore Size Distribution of a Needle Punched Non-Woven Geotextile (E-1)

- Variations in results: Figure 3.15 shows pore size distribution results of a non-woven geotextile (E-1) with wide variation. Possible reasons could be sample variation, non-saturation, pressure discrepancy etc. However, it is not a common phenomenon and only 1 out of 51 geotextiles showed this kind of variation.

Based on the pore structure and manufacturing process of geotextiles, the range of pore opening, O_{98} varies from geotextile to geotextile. Even in the same geotextile, individual specimen can provide different result. Therefore, box plot and whisker diagrams are used to calculate the minimum and maximum outliers for each geotextile.

3.3.1 Box Plot and Whisker Diagram

In the previous section, the results of capillary flow tests of a representative geotextile from each category were discussed. In addition, conflicting results of 2 needle punched non-woven geotextiles (E-1 and E-10) and 1 monofilament woven geotextile (A-4) were discussed.

Box plot and whisker diagrams were used based on the five-number summary: minimum, first quartile, mean, third quartile, and maximum (<http://www.physics.csbsju.edu/stats/box2.html>) to find out the outlier results of O_{98} . The box plot and whisker diagram consists of a box which lies in between first and third quartiles. The mean can also be indicated in the diagram. The "whiskers" are straight line extending from the ends of the box to the maximum and minimum values. A procedure to calculate the outliers in a box plot is discussed below.

Example to Calculate Outliers:

For a geotextile (E-1) with a range of bubble points of 157.5 – 675 microns, the five-number summary can be computed as follows:

Range of Bubble Point values, O_{98} (microns): 157.5, 425, 430, 430, 441, 450, 525, 642, and 675

Minimum = 157.5 microns

First quartile, $Q1 = 430$ microns

Mean = 463.94 microns

Third quartile, $Q3 = 525$ microns

Maximum = 675 microns

Interquartile range, $IQR = Q3 - Q1 = 95$ microns

Outliers = Any data point less than $Q1 - 1.5 \cdot IQR$, or any data point greater than $Q3 + 1.5 \cdot IQR$

Minimum non - outliers, $Q1 - 1.5 \cdot IQR = 430 - 1.5 \cdot 95 = 287.5$ microns;

Maximum non - outliers, $Q3 + 1.5 \cdot IQR = 525 + 1.5 \cdot 95 = 667.5$ microns

Therefore, for the geotextile E1, any bubble point (O_{98}) less than 287.5 microns and greater than 667.5 microns are considered as outliers (see Figure 3.16). Figure 3.16 shows a Box Plot and Whisker Diagram of a needle punched non-woven geotextile (E-1) which provides the maximum and minimum outliers.

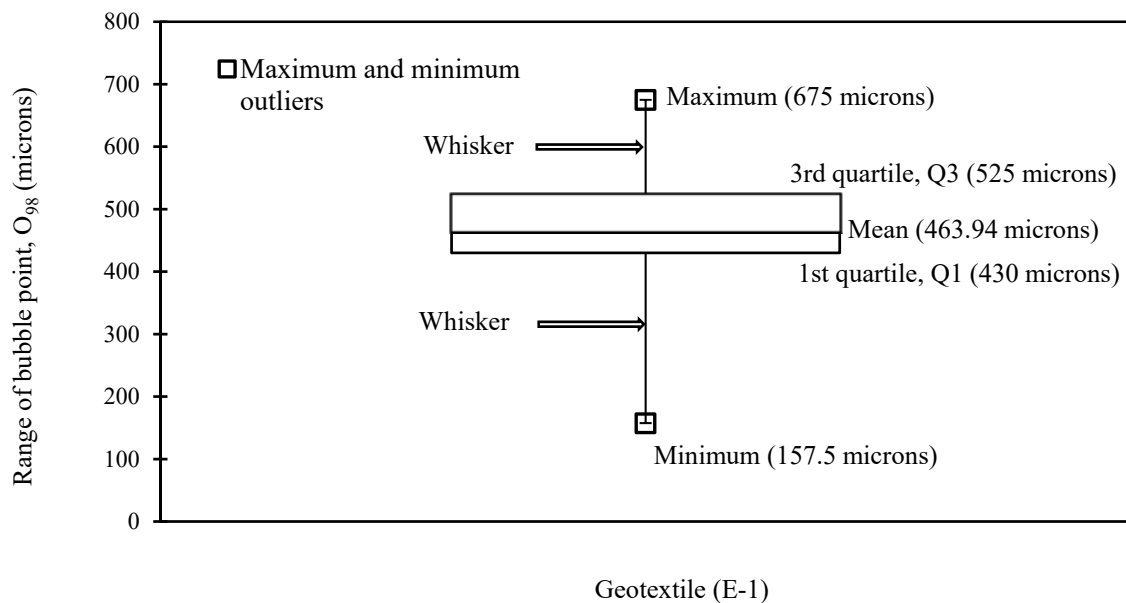


Figure 3.16: Box Plot and Whisker Diagram

Figure 3.17 shows the box plot and whisker diagram for a set of 7 monofilament geotextiles. The diagram shows that two monofilament geotextiles (A-1 and A-2) have a wide range of Bubble Point values, O_{98} and A-3 to A-7 have smaller range of Bubble Point values, O_{98} . Geotextiles with lesser mass per unit area (A-1 and A-3) has outliers as compared to the heavier geotextiles (A-6, A-7). The range of bubble point, O_{98} for A-1 (490 – 1100 microns) is found to be the largest among 7 geotextiles with a maximum outlier (1100 microns) in the range. Although, A-3 is not a heavy geotextile but has the smallest range of O_{98} (221 – 305 microns), it has a maximum outlier (305 microns). Following the calculation discussed in section 3.5.1, the minimum and maximum outliers are calculated from the box plot and whisker diagram for geotextiles A-1 and A-3 (see Table 3.2).

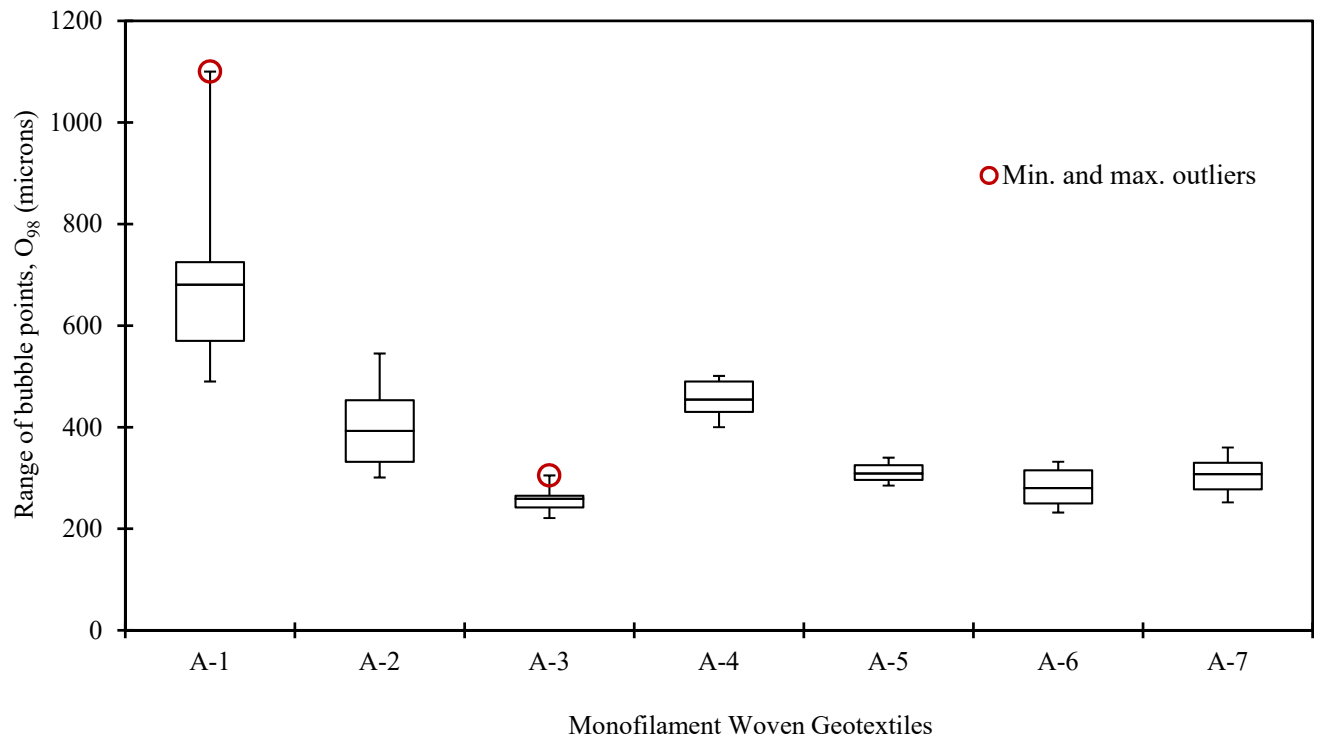


Figure 3.17: Box Plot and Whisker Diagram for a Set Of 7 Monofilament Woven Geotextiles

Table 3.2: Minimum and Maximum Outliers of Monofilament Woven Geotextiles.

Geotextiles	Maximum outliers, microns	Minimum outliers, microns
A-1	1100	N/A
A-3	305	N/A

N/A: Not available

Eleven slit film woven geotextiles were used in the analysis and the range of bubble point, O_{98} of each geotextile are plotted in Figure 3.18. B-7 shows the largest range of bubble point, O_{98} (340 – 500 microns) and B-10 gives the smallest range of bubble point, O_{98} (325 – 382 microns). Like monofilament, the minimum and maximum outliers were computed for slit film geotextiles. In Table 3.3, maximum and minimum outliers for B-7 and B-10 geotextiles are shown.

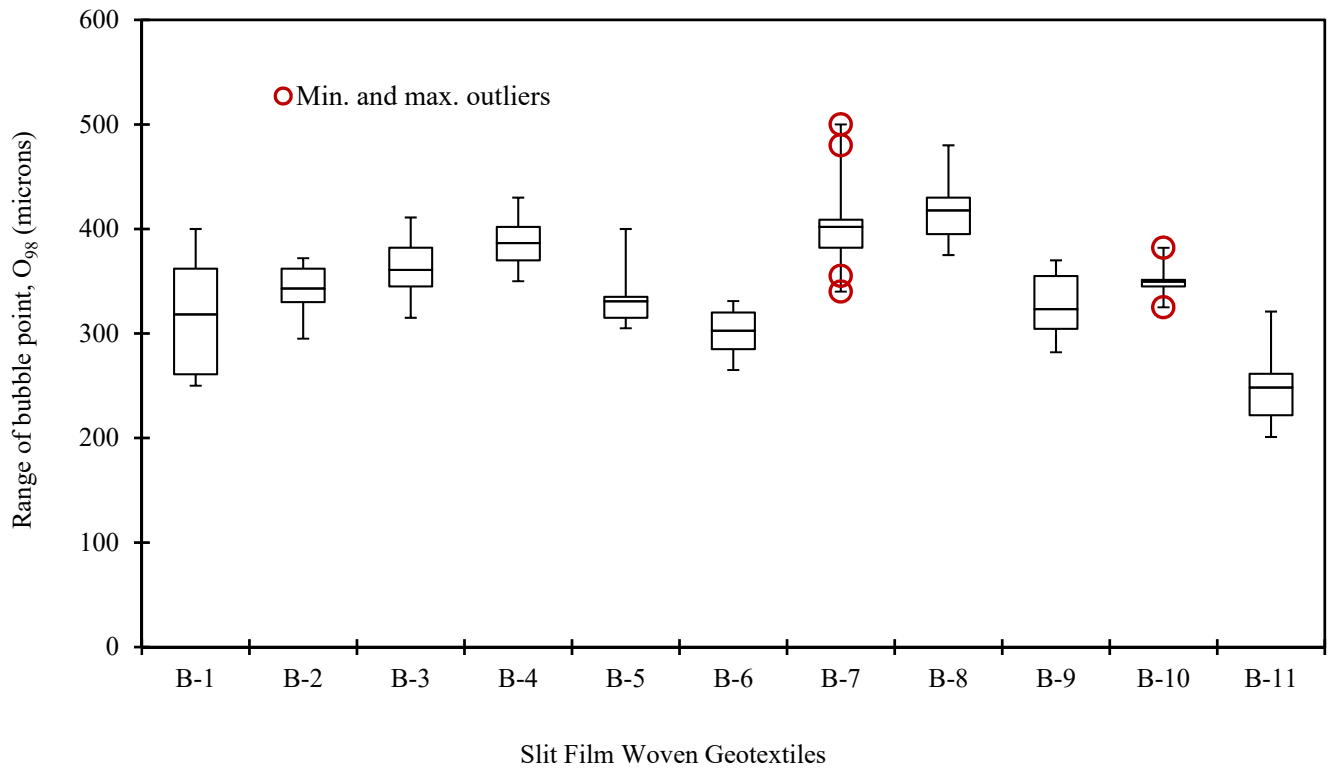


Figure 3.18: Box Plot and Whisker Diagram for a Set Of 11 Slit Film Woven Geotextiles

Table 3.3: Minimum and Maximum Outliers of Slit Film Woven Geotextiles

Geotextiles	Maximum outliers, microns	Minimum outliers, microns
B-7	480, 500	340, 355
B-10	382	325

Two multifilament woven geotextiles (813 – 1117 g/m² mass per unit area) were selected to perform the capillary flow test. The range of bubble point obtained from the testing is 190 – 640 microns. Figure 3.19 shows the range of bubble point of each multifilament geotextiles. The box plot showed an outlier for the multifilament (C-1) which is provided in Table 3.4.

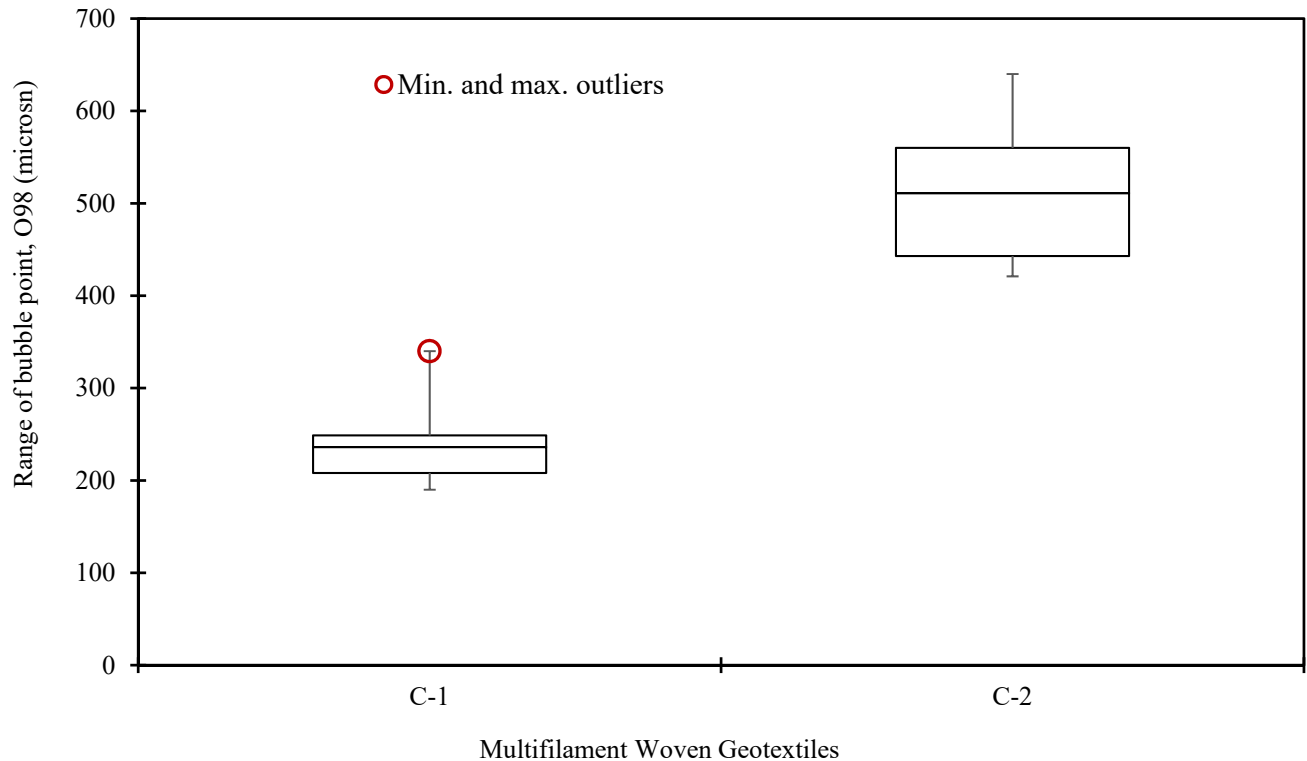


Figure 3.19: Box Plot and Whisker Diagram for a Set Of 2 Multifilament Woven Geotextiles

Table 3.4: Minimum and Maximum Outliers of Multifilament Woven Geotextiles.

Geotextiles	Maximum outliers, microns	Minimum outliers, microns
C-1	340	N/A

N/A: Not available

Figure 3.20 shows the box plot and whisker diagram of a group of geotextiles including 8 heat-bonded geotextiles with a range of mass per unit area of 90 – 290 g/m². Among 8 heat bonded non-woven geotextiles, D-5 (136 g/m²) shows the largest range of bubble point, O₉₈ of 262 – 450

microns and D-7 shows the smallest range of bubble point, O_{98} of 186 – 245 microns. No outlier was found from the box plot and whisker diagram drawn for heat-bonded geotextiles.

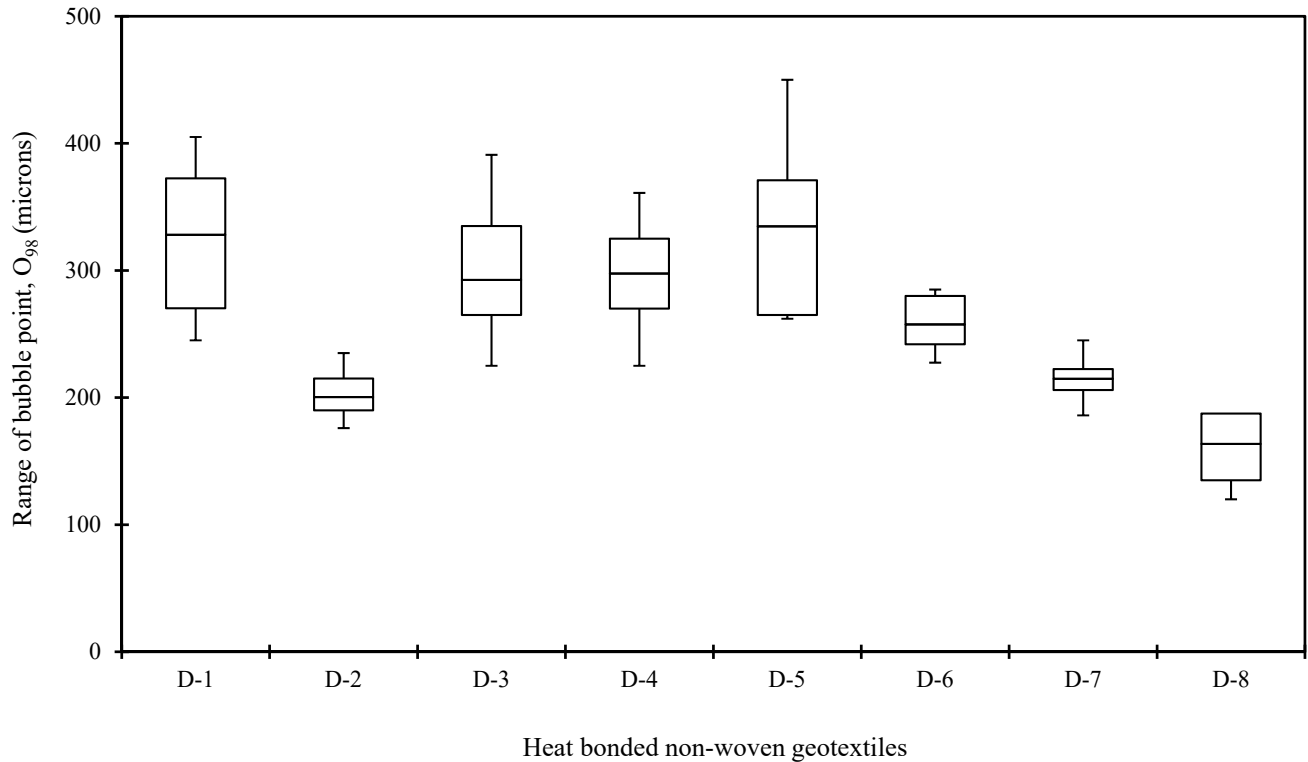


Figure 3.20: Box Plot and Whisker Diagram for a Set Of 8 Heat Bonded Non- Woven Geotextiles

A wide range of needle-punched non-woven geotextiles ($147 - 1006 \text{ g/m}^2$) were used in the analysis to draw the box plot and whisker diagram (see Figure 3.21) E-1, E-4 and E-8 showed a broad range of bubble point, O_{98} (157.5 – 675 microns, 255 – 510 microns, and 75 – 415 microns respectively); and E-13 and E-20 represent small range of bubble point, O_{98} (137.5 – 157.5 microns and 121 – 127.5 microns respectively). 9 needle punched geotextiles showed outliers in the box plot Figure 3.21. Table 3.5 also shows the minimum and maximum outliers of E-1, E-4, E-11, E-14 to E-17, E-19 and E-21.

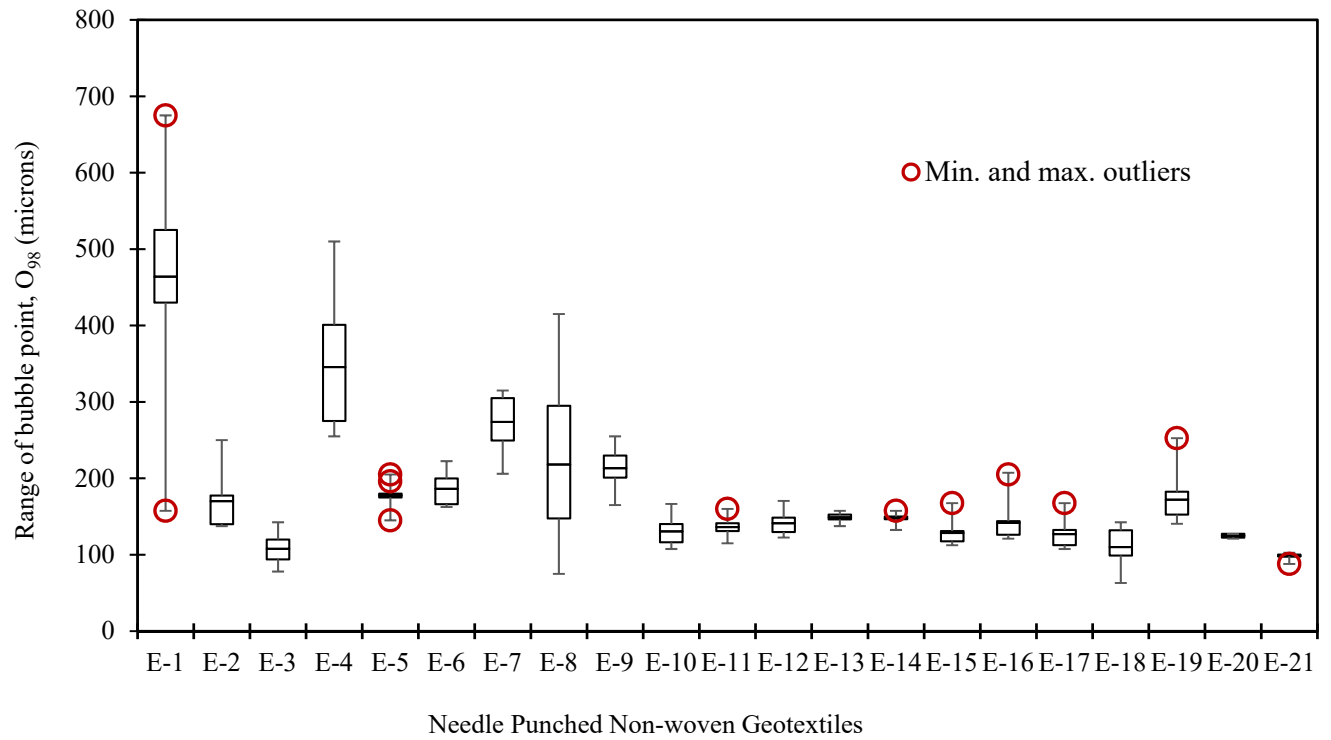


Figure 3.21: Box Plot and Whisker Diagram for a Set Of 21 Needle Punched Non- Woven Geotextiles

Table 3.5: Minimum and Maximum Outliers of Needle Punched Non-Woven Geotextiles.

Geotextiles	Maximum outliers, microns	Minimum outliers, microns
E-1	675	157.5
E-5	196, 205	145
E-11	160	N/A
E-14	157.5	N/A
E-15	167.5	N/A
E-16	205	N/A
E-17	167.5	N/A
E-19	252.5	N/A
E-21	N/A	88

N/A: Not available

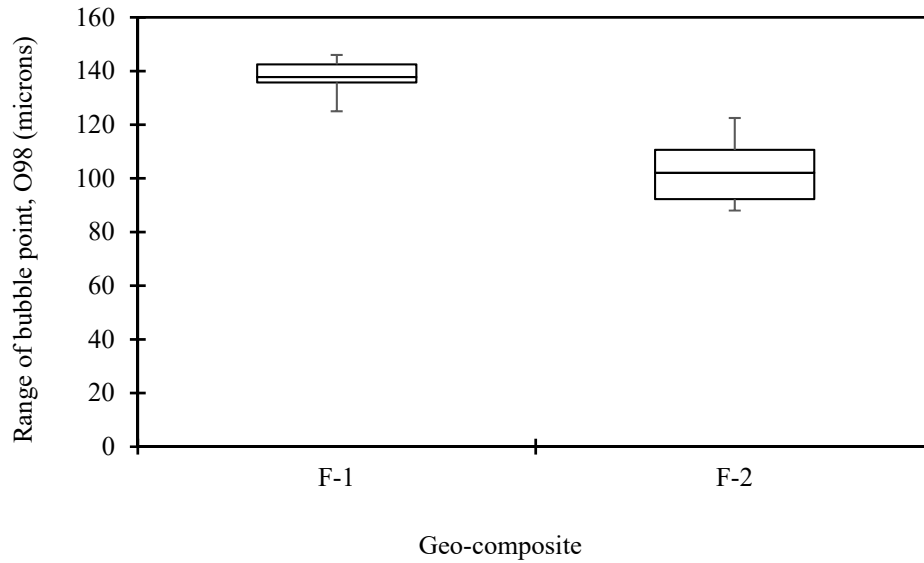


Figure 3.22: Box Plot and Whisker Diagram for a Set of 2 Geo-Composites

Figure 3.22 shows the range of bubble point, O_{98} (125 – 146 microns and 88 – 122.5 microns respectively) of two geo-composites. No minimum or maximum outlier could be found from the box plot and whisker diagram.

Two monofilament woven geotextiles (A-1 and A-3), 2 slit film woven geotextiles (B-7 and B-10), 1 multifilament woven geotextile (C-1), and 9 needle punched non-woven geotextiles (E-1, E-5, E-11, E-14, E-15, E-16, E-17, E-19, E-21) showed outliers in the range of pore opening (bubble point, O_{98}) obtained in the box plot and whisker diagram. The outliers could be an outcome of systematic error in the experiment, unsteady pressure transduce, diverse pore structure of woven and non-woven geotextiles, etc. To find a correlation between mass per unit area and the bubble point, O_{98} , the outliers are taken out from the analysis.

3.4 Relationships between O_{98} , O_{50} and O_{10} , and Mass per Unit Area of Geotextiles

Several researches were investigated to find a correlation between a physical property and a hydraulic property of geotextiles. Bhatia and Smith (1996), Vermeersch et al. (1996), Aydilek et al. (2006) and Elton (2007) proposed several correlations between mass per unit area and the largest pore openings, which provided a predicted pore opening for a given mass per unit area of a geotextile.

For this study, the Bubble Point values (O_{98}), a function of mass per unit area for monofilament and slit film woven geotextiles are plotted in Figure 3.23. For these plots, mean bubble point values were used after removing any minimum or maximum outliers. The bubble point, O_{98} of woven geotextiles, both monofilaments and slit films, do not show clear trend with the increasing of mass per unit area. Woven geotextiles are manufactured from the single layer fibers passing each other and the mass per unit area of woven geotextiles depends on the mass of fibers. The pore size of woven geotextiles mostly depends on the orientation of the fibers instead of the mass or thickness of fibers. Therefore, it is not surprising to find no relationship between O_{98} and mass per unit area for the monofilaments and slit film woven geotextiles.

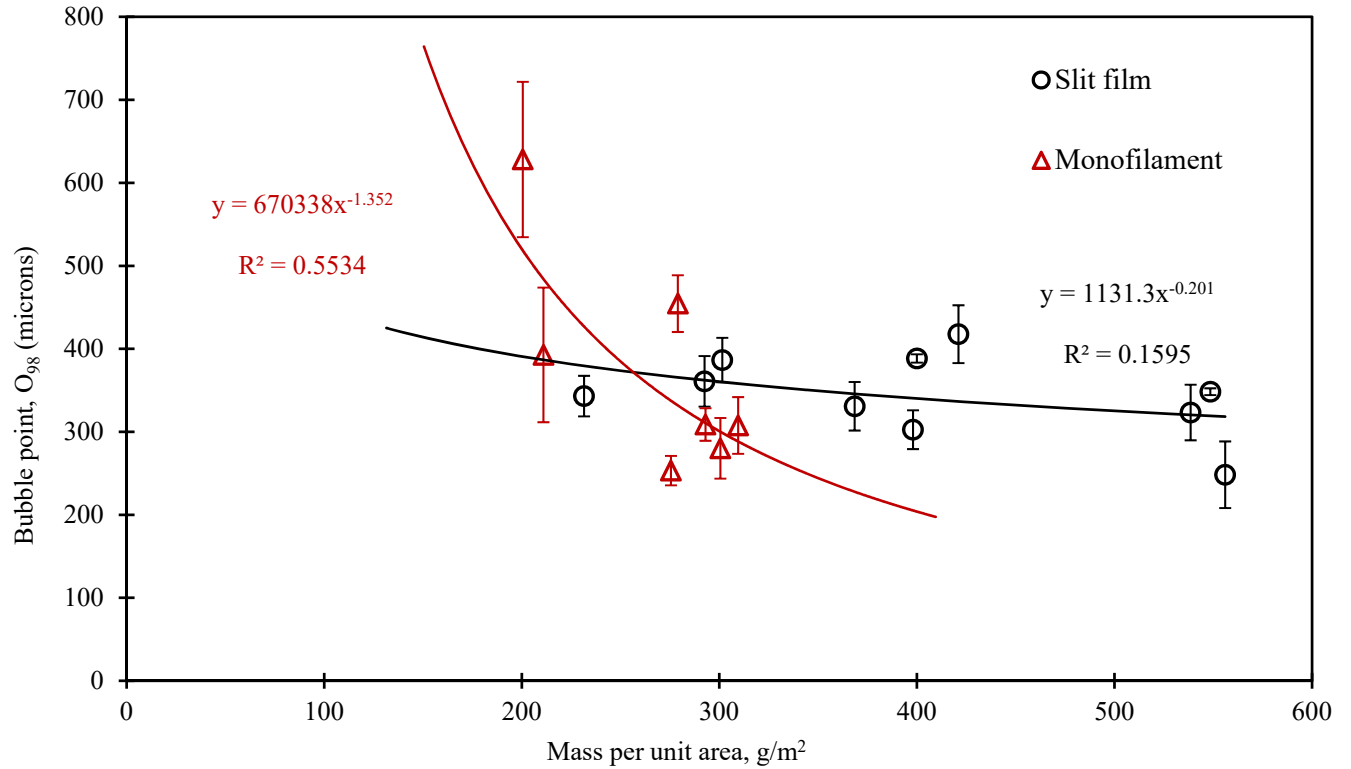
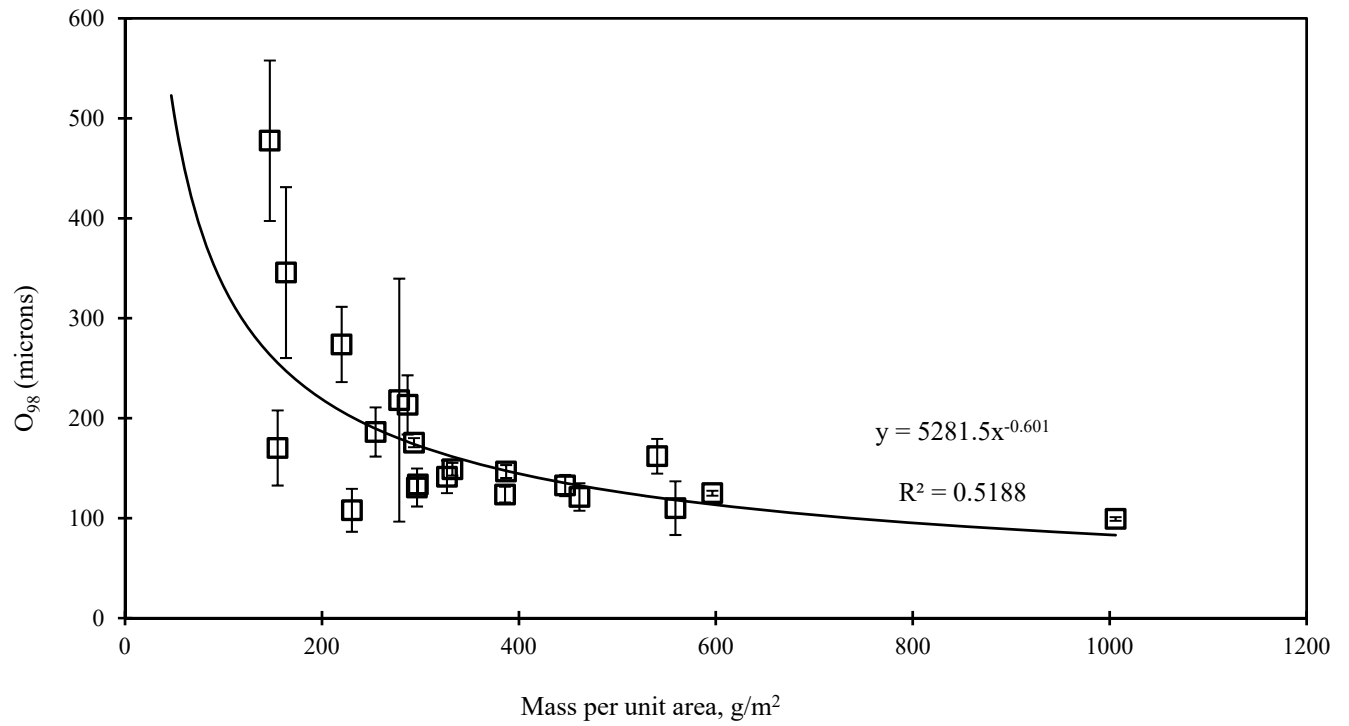
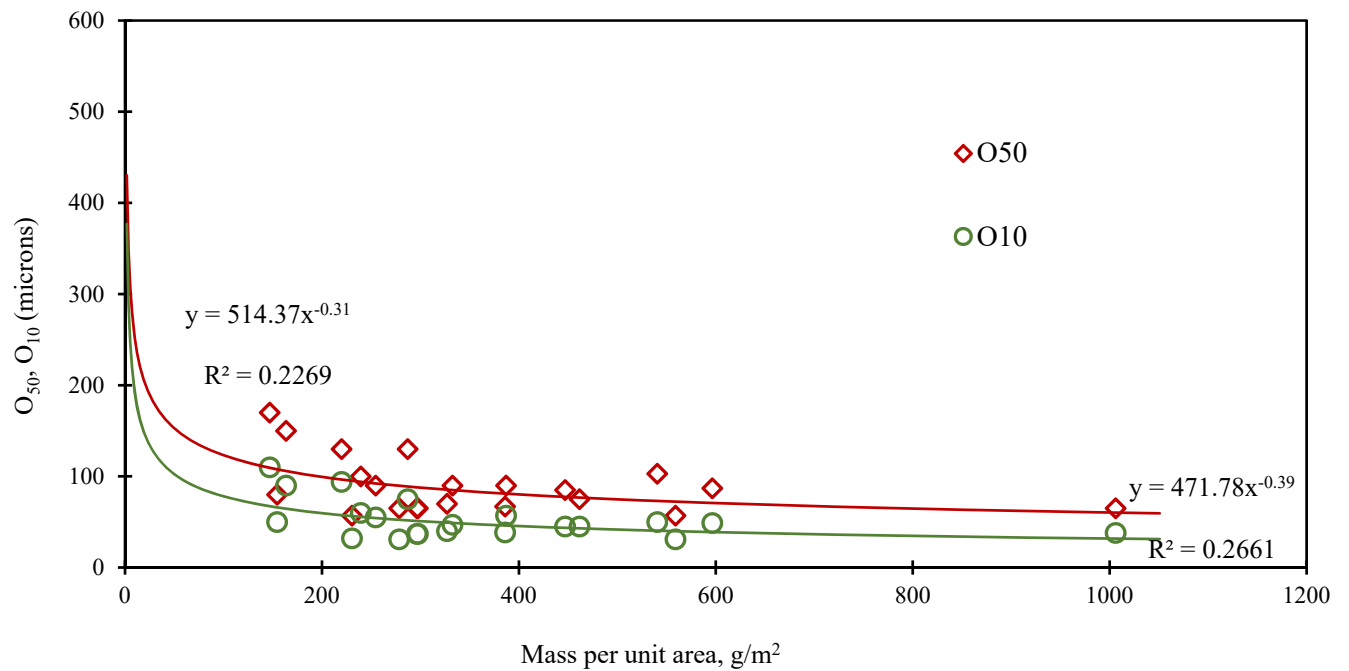


Figure 3.23: Bubble Point vs. Mass per Unit Area of Monofilament and Slit-film Woven Geotextiles

The same condition does not apply for non-woven geotextiles, either needle punched non-woven or heat bonded non-woven geotextiles. For both needle punched and heat bonded non-woven geotextiles, bubble point, O₉₈ decreases with the increasing mass per unit area (see Figure 3.24 and Figure 3.25). For needle punched non-woven geotextiles, O₁₀ and O₅₀ were also plotted against mass per unit area (see Figure 3.24 b).



(a)



(b)

Figure 3.24: O_{10} , O_{50} , and O_{98} vs. Mass per Unit Area of Needle Punched Non-Woven Geotextiles

For the needle punched non-woven geotextiles, the fibers run over one another randomly and leave anonymous spaces among each other, which creates a complex pore structure. Heavier non-woven geotextiles have many more fibers than thinner geotextiles. Therefore, the mass of fibers in the geotextile influence their pore size distribution. The needle punched non-woven geotextiles vary with a broad range of mass per unit area ($147 - 1006 \text{ g/m}^2$). In Figure 3.24, O_{98} , O_{50} and O_{10} values for all needle punched non-woven geotextiles are plotted. A decreasing trend of pore sizes is observed with the increasing mass per unit area.

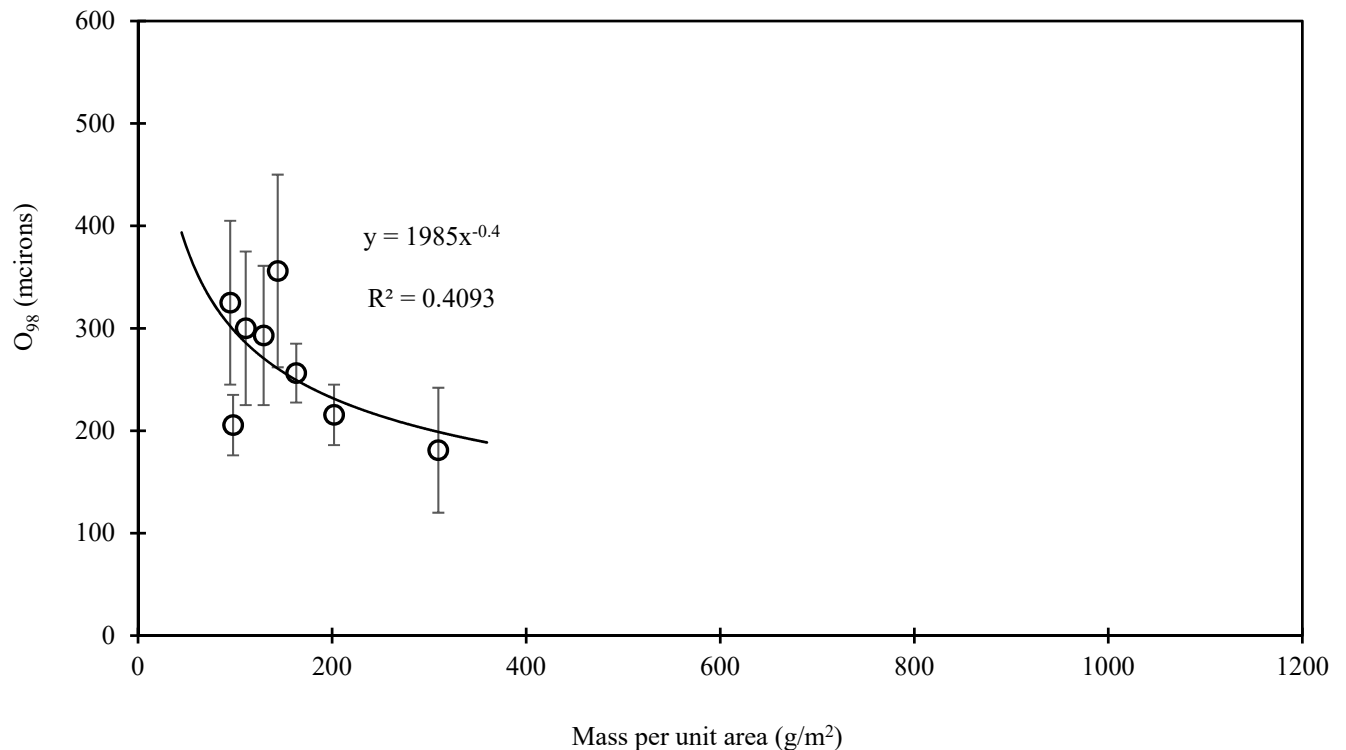


Figure 3.25: Bubble Point vs. Mass per Unit Area of Heat Bonded Non-Woven Geotextiles

On the other hand, the range of mass per unit area ($98 - 309 \text{ g/m}^2$) of heat bonded non-woven geotextiles is much lower compared to the needle punched non-woven geotextiles (see Figure 3.25). However, a decreasing trend was also found in the bubble point, O_{98} for heat bonded non-woven geotextiles with the increasing mass per unit area., but much different relationship.

Needle punched non-woven geotextiles have a broad range of Bubble Point (63 – 675 microns) along with the mass per unit area, which made a dramatic change in the relationship curve between O_{98} and mass per unit area. On the other hand, heat bonded non-woven geotextiles have a smaller range of pore openings (120 – 450 microns), and a flatter slope in the curve of heat bonded non-woven geotextiles was found with a completely different relation.

3.5 Dry Sieving Test

In the current study, most of the AOS results of geotextiles were obtained from the manufacturers. However, for all heat – bonded geotextiles, some woven geotextiles (A-6 and A-7) and needle – punched non – woven geotextiles (E-3, E-4, E-7, E-8, E-13, and E-18), dry sieving tests were conducted at Syracuse University. One needle – punched non – woven geotextile (E-21) could not be tested due to its high thickness.

ASTM D4751 – The Standard Test Method for Determining the Apparent Opening Size (AOS) was followed to perform the tests. Dry sieving test is based on the concept that glass beads of a specific diameter placed on a piece of a geotextile is sieved in a shaker to determine the percentage of beads passing through the geotextile, whether it is 5% or less. The repetition of the process with glass beads of different diameter provides apparent opening size (AOS, O_{95}) of a geotextile. In this test, a #4 sieve frame, a pan, a cover and a hoop to secure the geotextile inside the frame were used. A mechanical sieve shaker was used in the test to sieve the glass beads through the geotextile (see Figure 3.26).

Glass beads were sieved before performing the test to verify the diameter. 50 gm glass beads of known diameter were used in each test. The geotextile was cut into a size of 24 cm diameter, which has a cross-sectional area of 0.045 m^2 and a testing area of 0.0314 m^2 . Like Capillary flow test, the sample preparation was followed by soaking the specimens into clean water for an hour

and drying in the room temperature with a fan for 24 hours. The weight of the specimen was measured before soaking and after drying, to make sure that the weight is exactly same or less than before soaking and there is no water staying in the pores of the specimen.

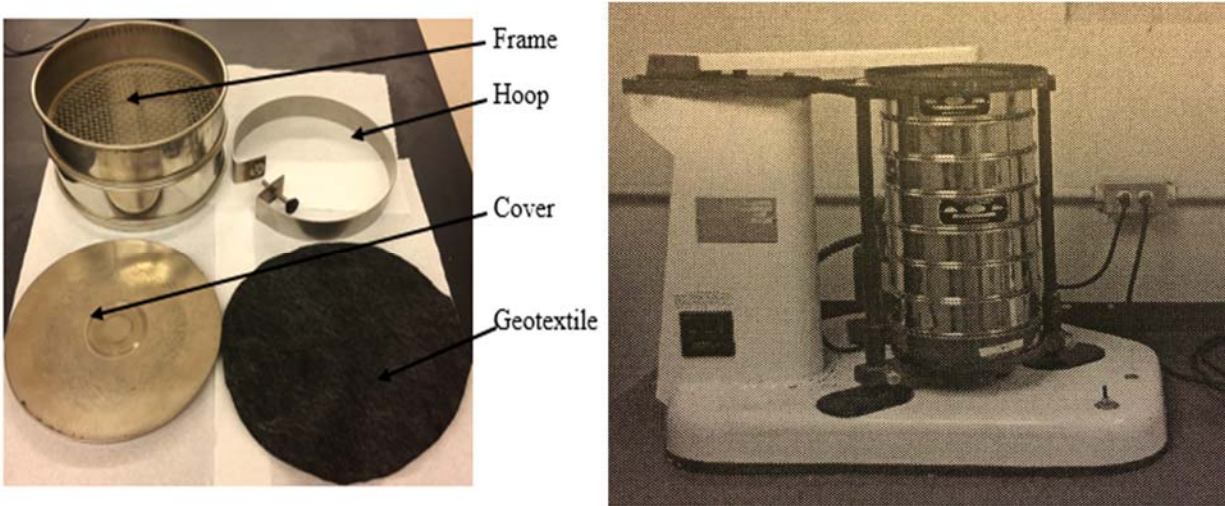


Figure 3.26: Dry sieving equipment and sieve shaker



Figure 3.27: Geotextile with glass beads secured in the frame

In the Dry sieving test, the geotextile cut into a specific diameter, is placed in the #4 sieve frame and a hoop was used to secure the geotextile inside the frame. Then the frame with geotextile was placed on the pan and 50 gm glass beads of known diameter were placed on the center of the

geotextile (see Figure 3.27). A cover was used on the frame. Then the frame was sieved in a mechanical shaker for 10 minutes. This test was conducted repeating the same technique with progressively larger beads until the percent passing of glass beads was 5% or less by weight. After sieving, the weight of glass beads in the pan and weight of geotextile with glass beads were measured and recorded. Approximately 5-6 tests were conducted for each type of geotextile. Dry sieving test is a time-consuming test. It takes several hours to complete the test for one geotextile. The geotextile with large thickness could not be used in the test. The geotextiles were secured in the frame with hoop, however, sagging was noticed with several specimens which might have some effects on the result. The AOS values were plotted a function of mass per unit area for needle punched (see Figure 3.28) and heat bonded (see Figure 3.29) non-woven geotextiles.

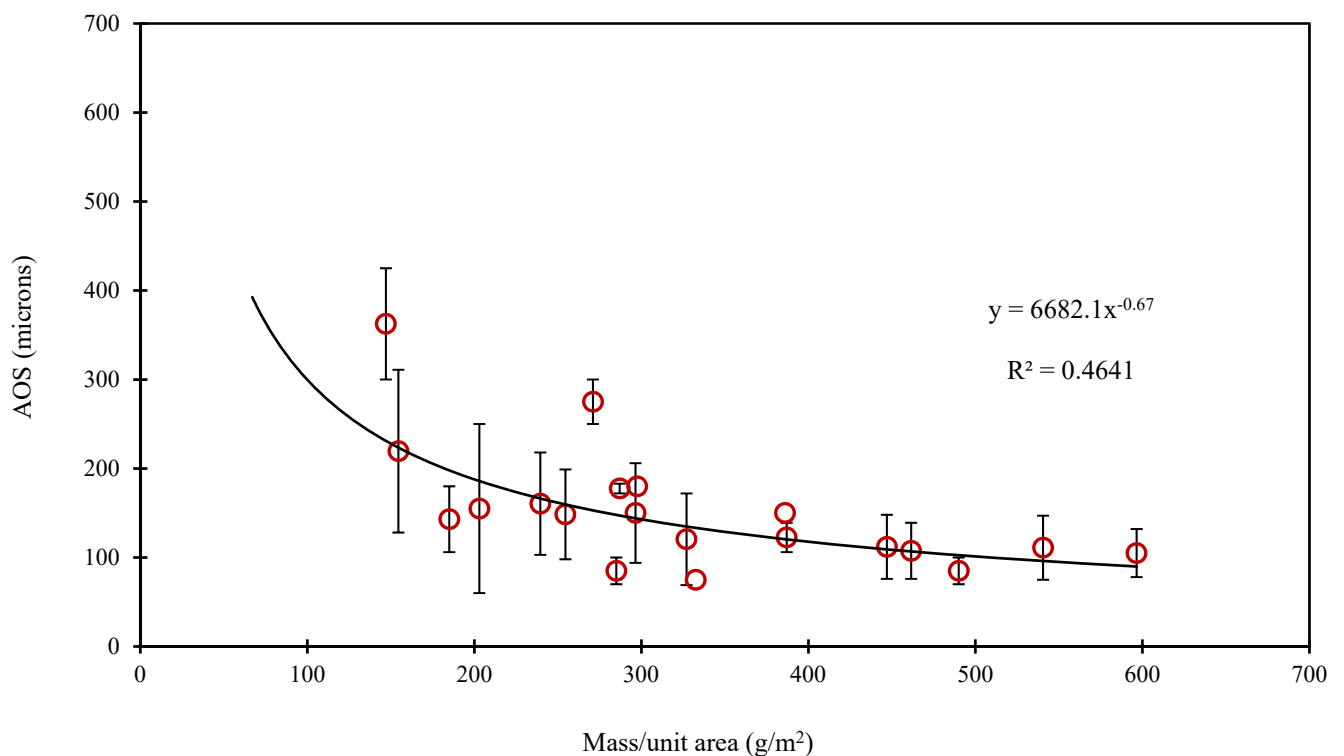


Figure 3.28: AOS vs. Mass per Unit Area for Needle Punched Non-Woven Geotextiles

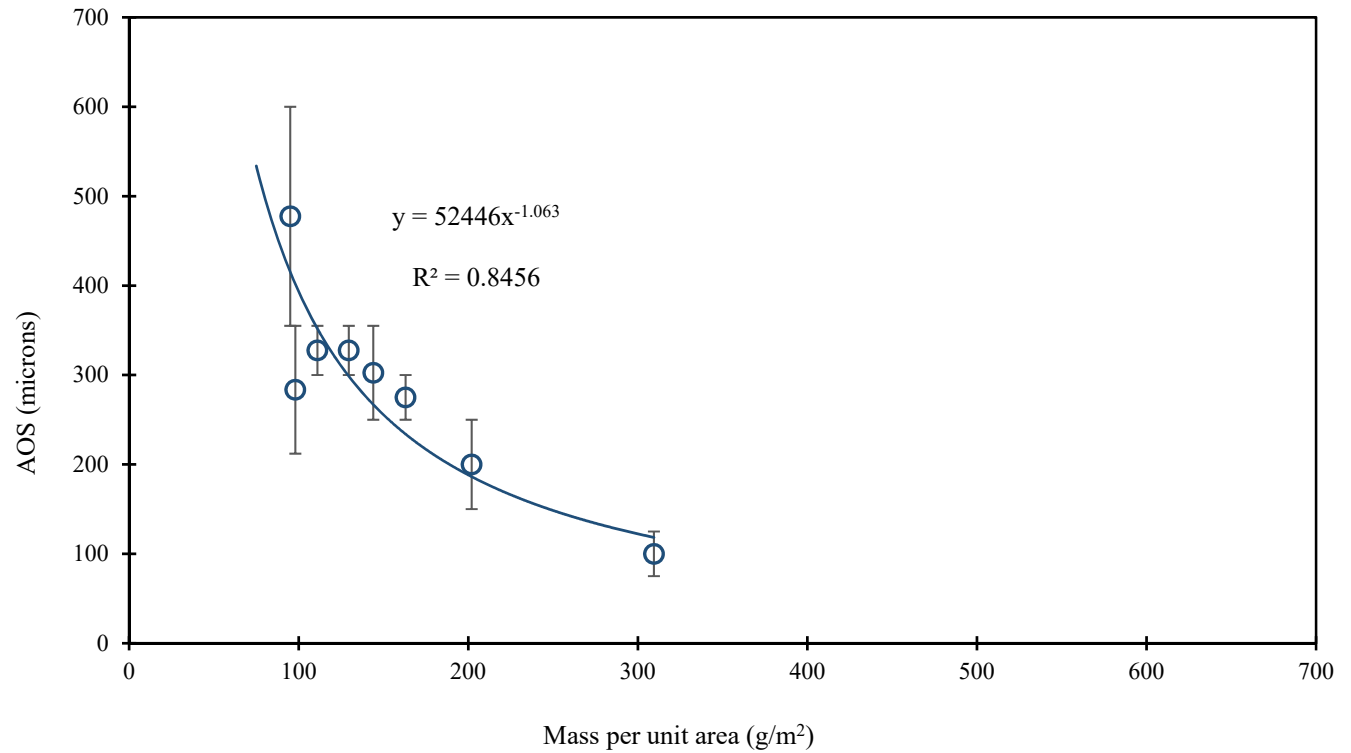


Figure 3.29: AOS vs. Mass per Unit Area for Heat Bonded Non-Woven Geotextiles

Figure 3.28 and Figure 3.29 showed that like the relationship between Bubble Point vs. mass per unit area, a decreasing trend of AOS was found with the increasing mass per unit area for needle punched and heat bonded non-woven geotextiles.

Table 3.6 shows the range of bubble point, O_{98} and AOS, O_{95} results of all types of geotextiles with standard deviation.

Table 3.6: Capillary Flow and Dry Sieving Test Results of Geotextiles

Geotextiles	Manufacturing process	Measured Bubble point O ₉₈ , microns	Standard deviation, σ	AOS, O ₉₅ * (microns)	Standard deviation, σ	Difference (microns)
A-1	Monofilament	490 - 740	176.78	425 - 850	300.52	65 - 110
A-2	Monofilament	301 - 545	172.53	300 - 504	144.25	1 - 41
A-3	Monofilament	221 - 305	59.40	150 - 212	43.84	71 - 93
A-4	Monofilament	400 - 501	71.42	426 - 430	2.83	26 - 71
A-5	Monofilament	232 - 332	70.71	355**	N/A	73
A-6	Monofilament	252 - 360	76.37	355 - 425**	49.50	65 - 103
A-7	Monofilament	285 - 340	38.89	300 - 425	88.39	15 - 85
B-1	Slit film	250 - 400	106.07	212 - 600	274.36	38 - 200
B-2	Slit film	295 - 372	54.45	518 - 585	47.38	213 - 223
B-3	Slit film	315 - 411	67.88	414 - 425	7.78	14 - 99
B-4	Slit film	350 - 430	56.57	422 - 424	1.41	6 - 72
B-5	Slit film	305 - 400	67.18	400 - 418	12.73	18 - 95
B-6	Slit film	265 - 331	46.67	271 - 388	82.73	6 - 57
B-7	Slit film	340 - 500	113.14	353 - 418	45.96	13 - 82
B-8	Slit film	375 - 480	74.25	333 - 655	227.69	42 - 175
B-9	Slit film	282 - 370	62.23	425	N/A	99
B-10	Slit film	325 - 382	40.31	420	N/A	66.5

Geotextiles	Manufacturing process	Measured Bubble point O ₉₈ , microns	Standard deviation, σ	AOS, O ₉₅ * (microns)	Standard deviation, σ	Difference (microns)
B-11	Slit film	201 - 301	70.71	271 - 388	82.73	70 - 87
C-1	Multifilament	190 - 340	106.07	150	N/A	115
C-2	Multifilament	421 - 630	147.79	600	N/A	74.5
D-1	Heat bonded	176 - 235	41.72	212 – 355**	101.12	36 - 120
D-2	Heat bonded	245 – 405	113.14	355 – 600**	173.24	110 - 195
D-3	Heat bonded	225 – 375	106.07	300 – 355**	38.89	20 - 75
D-4	Heat bonded	225 – 361	96.17	300 – 355**	38.89	6 - 75
D-5	Heat bonded	262 – 450	132.94	250 – 355**	74.25	12 - 95
D-6	Heat bonded	227.5 – 285	40.66	250 – 300**	35.36	15 - 22.5
D-7	Heat bonded	186 – 245	41.72	150 – 250**	70.71	5 - 36
D-8	Heat bonded	120 – 242	86.27	75 – 125**	35.36	45 - 117
E-1	Needle - punched	157.5 - 675	365.93	300 – 425**	88.39	142.5 - 250
E-2	Needle - punched	137.5 - 207.5	49.50	128 - 311	129.40	9.5 - 103.5
E-3	Needle - punched	78 - 142.5	45.61	106 – 180**	52.33	28 - 37.5
E-4	Needle - punched	255 - 415	113.14	60 – 250**	134.35	165 - 195
E-5	Needle - punched	145 – 205	42.43	103 - 218	81.32	13 - 42
E-6	Needle - punched	162.5 – 222.5	42.43	98 - 199	71.42	23.5 - 64.5
E-7	Needle - punched	206 - 315	77.07	250 – 300**	35.36	15 - 44

Geotextiles	Manufacturing process	Measured Bubble point O ₉₈ , microns	Standard deviation, σ	AOS, O ₉₅ * (microns)	Standard deviation, σ	Difference (microns)
E-8	Needle - punched	75 - 415	240.42	70 – 100**	21.21	5 - 315
E-9	Needle - punched	165 - 255	63.64	172 - 183	7.78	7 - 72
E-10	Needle - punched	107.5 - 166.5	41.72	94 - 206	79.20	13.5 - 39.5
E-11	Needle - punched	115 - 160	31.82	180	N/A	42.5
E-12	Needle - punched	122.5 - 170.5	33.94	69 - 172	72.83	2.5 - 53.5
E-13	Needle - punched	137.5 - 157.5	14.14	75**	N/A	72.5
E-14	Needle - punched	132.5 - 157.5	17.68	106 - 139	23.33	18.5 - 26.5
E-15	Needle - punched	112.5 - 167.5	38.89	150	N/A	10
E-16	Needle - punched	107.5 - 167.5	42.43	76 - 139	44.55	28.5 - 31.5
E-17	Needle - punched	121 - 205	59.40	76 - 148	50.91	45 - 57
E-18	Needle - punched	63 - 142.5	56.21	70 – 100**	21.21	7 - 42.5
E-19	Needle - punched	140.5 - 187.5	33.23	75 - 147	50.91	40.5 - 65.5
E-20	Needle - punched	121 - 127.5	4.60	78 - 132	38.18	4.5 - 43
E-21	Needle - punched	88 - 102.5	10.25	N/A	N/A	N/A
F-1	Geo-composite	125 - 146	14.85	75 - 88	9.19	50 - 58
F-2	Geo-composite	88 - 122.5	24.40	45	N/A	60.25

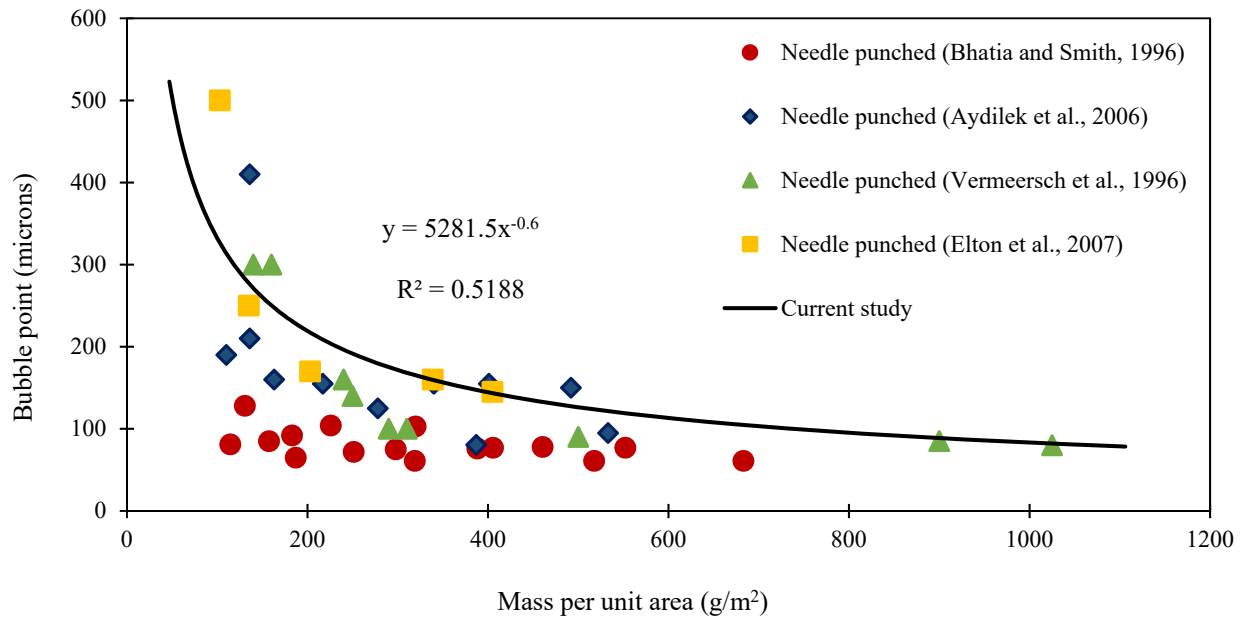
* Provided by the Manufacturers

** Conducted at Syracuse University

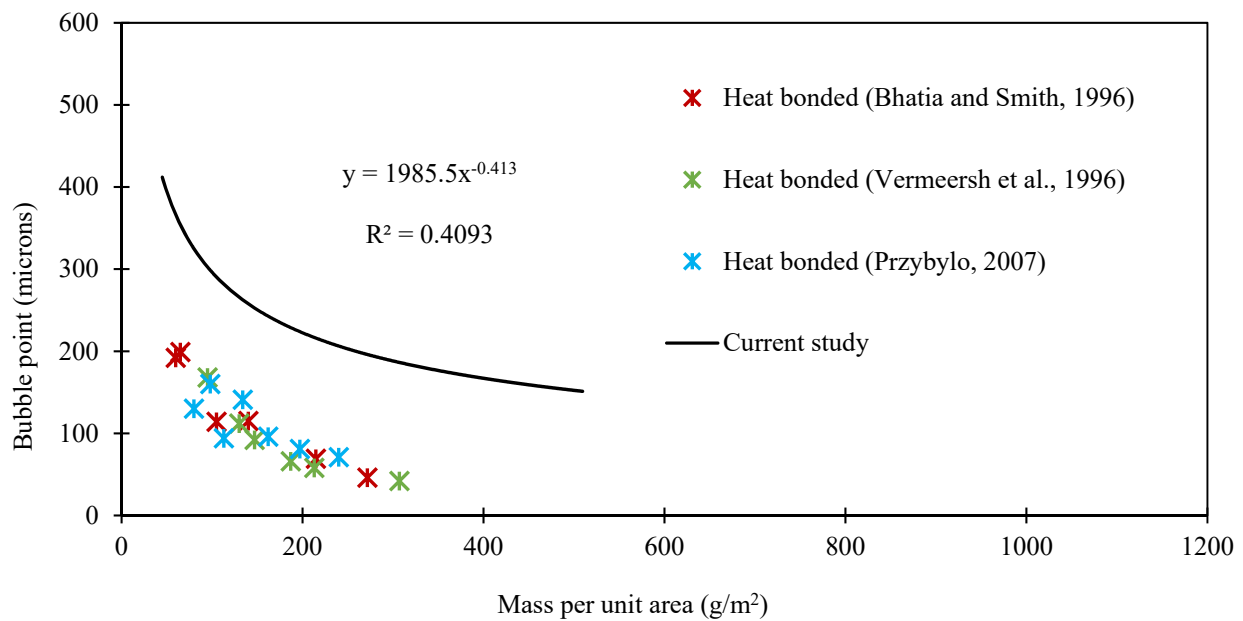
3.6 Previous studies

Bhatia and Smith (1996) showed that the staple fiber, needle-punched nonwoven geotextiles showed the least variation in Capillary flow test results. On the other hand, woven and heat bonded geotextiles with large openings showed a wide variation in Capillary flow test results. They also found that the bubble point, O_{98} of non-woven geotextiles decrease with the increasing mass per unit area (see Figure 3.30). However, woven geotextiles do not behave the same way. Vermeersch et al. (1996) selected 9 continuous filaments, polypropylene needle-punched non-woven geotextiles (mass per unit area = 140 – 1025 g/m²) and 6 continuous filaments, polypropylene heat-bonded non-woven geotextiles (mass per unit area = 95 – 307 g/m²) for capillary flow testing. They used Porofil® as a wetting liquid which has a surface tension of 16 mN/m and 170 Pa (1.28 mmHg) vapor pressure. The bubble point reported in the study was O_{100} instead of O_{98} . Like Bhatia et al. (1996), Vermeersch et al. (1996) also found that the bubble point (O_{100}) of needle punched and heat bonded non-woven geotextiles decreases with the increasing mass per unit area (see Figure 3.30).

Aydilek et al. (2006) used 8 monofilaments, 3 multifilaments and 7 slit film woven geotextiles (102 – 850 g/m²) and 10 needle punched and 1 heat bonded non-woven geotextiles (110 – 533 g/m²) to perform capillary flow test. Aydilek et al. (2006) used a device to perform the Capillary flow test which is manufactured in the University of Washington. The wetting liquid used in the testing was deionized water. They found that the relatively larger pore openings in woven geotextiles created problems during the bubble point test as a sufficient quantity of flow could not be sustained. Aydilek et al. (2006) reported the bubble point as O_{95} instead of O_{98} . They investigate that measured bubble points of non-woven geotextiles decrease with the increasing mass per unit area.



(a)



(b)

Figure 3.30: Bubble point vs. mass/unit area (a) needle-punched, (b) heat-bonded nonwoven geotextiles

Elton et al., 2007 from Auburn University conducted capillary flow test with 5 needle punched non-woven geotextiles (103 – 405 g/m² mass per unit area). The equipment used in the test was manufactured in Auburn University. They investigated that the bubble point results of needle punched non-woven geotextiles decrease with the increasing mass per unit area (see Figure 3.30 (a)).

Przybylo (2007) tested 12 heat – bonded non – woven textiles made of polypropylene (54 - 240 g/m²) with uniform fiber diameters (fiber diameter ranged from 27 to 50 microns in thickness) in his research at Syracuse University. The equipment used in the test was PMI automated CFP-1500 AEDLS-2C. He used Galwick as a wetting liquid for geotextiles (15.9 dynes/cm surface tension and 1/10th vapor pressure of Porewick). During testing a tortuosity factor of 0.715 was used for all textiles. It was found that the bubble points of heat bonded non-woven geotextiles decrease with the increasing mass per unit area (see Figure 3.30 (b)).

From the analysis conducted previously, it was found that the researchers have been using different types of Capillary flow devices in their study. However, in all studies it was reported that for needle punched and heat bonded non – woven geotextiles, the bubble point tends to decrease with the increase in mass per unit area (Bhatia and Smith (1996), Vermeersch et al. (1996), Aydilek et al. (2006), Elton et al. (2007), Przybylo (2007)). It can be noticed that most of the bubble point results obtained from the previous study fall apart from the range of current study. Only the results from Elton et al. (2007), few from Vermeersch et al. (1996) and Aydilek et al. (2006) are close to the range of current study. No such trend was reported for woven geotextiles in any study. These results validate the analysis conducted at Syracuse University.

3.7 Summary

- 20 woven geotextiles, 29 non-woven geotextiles, and 2 geo-composites were used in the Capillary flow test and pore size distribution results with various shapes were obtained for woven and non-woven geotextiles. 9 – 10 tests were conducted for each type of geotextile with individual specimens to obtain consistency in the results. O_{50} and O_{10} were obtained from the pore size distribution along with bubble point, O_{98} . Non-woven geotextiles have small to larger pores which provides “S” shaped pore size distribution. On the other hand, woven geotextiles have similar sized fibers moving over one another which results into almost uniform pore sizes. Therefore, the pore size distribution of woven geotextiles does not look like “S” shaped. The deviation in the test results were also described in the study.
- To find out the minimum and maximum outliers, box plot and whisker diagrams were used in the analysis for 7 kinds of geotextiles (monofilament, slit film, fibrillated fill, and multifilament woven geotextiles, needle punched and heat bonded non-woven geotextiles, and geo-composites). Two monofilament woven, 2 slit film woven, 1 multifilament woven and 9 needle punched non-woven geotextiles showed outliers in the box and whisker diagram.
- From the results plotted for pore openings vs. mass per unit area, it was found that O_{98} , O_{50} and O_{10} of non-woven geotextiles decrease with the increasing mass per unit area. However, no such trend could be found for woven geotextiles. The previous analysis conducted by Bhatia (1996), Vermeersch et al. (1996), Aydilek (2006), Elton et al (2007), and Przybylo (2007) were investigated as well and it was found that the bubble points of

non-woven geotextiles decrease with the increasing mass per unit area which validates the current study.

3.8 References

- ASTM D4404, “Standard Test Method for Determination of Pore Volume and Pore Volume Distribution of Soil and Rock by Mercury Intrusion Porosimetry”, American Society for Testing and Materials, West Conshohocken, Pennsylvania, USA.
- ASTM D6767-16 Standard Test Method for Pore Size Characteristics of Geotextiles by Capillary Flow Test, ASTM International, West Conshohocken, PA, 2014.
- ASTM D4751-16 Standard Test Methods for Determining Apparent Opening Size of a Geotextile, ASTM International, West Conshohocken, PA, 2016.
- ASTM F316, “Standard Test Method for Pore Size Characteristics of Membrane Filters by Bubble Point and Mean Flow Pore Test”, American Society for Testing and Materials, West Conshohocken, Pennsylvania, USA.
- Aydilek, A. H., & Edil, T. B. (2003). Evaluation of woven geotextile pore structure parameters using image analysis. (2003): 1-12.
- Aydilek, A. H., D'Hondt, D., & Holtz, R. D. (2006). Comparative evaluation of geotextile pore sizes using bubble point test and image analysis. (2006): 1-9.
- Bhatia, S.K., Huang, Q. and Smith, J., 1993, “Application of Digital Image Processing in Morphological Analysis of Geotextiles”, Proceedings of Conference on Digital Image Processing: Techniques and Applications in Civil Engineering, ASCE, proceedings of a symposium held in Kona, Hawaii, USA, February-March 1993, 95-108.

- Bhatia, S.K. and Smith, J.L., 1995, “Application of the Bubble Point Method to the Characterization of the Pore-Size Distribution of Geotextiles”, ASTM Geotechnical Testing Journal, Vol. 18, No. 1, 94-105.
- Bhatia, S. K., & Smith, J. L. (1996). Geotextile characterization and pore-size distribution: Part I. A review of manufacturing processes. *Geosynthetics International*, 3(1), 85-105.
- Bhatia, S. K., & Smith, J. L. (1996). Geotextile characterization and pore-size distribution: Part II. A review of test methods and results. *Geosynthetics International*, 3(2), 155-180.
- Bhatia, S. K., & Smith, J. L. (1994). Comparative study of bubble point method and mercury intrusion porosimetry techniques for characterizing the pore-size distribution of geotextiles. *Geotextiles and Geomembranes*, 13(10), 679-702.
- Blond, Eric; Vermeersch, O. G.; and Diederich, Romain (2015). A Comprehensive Analysis of the Measurement Techniques used to Determine Geotextile Opening Size: AOS, FOS, O90, and ‘Bubble Point’. *Geosynthetics 2015*, February 15-18, Portland, Oregon.
- Calhoun, C.C., Jr., 1972, “Development of Design Criteria and Acceptance Specifications for Plastic Filter Cloth”, Technical Report F-72-7, U.S. Army Corps of Engineers Waterways Experimental Station, Vicksburg, Mississippi, USA, 105.
- Cap.Fl.5-12- 09 Capillary Flow Porometer 7.0, Porous Materials Inc.
- Christopher, B.R. and Holtz, R.D., 1985, “Geotextile Engineering Manual”, U.S. Department of Transportation, Federal Highway Administration, Washington, DC, USA, Report No. FHWA-TS-86/203, March 1985, 1044.
- Elsharief, A.H. and Lovell, C.W., 1996, “Determination and Comparison of Structural Properties of Nonwoven Geotextiles”, *Recent Developments in Geotextile Filters and*

Prefabricated Drainage Geocomposites, Bhatia, S.K. and Suits, L.D., Editors, ASTM Special Technical Publication 1281, proceedings of a symposium held in Denver, Colorado, USA, June 1995, in press.

- Elton, D. J., Hayes, D. W., & Adanur, S. (2006). Bubble point testing of geotextiles: apparatus and operation. (2006): 1-8.
- Elton, D. J., & Hayes, D. W. (2007). The Bubble Point Method for Characterizing Geotextile Pore Size. In Geosynthetics in Reinforcement and Hydraulic Applications (1-10). ASCE.
- Fayoux, D., 1977, “Filtration Hydro dynamique des Sols par des Textiles”, Proceedings of the International Conference on the Use of Fabrics in Geotechnics, Vol. 2, Paris, France, April 1977, 329-332. (in French)
- Giroud, J.P., 1982, “Filter Criteria for Geotextiles”, Proceedings of the Second International Conference on Geotextiles, IFAI, Vol. 1, Las Vegas, Nevada, USA, August 1982, 103-108.
- Gourc, J.P., 1982, “Quelques Aspects du Comportement des Géotextiles en Mécanique des Sols”, Thèse de Docteur des Sciences, Université Joseph Fourier, Grenoble, France, 249 (in French).
- Ingold, T.S. and Miller, K.S., 1988, “Geotextiles Handbook”, Thomas Telford Ltd., London, United Kingdom, 152.
- Joseph, M.L., 1981, “Introductory Textile Science”, 4th Edition, CBS Publishing, New York, New York, USA, 406.
- Khachan, M. M. (2016). Sustainable and innovative approaches for geotextile tube dewatering technology. PhD Dissertation. Syracuse University, NY, USA.

- Kiffle, Z. B., Bhatia, S. K., Khachan, M. M., & Jackson, E. K. (2014). Effect of pore size distribution on sediment retention and passing. In 10th International Conference on Geosynthetics, ICG 2014 Deutsche Gesellschaft für Geotechnik e. V.
- Koerner, R. M., & Koerner, G. R. (2014). On the Need for a Better Test Method Than Dry or Wet Sieving to Obtain the Characteristic Opening Size for Geotextile Filter Design Purposes. Geosynthetic Institute's White Paper, 31.
- Kulter, H., 1985, "Non-Woven Bonded Fabrics", Lunenschloss, J. and Albrecht, W., Eds., Ellis Horwood, Ltd., Chichester, United Kingdom, 178.
- Kutay, M. E., & Aydilek, A. H. (2004). Retention performance of geotextile containers confining geomaterials. *Geosynthetics International*, 11(2), 100-113.
- Lawson, C. R. (2008). Geotextile containment for hydraulic and environmental engineering. *Geosynthetics International*, 15(6), 384-427.
- Liao, K., & Bhatia, S. K. (2005). Geotextile tube: filtration performance of woven geotextiles under pressure. *Proceedings of NAGS*, 1-15.
- Lombard, G. and Rollin, A., 1987, "Filtration Behavior Analysis of Thin Heat Bonded Geotextiles", *Proceedings of Geosynthetics '87*, IFAI, Vol. 2, New Orleans, Louisiana, USA, February 1987, 482-492.
- Lydon, R., Mayer, E., & Rideal, G. R. (2004, April). Comparative methods for the pore size distribution of woven and metal filter media. In 9th World Filtration Congress. (1-6)
- Masounave, J., Denis, R. and Rollin, A.L., 1980, "Prediction of Hydraulic Behavior of Synthetic Non-Woven Filter Fabrics Used in Geotechnical Works", *Canadian Geotechnical Journal*, Vol. 17, No. 4, 517-525.

- Moraci, N., Mandaglio, M.C., Salmi, M. (2016). Long term behavior of woven and nonwoven geotextile filters. *GeoAmericas 2016*, vol. 1, 740-749.
- Mori, H., Miki, H., & Tsuneoka, N. (2002). The geo-tube method for dioxin-contaminated soil. *Geotextiles and Geomembranes*, 20(5), 281-288.
- Mlynarek, J., Lafleur, J., Rollin, R. and Lombard, G., 1993, "Filtration Opening Size of Geotextiles by Hydrodynamic Sieving", *ASTM Geotechnical Testing Journal*, Vol. 16, No. 1, 61-69.
- Muthukumaran, A. E., & Ilamparuthi, K. (2006). Laboratory studies on geotextile filters as used in geotextile tube dewatering. *Geotextiles and Geomembranes*, 24(4), 210-219.
- Palmeira, E. M., Fannin, R. J., & Vaid, Y. P. (1996). A study on the behavior of soil geotextile systems in filtration tests. *Canadian Geotechnical Journal*, 33(4), 899-912.
- Palmeira, E. M., & Gardoni, M. G. (2000). The influence of partial clogging and pressure on the behavior of geotextiles in drainage systems. *Geosynthetics International*, 7(4-6), 403-431.
- Prapaharan, S., Holtz, R.D. and Luna, J.D., 1989, "Pore Size Distribution of Nonwoven Geotextiles", *ASTM Geotechnical Testing Journal*, Vol. 12, No. 4, 261-268.
- Przybylo, Lukasz (2007). An investigation of the Bubble Point method and Capillary flow porometry for geotextiles characterization. MS Thesis. Syracuse University, NY, USA.
- Rollin, A.L., Masounave, J. and Dallaire, G., 1977, "Etudes des propriétés hydrauliques des membranes non-tissées", *Proceedings of the International Conference on the Use of Fabrics in Geotechnics*, Vol. 2, Paris, France, April 1977, 201-206. (In French)

- Saathoff, F. and Kohlhase, S., 1986, "Research at the Franzius-Institut on Geotextile Filters in Hydraulic Engineering," Proceedings of the Fifth Congress Asian and Pacific Regional Division, ADP/IAHR, Seoul, Korea, 9-10.
- Satyamurthy, R., & Bhatia, S. K. (2009). Effect of polymer conditioning on dewatering characteristics of fine sediment slurry using geotextiles. *Geosynthetics International*, 16(2), 83-96.
- Siva, U. and Bhatia, S.K., 1993, "Rapid Filtration Performance Tests for Nonwoven Geotextiles with Silty Sands", Proceedings of Geosynthetics '93, IFAI, Vol. 1, Vancouver, British Columbia, Canada, March 1993, 483-500.
- Smith, J. L., & Bhatia, S. K. (1995). Application of the bubble point method to the characterization of the pore-size distribution of geotextiles. 94-105.
- Smith, J.L. (1996). The pore size distribution of geotextiles. MS Thesis. Syracuse University, Syracuse, NY, USA.
- Vermeersch, O. G., & Mlynarek, J. (1996). Determination of the pore size distribution of nonwoven geotextiles by a modified capillary flow porometry technique. In *Recent developments in geotextile filters and prefabricated drainage geocomposites*. ASTM International.
- Washburn, E.W. (1921). Proceedings of the National Academy of Science, Vol. 7, No. 115.

Chapter 4 Bubble Point Results: Correlations

4.1 Introduction

For the last 15 years, extensive studies have been carried out to find a common standard for measuring the largest pore size of geotextiles. However, different standards are used in different countries as a practice to measure the pore sizes of geotextiles. The pore sizes of a geotextile differ based on the variation in standards and devices. In USA, Dry sieving (ASTM D4751) is a common standard to measure the O_{95} (AOS) of geotextiles, which is one of the major properties used to evaluate geotextile retention performance. Despite of the disadvantages (electrostatic effects, clogging of glass beads etc.) encountered with the dry sieving test, in the USA, most of the geotextile filters are designed based on the AOS, O_{95} values. Along with the largest pore, smaller pores also play an important role in the life of geotextile as a filter (Rankilior 1981, Giroud 1982, Christopher and Holtz 1985). Therefore, researchers have been looking for a method to measure the smaller pores as well as larger pores of geotextiles. Besides Dry sieving, Capillary flow test is an approved standard in the US which can provide a complete pore size distribution with the largest pore size (O_{98}) of a geotextile. Despite of numerous advantages of ASTM D 6767, this test is not widely used in USA. Therefore, an ASTM meeting was held at Syracuse University in the summer of May 4th, 2015, having participants from industries and research institution, to come up with a correlation between Dry sieving test and Capillary flow test results.

For the last 20 years, ASTM D 4751 is used to determine the apparent opening size (AOS, O_{95}) of a geotextile in the industries and research institutions. In the current standard of ASTM D4751-16, two methods of calculating pore size of a geotextile are presented; method A covers the determination of AOS, O_{95} by sieving glass beads through a geotextile and method B deals

with the capillary flow test by pressurizing the pores to overcome the capillary attraction. The new addition to the ASTM D 4751, method B follows ASTM D6767 to obtain the pore opening (bubble point, O_{98}) of geotextiles. It means, capillary flow test has already been accepted as an alternative method to dry sieving test for determining the pore size of geotextiles. However, it is noted in the ASTM D4751-16 that the AOS, O_{95} obtained by the dry sieving test may not be precisely identical to the bubble point, O_{98} obtained by the ASTM D6767. Capillary flow test was recommended to use as an alternative test with proper correlation with dry sieving test and established requirements of the test method for distinct types of geotextiles. The testing procedure of capillary flow test is described in ASTM D4751 following ASTM D6767. A set of three capillary flow tests are suggested to establish a correlation between the results obtained by ASTM D4751 and ASTM D6767.

4.2 Correlation between Capillary Flow and Dry Sieving Test

4.2.1 Current study

In this study, Capillary flow test and Dry sieving test results of a wide range of woven ($190 - 1100 \text{ g/m}^2$), non – woven ($88 - 1075 \text{ g/m}^2$) geotextiles and geo-composites ($534 - 879 \text{ g/m}^2$) from different manufacturers, correlation between these two types of test results is obtained. For many geotextiles, the AOS values were provided by the manufacturers. For seventeen geotextiles (2 monofilaments woven, 7 needle punched non-woven, and 8 heat bonded non-woven geotextiles), for which dry sieving test results were not available, dry sieving tests were conducted. The ASTM D4751 was followed to perform the tests. The glass beads was used in the test were standardized according to the ASTM D4751 and 5 to 6 tests were performed for each type of geotextile to obtain the AOS as a range rather than a single number.

Figure 4.1 shows a correlation between bubble point and AOS of a set of 7 monofilament, 11 slit-film and 2 multifilament woven geotextiles. The best fitted line plotted provides an equation to calculate an AOS value for each corresponding bubble point value of the geotextile. The value of R^2 (coefficient of determination) obtained from the plot is 0.62. R^2 is a statistical measure which determines the degree of explanation of how the output variable is equivalent to the input variable. $R^2 = 0.62$ means 62% AOS values obtained from the test are comparable to the bubble point values. The best fitted line should not be extended beyond a certain bubble point value (293 microns). Beyond this limit, the correlation is not valid because no result exists below the range.

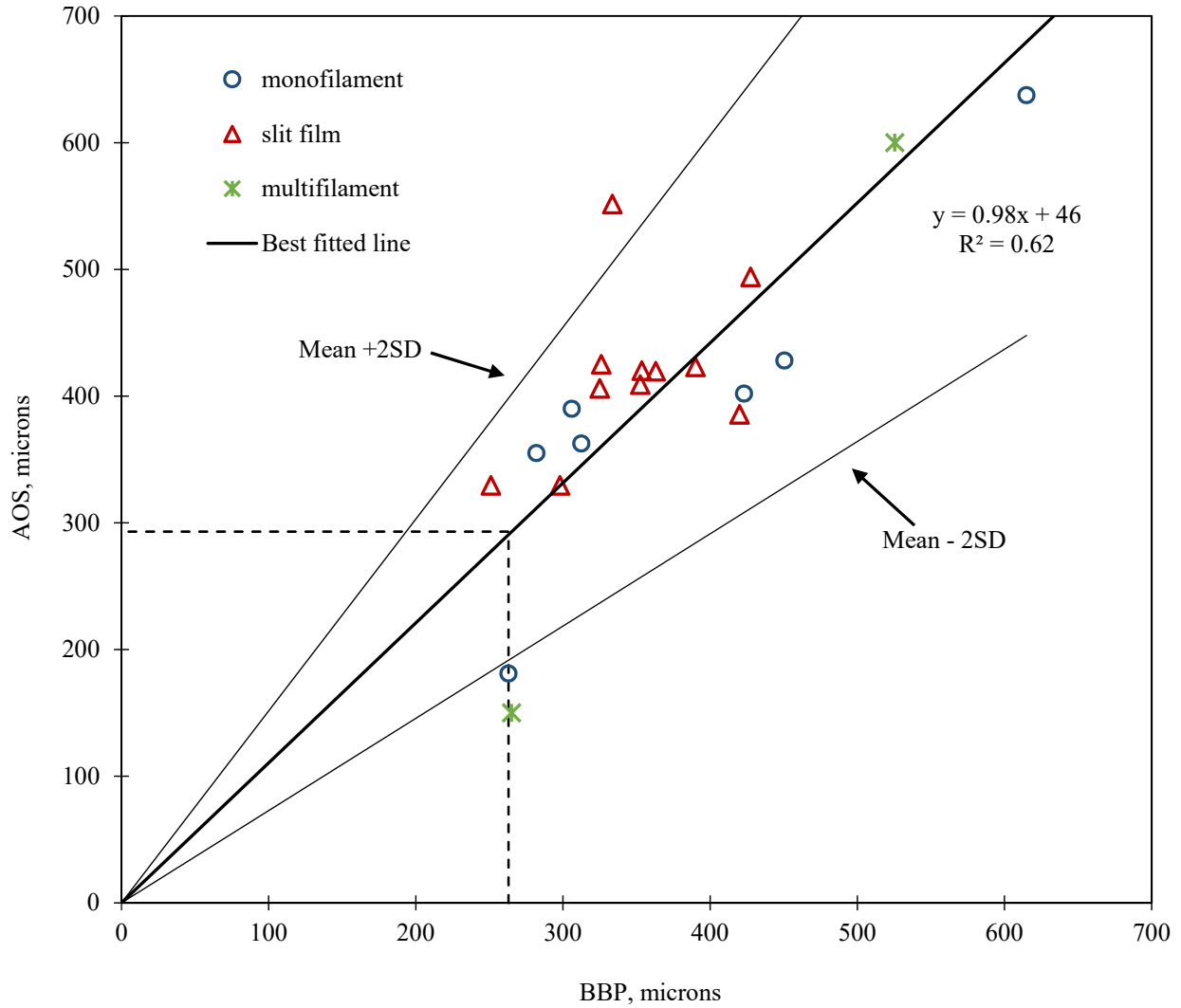


Figure 4.1: Correlation between Bubble Point and AOS of Woven Geotextiles

The best fitted line shows a positive slope which indicates an increasing trend of AOS corresponding to bubble point for each monofilament geotextile. In Figure 4.1, the range of AOS and bubble point values are presented with mean \pm 2SD (a band around the mean with a width of two standard deviations). According to the three-sigma rule of thumb, mean \pm 2SD is called 95% confidence level as well. Figure 4.1 shows that 1 out of 2 multifilaments has the smallest bubble point and one monofilament has the largest bubble point value. The equation presented with the best fitted line provides comparable AOS against a bubble point for each woven

geotextile. For any bubble point in the equation, $y = 0.98x + 46$, provides a larger AOS of a woven geotextile. If bubble point of a woven geotextile is 300 microns, using the equation from Figure 4.1 the AOS can be obtained as follows:

$$y = 0.98 * x + 46$$

$$\text{AOS, O95} = 0.98 * 300 + 46 = 340 \text{ microns}$$

Theoretically 15 out of 20 geotextiles showed larger AOS values than the bubble point values. However, 3 monofilament (A-2 to A-4) and 1 multifilament (C-1) woven geotextiles provided smaller AOS values than bubble point values. Therefore, the correlation for all woven geotextiles presented in this study, should not be considered valid for all types of woven geotextiles, there might be some deviation which should be evaluated properly.

Relationship between Bubble Point and AOS of 8 heat bonded and 21 needle punched non-woven geotextiles is shown in Figure 4.2. A best fitted curve represented with a linear equation, $y = 0.97x - 13$, provides a positive correlation with 61% possibility to obtain AOS results comparable to the corresponding bubble point result of each non-woven geotextile (see Figure 4.2). Any bubble point in the equation provides a smaller AOS for a non-woven geotextile.

However, based on the capillary flow and dry sieving test results, 5 out of 8 heat bonded (D-1 to D-4 and D-6) and 6 out of 21 needle punched (E-2, E-3, E-7, E-10, E-11, and E-15) non-woven geotextiles had larger AOS values than bubble point. It was also noticed that for heat bonded geotextiles, a small range of bubble point (181 – 356 microns) provided a broad range of AOS (100 – 477.5 microns). However, for needle punched geotextiles, the range of bubble point is 124 – 416 microns and AOS is 75 – 362.5 microns respectively. The range of possible AOS and bubble point values were showed with mean \pm 2SD. Beyond a value of 105 microns of bubble

point and 75 microns of AOS, the correlation is not reliable for any heat bonded and needle punched non-woven geotextile because no result is available in the correlation below this limit.

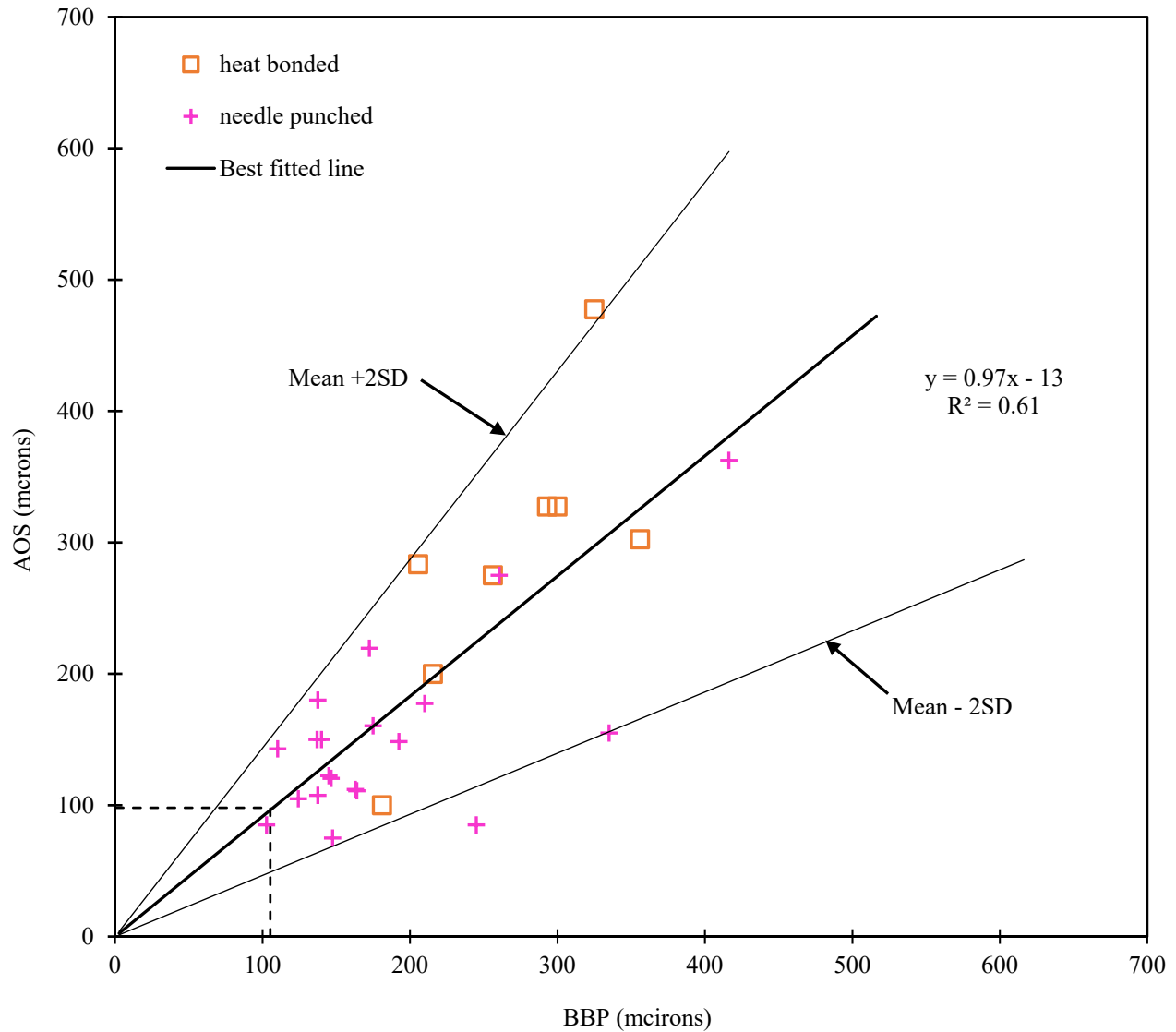


Figure 4.2: Correlation between Bubble Point and AOS of Non- Woven Geotextiles

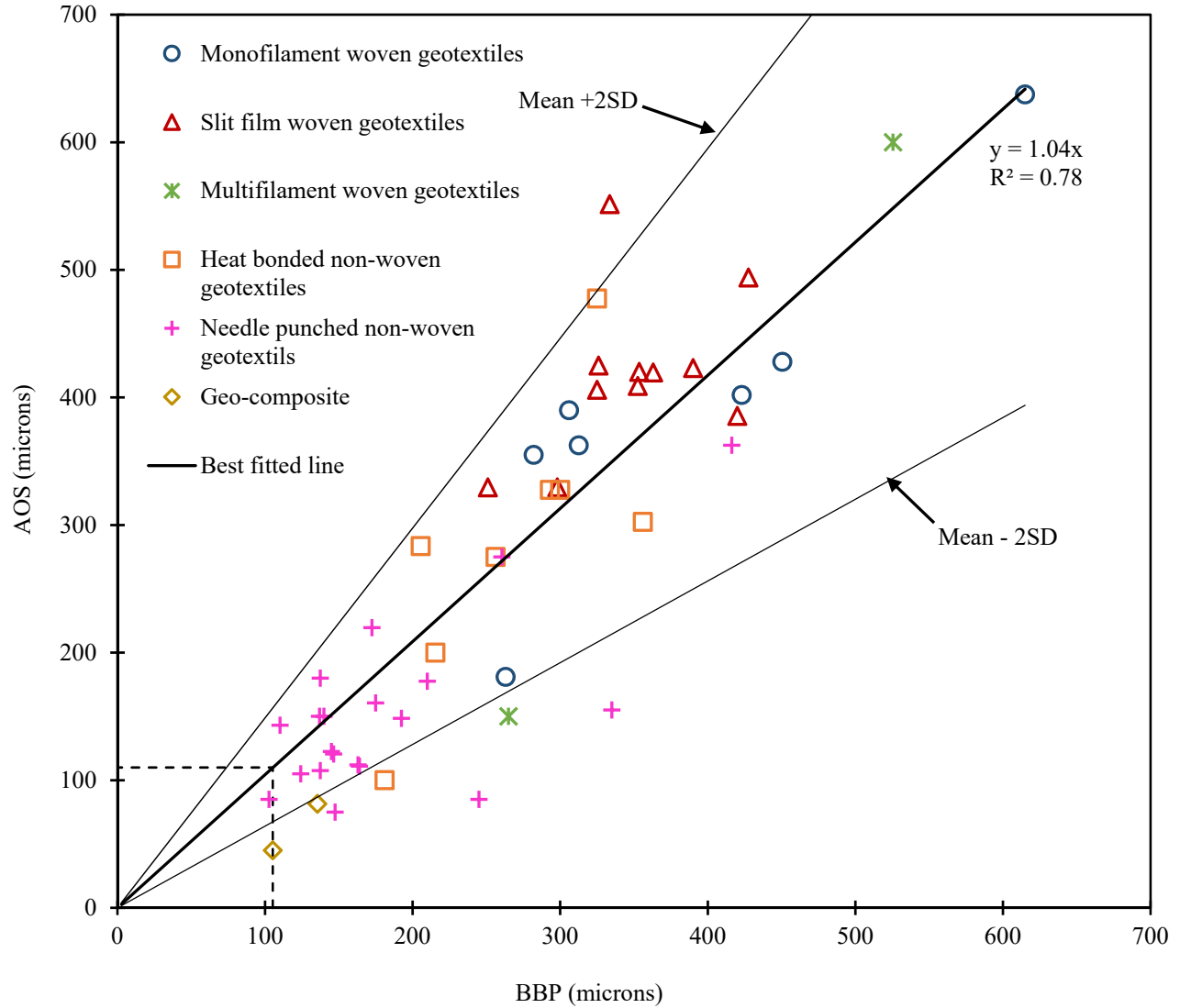


Figure 4.3: Correlation between Bubble Point, O_{98} and AOS, O_{95} of All Geotextiles

Figure 4.3 showed a correlation between bubble point and AOS for all 51 geotextiles (a combination of woven, non-woven and composite geotextiles). A positive linear relation is found with an increasing trend of AOS corresponding to a bubble point for each geotextile irrespective to manufacturing process (woven or non-woven). However, based on the test results, not all geotextiles provided larger AOS compared to bubble point value. For the tested geotextiles, 26 out of 51 geotextiles provided larger AOS results than the equivalent bubble point results. A

value of 0.78 of R^2 indicates that 78% AOS results can be justified precisely corresponding to the bubble point results. Mean \pm 2SD plotted in Figure 4.3 provided the range of maximum AOS and bubble point values. The combined plot shows that monofilament geotextiles have a wide range of bubble point and AOS results. On the other hand, the results of needle punched non-woven geotextiles are in the narrow range (between 100 to 300 microns). The least bubble point and AOS values are provided by a geo-composite.

4.2.2 Previous studies

Few studies have been conducted to correlate the bubble point with AOS for both woven and non-woven geotextiles. However, different devices and saturating liquids were used in the tests. Due to the variation in device and saturating liquids, different conclusions have been made from the correlation. Table 4.1 summarizes the details of some of the previous studies. In Figure 4.4 the bubble point and AOS results of previous studies are compared with the current study.

Table 4.1: Previous Studies (Bhatia and Smith (1996), Elton et al. (2006), Aydilek et al. (2006), TENCATE (2015))

Reference	Equipment	Liquid	Geotextile	Mass per unit area (g/m ²)	Bubble point, O ₉₈ (microns)	AOS, O ₉₅ (microns)
Bhatia and Smith (1996)	PMI automated Perm-Porometer (Model No. APP-200)	Porewick with a surface tension of 0.0163 g/cm	4 slit film woven geotextiles	155.27 – 397.06	115 – 407	321 – 494
			2 multifilament woven geotextiles	407.67 – 687.86	158 - 183	200 – 346
			16 needle-punched non-woven geotextiles	114.6 – 683.05	61 - 128	67 – 260
			6 heat-bonded non-woven geotextiles	59.8 – 271.65	46 - 199	63 - 571
Elton et al. (2006)	Device designed by the research institution	No information was found	2 needle-punched non-woven geotextiles	203 – 339	160 – 170	360 - 370

Aydilek, et al. (2006)	Device manufactured in the University of Washington	Water	8 monofilament woven geotextiles	120 – 490	295 – 920	212 – 650
			7 slit film woven geotextiles	102 – 291	190 – 585	212 – 425
			3 multifilament woven geotextiles	257 – 850	285 – 920	150 - 600
			11 needle-punched non-woven geotextiles	110 – 533	80.5 – 410	106 - 300
TENCATE (2015)	PMI porometer	No information was found	8 monofilament woven geotextiles (woven	No information was found	277 – 421	300 - 425

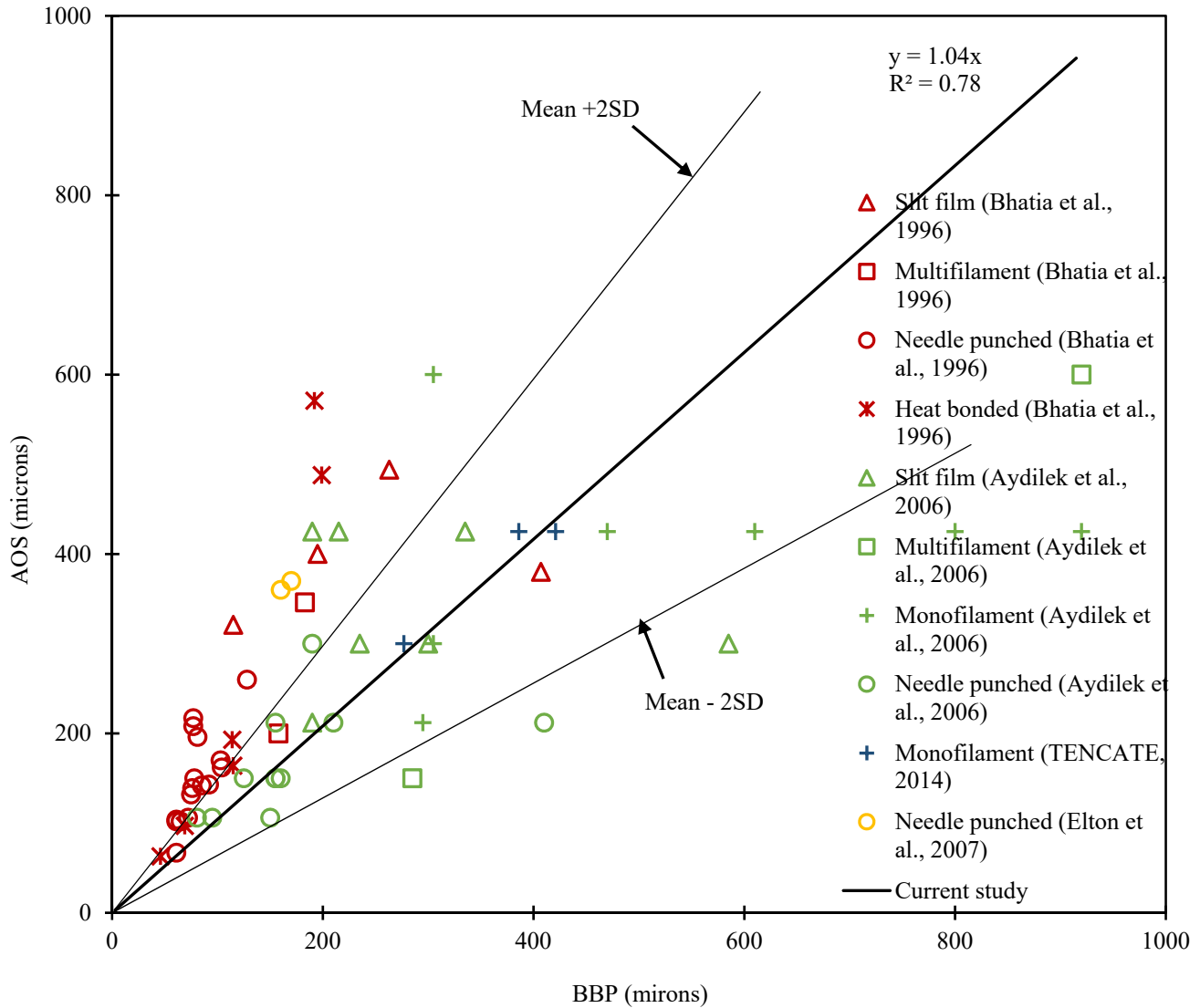


Figure 4.4: Correlation between Bubble Point, O_{98} and AOS, O_{95} of All Geotextiles (Bhatia et al. (1996), Aydilek et al. (2006), Elton et al. (2007) and TENCATE (2014))

Figure 4.4 showed a correlation between bubble point and AOS results of all geotextiles tested by Bhatia et al. (1996), Aydilek et al. (2006), Elton et al. (2007) and TENCATE (2014)). The results obtained by Aydilek et al. (2006) were mostly scattered and provided the largest range of bubble point (80 – 610 microns). The results obtained by Bhatia et al. (1996) showed least variation in the bubble point results. The straight line plotted with an equation, $y = 1.04x$ and R^2

= 0.78, showed the test results of Capillary flow and Dry sieving test obtained in the current study. The results of mostly non-woven geotextiles (except Elton et al., 2006) in the previous study are close to the current study, results of few heat bonded non-woven geotextiles performed by Bhatia et al. (1996) fall in the range of current study. The woven geotextiles (monofilament, slit film and multifilament) are falling apart from the test results in the current study. Bhatia et al. (1996) and Elton et al. (2006) showed an increasing trend of AOS in their results compared to bubble point. The results obtained by Aydilek et al. (2006) do not show the similar trend of increasing AOS for all geotextiles. The range of maximum AOS and bubble point values were shown with mean +/- 2SD, which represents 95% confidence level (three-sigma rule of thumb). Most of the results obtained by Bhatia et al. (1996) and Elton et al. (2007) did not fall into the range of 95% confidence level of current study.

4.3 Comparison of Filtration Opening Size and Bubble Point

Based on a large number of experimental data and theoretical concepts, Giroud (1996) established a mathematical equation which relates fiber diameter, fiber density, porosity and thickness of a geotextile with the pore opening (filtration opening) of non-woven geotextile. The equation is as follows:

$$\frac{O_F}{d_f} \approx \frac{1}{\sqrt{1-n}} - 1 + \frac{10n}{(1-n) t_{GT} / d_f} \quad 4.1$$

Where, O_F = filtration opening size, mm

d_f = diameter of fiber, mm

t_{GT} = thickness of a non-woven geotextile, mm

n = porosity of a non-woven geotextile

On the right side in the equation, the factor 10 was obtained through calibration with many experimental data. The porosity (n) of a non-woven geotextile can be calculated using the following equation.

$$n = 1 - \frac{\mu_{GT}}{\rho_f t_{GT}} \quad 4.2$$

Where, μ_{GT} = mass per unit area of non-woven geotextile, g/m^2

ρ_f = density of fiber, g/m^3

t_{GT} = thickness of non-woven geotextile, m

The theoretical filtration opening (O_f) size of 21 needle punched non-woven geotextiles were calculated using the equation 4.1 given by Giroud, and compared with the pore opening, O_{98} obtained by the Capillary flow test. For all non-woven geotextiles, the mass per unit area and thickness of geotextiles were measured at Syracuse University (see Table 4.2). The fiber diameter information was collected from the manufacturers and a typical fiber density (density of Polypropylene = 946 kg/m^3 , <https://en.wikipedia.org/wiki/Polypropylene>) was used in the analysis. Table 4.2 shows the physical properties of the non-woven geotextiles used to calculate the filtration opening sizes. Since all geotextiles were made of polypropylene, fiber density was used as 946 kg/m^3 for the calculations. Equation 4.2 was used to calculate the porosity of the non-woven geotextile which used mass per unit area and thickness of geotextile and fiber density. In Figure 4.5, the filtration opening size (O_f) and O_{98} are plotted against the mass per unit area of non-woven geotextiles. As it can be seen that for lighter geotextiles, the bubble point (O_{98}) values are generally larger than the filtration opening sizes and the difference decreases with increasing mass per unit area. A correlation in the pore openings is plotted in Figure 4.5 and Figure 4.6 respectively.

Table 4.2: Physical Properties of Non-Woven Geotextiles

Geotextiles	Mass per unit area, g/m ²	Thickness, mm	Diameter of fiber, microns	Porosity, n
E-1	147	0.765	38.5	0.796
E-2	154.5	0.765	36.7	0.786
E-3	230.5	1.095	38.5	0.777
E-4	163.5	0.855	38.5	0.797
E-5	239.5	1.17	45	0.783
E-6	254.5	0.945	40	0.715
E-7	220	1.095	38.5	0.787
E-8	278.5	1.365	38.5	0.784
E-9	287	1.74	32	0.825
E-10	296.5	1.24	36	0.747
E-11	297.5	0.925	38.5	0.660
E-12	327	1.34	38.7	0.742
E-13	332.5	1.755	38.5	0.799
E-14	387	2.54	38.5	0.838
E-15	386	1.67	38.5	0.755
E-16	447	2.005	40	0.764
E-17	461.5	2.03	36	0.759
E-18	559	2.685	38.5	0.779
E-19	540.5	3.795	38.5	0.849
E-20	596.5	3.745	35	0.831
E-21	1006	5.85	38.5	0.818

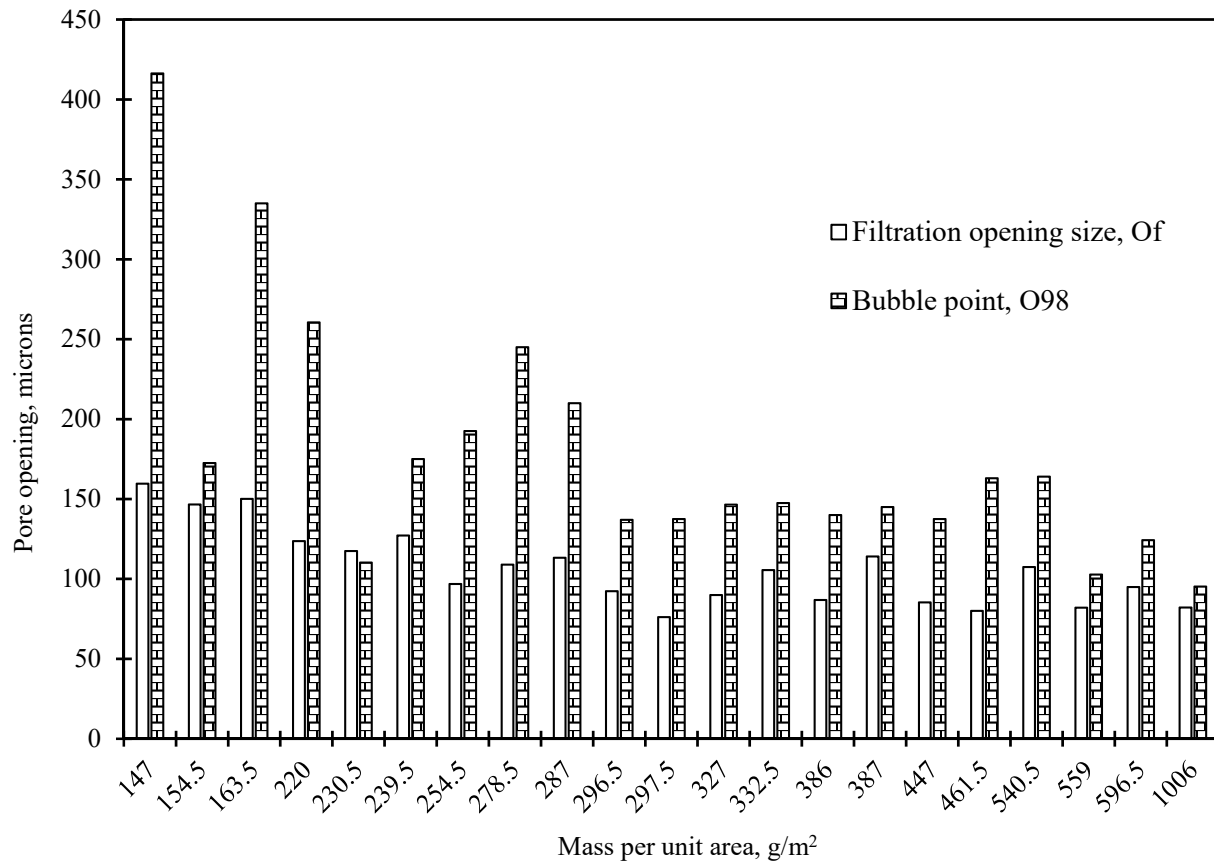


Figure 4.5: Theoretical and Measured Pore Openings vs. Mass Per Unit Area of Needle Punched Non-Woven Geotextiles

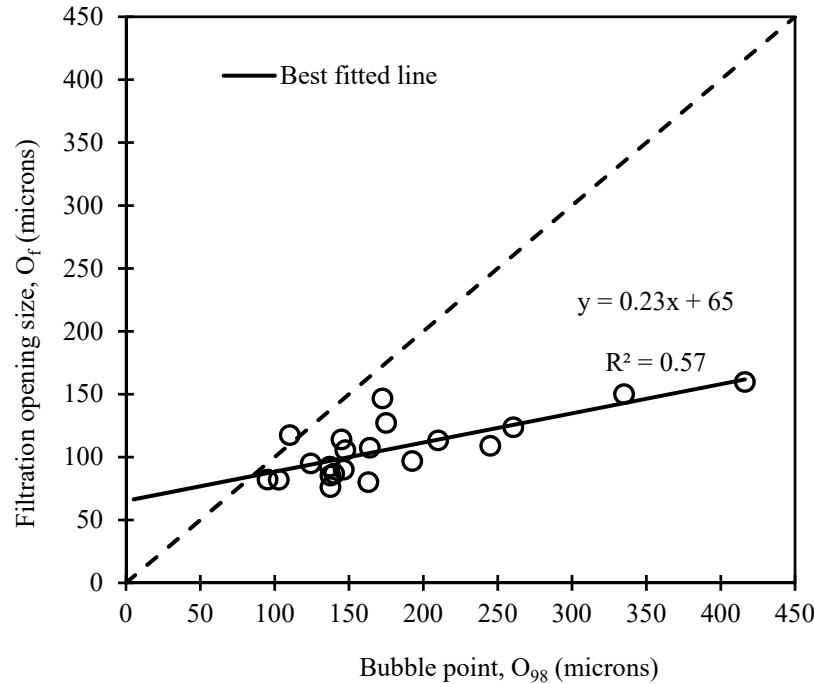


Figure 4.6: Bubble Point vs. Theoretical Pore Openings of Needle Punched Non-Woven Geotextiles

A correlation between O_f and O_{98} is given in Figure 4.6 and it can be seen that only 57% filtration opening sizes could be predicted from the bubble points, however, for several geotextiles, the bubble point is two times larger than the filtration opening sizes. It can be seen that the difference between bubble point and filtration opening size increases with the increasing bubble point values. The geotextiles with smaller O_{98} showed less variation with filtration opening size than the geotextiles with larger O_{98} values.

4.4 Performance Tests

The proper utilization of water bodies and related infrastructures including drainage channels, reservoirs, lagoons, ponds and lakes etc., require an extensive and improved knowledge for the dewatering of dredging sediments. Geotextiles are predominantly used for dewatering high water slurries and proved to be the most time and cost efficient way (Barrington et al. 1998; Henry et al. 1999; Fowler et al. 2002; Mori et al. 2002). For this purpose, several methods have been using

including pressurized and non-pressurized techniques to dewater the dredged sediments. The water content of these dredged sediments can be as high as 800% and very low shear strength before dewatering (Pilarczyk 2000, Moo-Young et al. 2002). To ensure high tensile strength to carry the high-water content sediments, the high tensile strength woven geotextiles are seamed together to manufacture the geotextile tubes. The sediments are pumped into the tubes as a slurry and allowed to settle down and the water filters through the pores of the geotextile tubes. The pore sizes of the geotextile tubes play an important role in dewatering. The dewatering of fine grained sediments may cause excessive piping due to the large pores of geotextile tubes, therefore, the geotextiles are selected carefully during the manufacturing of tubes. To ensure the long-term performance of geotextile tubes, two major factors including soil piping and clogging are important. The geotextile should be selected in a way that it will not be clogged and soil piping will be minimal. Therefore, soil retention is an important criterion, especially in a case of high water content slurries. In addition, the formation of filter cake during dewatering plays a crucial role in filtration, since it controls the piping of fine grained materials, provides soil retention and prevents excessive clogging of the filter. Several methods are used to evaluate the filter cake formation and its properties including, Pressure filtration test (Montero and Overmann (1990); Moo-Young et al. (1999); Moo-Young et al. (2002); Aydilek and Edil (2002, 2003); Kutay and Aydilek (2004); Liao and Bhatia (2005)), Hanging bag test (Baker et al. (2002); and Falling head dewatering test (Huang and Luo (2007)), etc.

In this study, relationships between geotextile filter performance and its relationship to pore openings is evaluated by conducting two different types of tests: 1-D filtration (Falling-head test) and Pressurized 2-D test. The falling-head tests were performed with 6 woven and 6 non-woven geotextiles which have similar O_{98} but different pore size distributions. The 2-D tests were

performed with 1 slit film and 1 multifilament woven geotextiles, 2 geo-composites, 6 needle-punched non-woven geotextiles. The selected geotextiles had a range of pore size distribution and permutableabilities.

4.4.1 1-D Filtration Test (Falling Head Test)

Several studies have been carried out to evaluate dewatering and sediment retention of high water content slurries with a variety of geotextiles using falling-head test (Kutay and Aydielk (2004); Liao and Bhatia, (2005); Muthukumaran and Ilmaparuthi (2006); and Kiffle et al. (2014)). According to Kutay and Aydielk (2004), the retention performance of a geotextile tube depends on several factors including apparent opening size (AOS, O₉₅), permittivity, and water content of slurry. Kiffle et al. (2014) study was the only one that investigated the role of pore size distribution of geotextiles on sediment retention of high water content of slurries. However, their study was limited to 2 pairs of geotextiles only.

Many researchers have developed sediment retention and geotextile clogging criteria for both woven and non-woven geotextiles for high water content slurries. For the retention purpose, the larger pore sizes of geotextiles (O₅₀ – O₉₅) and particle sizes (d₅₀ – d₉₅) are usually used. The clogging criteria include small pore openings of geotextiles (O₄₀) and sediments (d₁₅). Moo-Young and Tucker (2002) used three high strength woven geotextiles (two are made of polypropylene and one is made of polyester fiber) of AOS of 212 – 425 microns, to perform vacuum filtration test to evaluate the filtration and retention capacity of geotextiles. The high-water content (250%, 500%, and 1200%) slurries were used. The range of the piping rate reported was 25 – 2173 g/m², which was less than the piping rate limit of 2500 g/m² (Lafleur et al., 1989). Moo-Young and Tucker (2002) also investigated that as a clogging criterion, the

allowable range of percent open area (POA) of woven geotextile is 1 – 5 percent. No further information was available for the measurement of clogging.

Aydilek (2006) used 4 monofilament, 4 slit film and 1 multifilament woven geotextiles of O_{95} of 130 – 665 microns to evaluate the filtration performance of soil-geotextile system using RETAIN and compare with the laboratory soil-geotextile filtration tests. The soil used in the test was silty sand (USCS classification) with a specific gravity of 2.67. No further information was found for soil, water content and laboratory test. The range of measured and predicted piping rate were 100 – 3900 g/m² and 471 – 4809 g/m² respectively. The clogging of geotextile was measured by comparing the ratio of permeability of clean and clogged geotextiles.

Muthukumaran et al. (2006) used 4 woven geotextiles (90 – 600 microns AOS) to perform the Standard Filtration test with unidirectional flow. The sediments used in the test including harbor sediments and fly ash to prepare the slurry with 80% - 320% water content. The following retention criteria were proposed by Muthukumaran et al. (2006): AOS of the geotextiles ≤ 425 microns; $40 < AOS/d_{15} < 125$; and $0.3 < AOS (d_{85}/d_{15}) < 1.7$.

Liao and Bhatia (2008) used one high strength polypropylene monofilament woven geotextile ($O_{95} = 443$ microns) and two high strength polyester multifilament woven geotextiles ($O_{95} = 218$ - 307 microns) to perform pressure filtration test using three soils (Cayuga Lake sediments, Ottawa clean sand, and silt) with a water content of 100%, 200%, 300% and 400%. They found that the filtration efficiency of the coarse-grained materials decreases a little bit (3%) with the increasing water content (100% - 400%), however, the filtration efficiency of fine-grained materials decreases 10% with the increasing water content (100% - 400%). The range of piping obtained in the test was reported as 152.64 – 252.48 g/m² and piping increases with the increasing pressure.

Palmeira and Gardoni (2000) used eight needle punched non-woven geotextiles (60 – 500 microns FOS) to evaluate the behavior of partially clogged geotextiles using compressibility, transmissivity and permittivity tests. The soil sediments used in the clogging tests included residual quartzite soil, sand, clayey sand, 4 types of glass beads. Several tests including vibration (laboratory test), water flow, compaction (laboratory and field tests) were used to clog the geotextiles. The range of impregnation level or degree of clogging (ratio of mass of soil particles in the geotextile voids and mass of geotextile fibers) reported was 0.2 to 15.0. The large values of degree of clogging were obtained when vibration was applied to clog the geotextiles.

Palmeira and Galvis (2016) used 7 needle punched non-woven geotextiles (200 – 1800g/m² mass per unit area and 60 – 130 microns FOS) to evaluate the behavior of partially clogged geotextiles with glass beads using vibration to favor the penetration of beads in the voids. The range of impregnation level or degree of clogging reported was 0.5 to 3.0. It was found that the degree of clogging decreased with the increasing O_{95}/d_f and O_{98}/d_f where, d_f = diameter of fiber ($d_f = 0.027$ mm for geotextile).

Table 4.3 shows the existing criteria followed to select geotextile filter for high water content sediments.

Table 4.3: Geotextile Filter Selection Criteria with High-Water Content Slurry

Criteria	Soil and Geotextile type	Reference
Retention: $O_{95}/D_{85} < 1$ Clogging: POA (%) = 1-5	Sandy or silty slurry; Woven geotextile	Moo-Young and Tucker (2002)
Retention: $O_{95} < 0.3$ mm or $O_{90}/D_{90} = 2-5$	Clayey slurry; Woven geotextile	Moo-Young and Tucker (2002)
Retention: $O_{85}/D_{50} < 1$ for all POA	Silty sand slurry; Woven geotextile	Aydilek (2006)
Clogging: $O_{40}/D_{15} > 1$ for POA < 8 $O_{40}/D_{30} > 1$ for POA > 8	Silty sand slurry; Woven geotextile	Aydilek (2006)
AOS < 0.425 mm $40 < AOS/D_{15} < 125$	Silty slurries; Woven geotextile	Muthukumaran and Ilmaparuthi (2006)

0.3<AOS x D85/D15 <1.7		
Filtration efficiency decreases 3% with increasing water content, 100% - 400%	Coarse-grained	Liao and Bhatia (2008)
Filtration efficiency decreases 10% with increasing water content, 100% - 400%	Fine-grained	Liao and Bhatia (2008)

To further investigate the influence of a complete pore size distribution on the soil retention performance of a geotextile with high water content slurries, 1-D filtration tests (Falling head test) were conducted on 6 pairs (3 pairs of woven and 3 pairs of non-woven geotextiles) having similar bubble point (O_{98}) but different pore size distribution (see Table 4.4 and Figure 4.7).

Table 4.4: Physical properties of geotextiles used in the test

Pairs	Geotextiles	Manufacturing process	Thickness (mm)	Bubble point, O_{98} (microns)	O_{50} (microns)	O_{10} (microns)	Permittivity (sec^{-1})
1	A-5	Woven	0.82 – 0.89	285 – 340	200	170	0.9
	A-7	Woven	0.48 – 0.49	252 – 360	280	250	0.96
2	A-4	Woven	0.74 – 0.82	400 – 501	430	390	1.5
	B-8	Woven	1.04 – 1.25	375 – 480	377	277	0.4
3	B-3	Woven	0.83 – 0.88	315 – 411	200	127	0.9
	B-5	Woven	1.1 – 1.15	305 – 400	275	210	0.9
4	E-10	Non-woven	1.14 – 1.34	107.5 – 166.5	65	37	1.4
	E-17	Non-woven	1.93 – 2.13	107.5 – 167.5	75	45	0.8
5	E-12	Non-woven	1.18 – 1.5	122.5 – 170.5	70	40	0.8
	E-14	Non-woven	2.2 – 2.88	132.5 – 157.5	90	57	1.0
6	E-16	Non-woven	1.87 – 2.14	121 – 205	85	45	0.7
	E-19	Non-woven	3.47 – 4.12	140.5 – 187.5	103	50	0.9

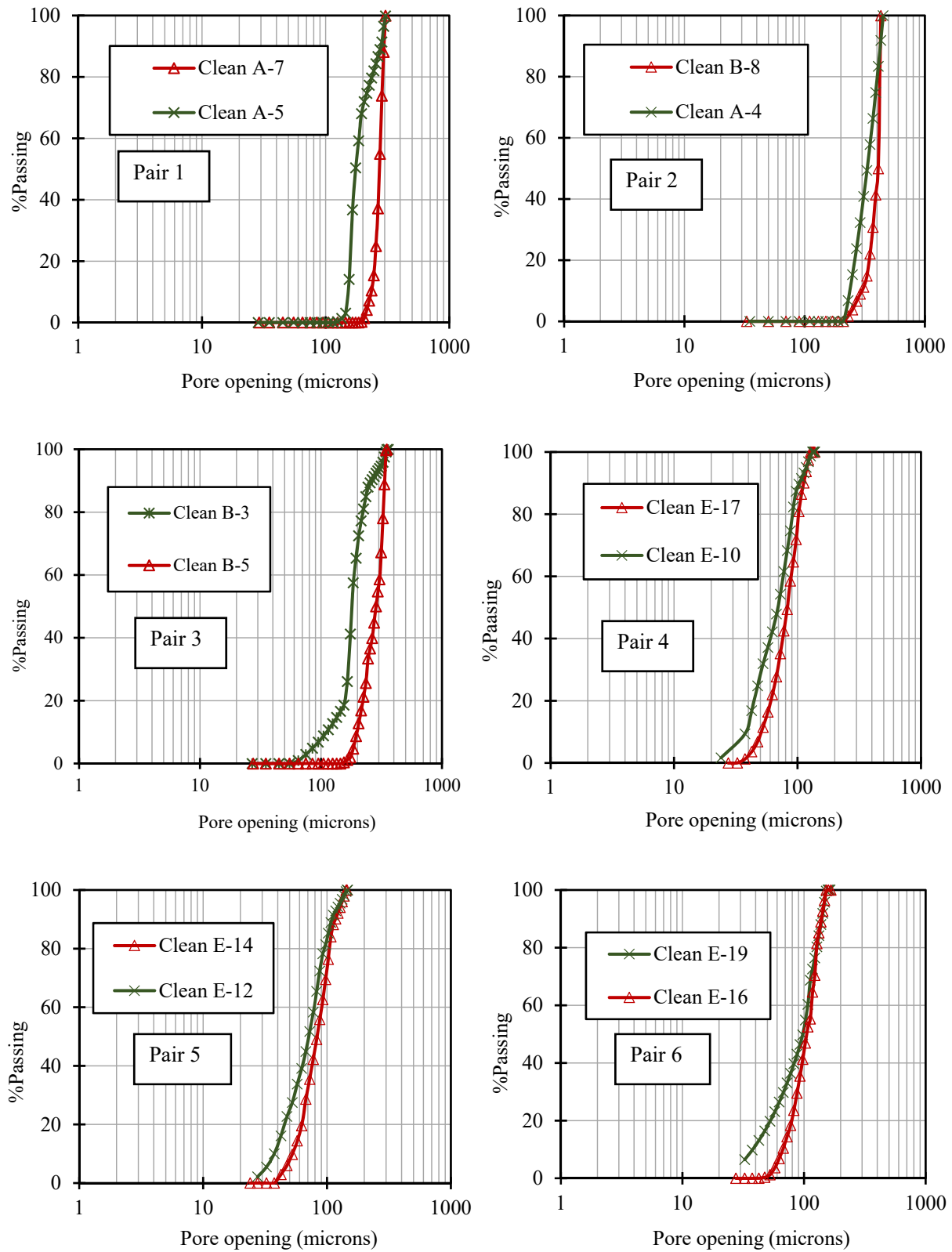


Figure 4.7: Pore Size Distribution of Six Pairs of Geotextiles used for 1-D Filtration Test

The soil sediments used in this test were obtained from U.S. Silica and local aggregate quarry in Syracuse area, identified as Standard silica and Tully silt respectively. Silica sand is standardized by ASTM C-778-03, 20/30 silica type. On the other hand, Tully silt includes 20% coarse fraction particles passing through US standard sieve No. 80 (180 microns), and the remaining 80% particles passing through sieve No. 200 (75 microns) (Satyamurthy and Bhatia, 2009). A slurry with 50% standard silica and 50% Tully silt were made and physical properties of the slurry are provided in Table 4.5.

Table 4.5: Properties of Slurry (50% Standard Silica and 50% Tully Silt)

D ₁₀ (microns)	D ₁₅ (microns)	D ₃₀ (microns)	D ₅₀ (microns)	D ₆₀ (microns)	D ₈₅ (microns)	C _u	C _c
14	30	75	175	312	1060	22.29	1.29

*C_u, coefficient of uniformity = d_{60}/d_{10} and *C_c, coefficient of curvature = $(d_{30})^2/(d_{10} \times d_{60})$

In this test, 600 ml of w% = 882.35% (10% solid content), w% = 400% (20% solid content) and w% = 232.56% (130% solid content) water content, solid slurry was mixed using a jar test apparatus for 3 minutes. A cylindrical reservoir (72 mm diameter and 170 mm height) is used in the test holding 600 ml slurry and a threaded base that secures the geotextiles specimen (8.5 cm diameter) over a perforated steel plate and controls the effluent flow. Before starting the test, the geotextile is saturated with distilled water to ensure spontaneous flow of fluid. The valve was closed to secure the formation of filter cake on retention. After mixing the slurry properly, the mixture was poured into a test tube immediately and the valve was remained closed until the filling process was done. The details of the test setup and equipment are discussed by Khachan, 2016. The drainage continued until no further flow was identified from the filtrate. No pressure

was applied in the test. During the test, the flow was measured with a scale, A&D EW-12KI and the data was recorded in a computer in every 5 seconds (see Figure 4.8).

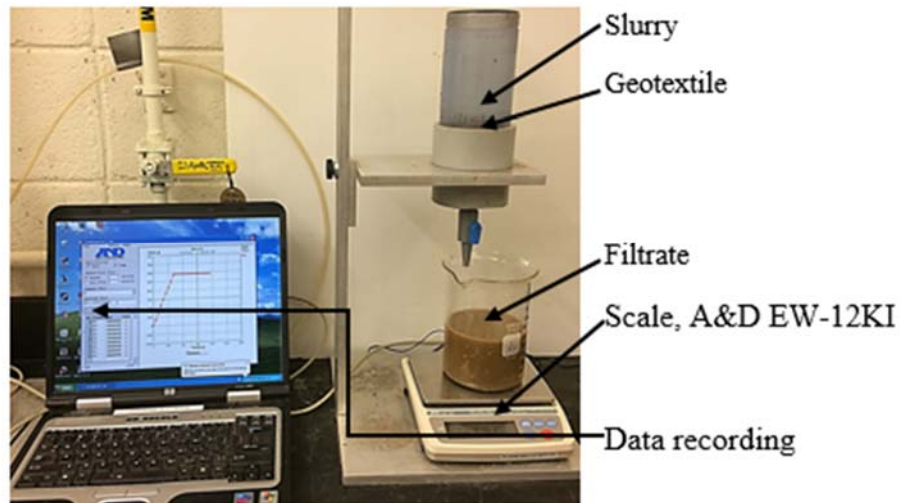
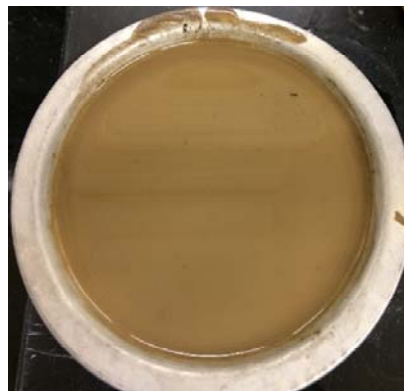


Figure 4.8: 1-D Filtration Test Setup

Upon completion of the test, dewatering rate, filter cake percent solids, filter cake water content, and soil loss were evaluated. The clogged geotextiles were saved and dried for 24 hours to perform capillary flow test and obtain the degree of clogging. From the filtrate, total mass of the sediments piping was calculated. After the test was completed, the filter cake was collected in a can and its weight was measured using A&D EW-12KI (see Figure 4.9).



$$w\% = 232.56\%$$

Figure 4.9: Filter Cake Obtained from the Test with E-19

The percentage of soil loss is defined as the ratio of dry weight of soil passing through geotextile and initial total weight of dry soil in the 600-ml slurry, expressed in percentage.

$$\% \text{ Soil loss} = \frac{\text{total dry weight of soil passing through geotextile}}{\text{total initial weight of dry soil}} * 100 \quad 4.3$$

Along with the % soil loss, from the falling-head test, piping rate and degree of clogging were calculated in this study.

$$\text{Piping rate} = \frac{\text{total dry weight of soil passing through geotextile}}{\text{cross-sectional area of geotextile}} \text{ g/m}^2 \quad 4.4$$

$$\text{Degree of clogging} = \frac{\text{mass of soil particles in the geotextile voids}}{\text{mass of geotextile fibers}} \quad 4.5$$

The results of the 1-D filtration tests for water content of 882.35%, 400% and 232.56% are provided in Table 4.6.

Table 4.6: 1-D Filtration (Falling-Head Test) Test Results

w% = 882.35% (10% Solid content)						
Geotextiles	% Soil loss		Piping rate (g/m ²)		Water content in filter cake (%)	
	Trial 1	Trial 2	Trial 1	Trial 2	Trial 1	Trial 2
A-5	22.21	22.64	2661.26	2714.13	27.06	26.58
A-7	26.76	16.94	3207.61	2030.31	29.21	33.11
A-4	18.39	22.87	2204.79	2740.57	33.73	37.31
B-8	21.1	18.7	2528.73	2241.09	32.5	26.75
B-3	24.17	20	2897.43	2396.89	30.67	31.42
B-5	21.76	23.82	2608.39	2855.13	29.85	26.47
E-10	14.4	16.77	1722.59	2013.751	29.59	31.89
E-17	11.89	12.28	1424.95	1472.47	23.96	26.48
E-12	11.9	13.95	1479.25	1619.093	33.15	36.30
E-14	19.25	21.04	2400	2429.045	32.91	38.08
E-16	7.04	8.84	878	1025.42	36.69	37.38
E-19	8.99	9.21	1077.00	1104.88	41.01	41.55

w% = 400% (20% Solid content)						
Geotextiles	% Soil loss		Piping rate (g/m ²)		Water content in filter cake (%)	
	Trial 1	Trial 2	Trial 1	Trial 2	Trial 1	Trial 2
A-5	28.93	24.4	7648.92	6450.47	29.16	27.86
A-7	27.27	24.62	7208.32	6510.39	35.32	29.74
A-4	25.3	25.06	6697.22	6626.72	33.87	31.3
B-8	18.2	20.04	4811.42	5297.85	29.78	29.42
B-3	25.26	25.86	6679.59	6838.21	26.68	28.94
B-5	21.7	19.6	5736.69	5181.53	31.34	30.67
E-10	11.2	13.36	2960.87	3531.9	28.66	29.46
E-17	15.95	16.39	4216.6	4334.687	28.85	30.43
E-12	10.65	12.49	3005.19	3113.95	25.56	26.67
E-14	13.13	15.29	3699	815.98	28.69	31.62
E-16	14.9	16.96	3939.02	4485.37	29.4	31.78
E-19	11.89	12.95	5406.45	5890.69	25.95	26.78

w% = 232.56% (30% Solid content)						
Geotextiles	% Soil loss		Piping rate (g/m ²)		Water content in filter cake (%)	
	Trial 1	Trial 2	Trial 1	Trial 2	Trial 1	Trial 2
A-5	22.79	19.08	10364.822	8679.94	26.76	26.15
A-7	27.31	23.24	12421.57	10571.02	21.15	27.42
A-4	25.08	24.18	11404.6	10998.71	29.5	27.36
B-8	16.71	17.1	7598.13	7775.47	25.64	29.5
B-3	21	23.11	9552.34	10509.34	24.31	28.05
B-5	24.45	23.48	11120.9	10680.3	27.94	27.51
E-10	14.92	16.46	6784.21	7487.9	25.59	26.88
E-17	8.55	11.24	3887.73	2971.44	25.45	27.01
E-12	20.26	23.93	9879.38	10215.79	27.5	30.37
E-14	14.25	17.14	6967.55	7308.09	24.66	27.27
E-16	8.50	11.11	3864.99	5052.88	24.64	26.76
E-19	11.89	12.95	5406.45	5890.69	25.95	26.76

Three different retention criteria have been developed for woven geotextiles and sand-silty slurries. In these, O₉₅, O₉₀ and O₈₅ are compared with D₈₅, D₉₀ and D₅₀ of the sediments. In Figure 4.10, ratio of O₉₈/d₈₅ are plotted against piping rate for three different water content slurries.

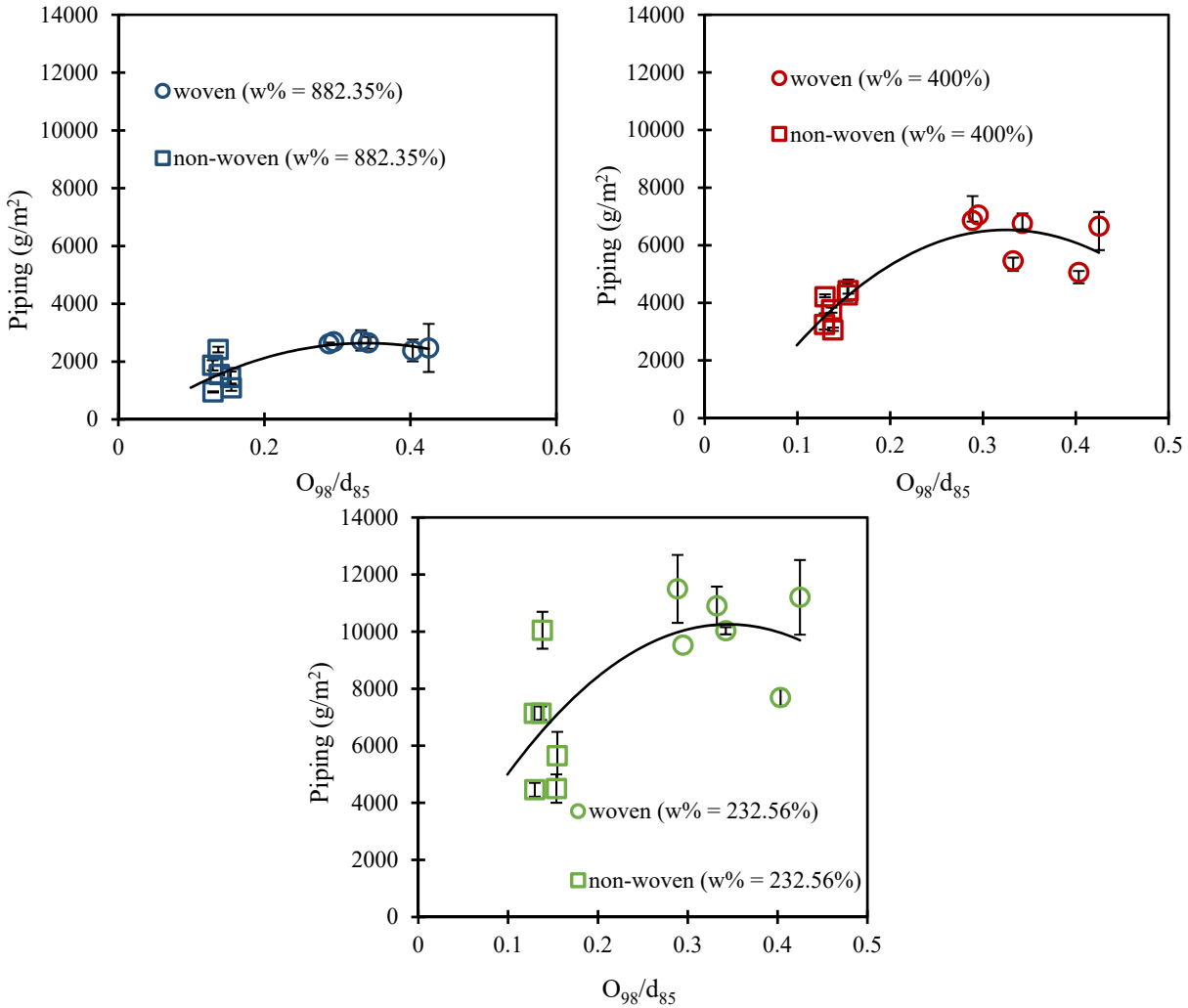


Figure 4.10: 1-D Filtration Test Piping Rate Results Against O_{98}/d_{85} for the Soil-Geotextile Systems

The highest piping occurred for a 232.56% water content (30% solid content) and the piping rate for 882.35% water content (10% solid content) was the least for both woven and non-woven geotextiles. The woven geotextiles selected for the tests showed a broad range of pore sizes, whereas, non-woven geotextiles had a narrow range of O_{98} . Woven geotextiles showed higher piping rate than non-woven geotextiles for all three water content slurries. It was found that for all three water content slurries, piping increases for the value of $O_{98}/d_{85} = 0 - 0.3$, and after that range piping remains stable. For a range of $O_{98}/d_{85} = 0 - 0.3$, piping increases up to 3000 g/m^2 ,

7000 g/m² and 11,000 g/m² in terms of 882.35%, 400% and 232.56% water content respectively.

Moo-Young and Tucker (2002) suggested an allowable limit of piping rate of 2500 g/m² in their study. However, in this study, the highest piping reported for woven and non-woven geotextiles with 232.56% water content, are almost 12,500 g/m² and 11,000 g/m². With the increase in pore sizes, not a significant change in piping was noticed in Figure 4.10. Table 4.7 shows the applicability of the existing retention and clogging criteria observed in the current study.

Table 4.7: Applicability of the Existing Criteria

Geotextiles	Existing criteria						
	Moo-Young and Tucker (2002): Retention - O95/D85<1	Moo-Young and Tucker (2002): Retention - O95<0.3 mm or O90/D90=2-5	Aydilek (2006): Retention - O85/D50<1 for all POA	Aydilek (2006): Clogging: O40/D15 >1 for POA <8 O40/D30>1 for POA >8	Muthukumaran and Ilmaparuthi (2006): 40<AOS/D15 <125	Muthukumaran and Ilmaparuthi (2006): AOS<0.425 mm	Muthukumaran and Ilmaparuthi (2006): 0.3<AOS (D85/D15) <1.7
A-5	OK	OK	Not OK	OK	OK	OK	Not OK
A-7	OK	OK	Not OK	OK	OK	OK	Not OK
A-4	OK	OK	Not OK	OK	OK	Not OK	Not OK
B-8	OK	OK	Not OK	OK	OK	Not OK	Not OK
B-3	OK	OK	Not OK	OK	OK	OK	Not OK
B-5	OK	OK	Not OK	OK	OK	OK	Not OK
E-10	OK	OK	OK	Not OK	OK	OK	Not OK
E-17	OK	OK	OK	Not OK	OK	OK	Not OK
E-12	OK	OK	OK	Not OK	OK	OK	Not OK
E-14	OK	OK	OK	OK	OK	OK	Not OK
E-16	OK	OK	OK	OK	OK	OK	Not OK
E-19	OK	OK	OK	OK	OK	OK	Not OK

In Table 4.7, it was found that most of the existing criteria were satisfied for geotextile-slurry performance in the current study. However, the performance depends on the water content of slurry, which is not mentioned by any existing study. In addition, the allowable piping rate is not mentioned as well, therefore, these criteria cannot be considered as complete.

After 1-D filtration tests were completed, the clogged geotextiles (see Figure 4.11) were saved and Capillary flow tests were performed to evaluate the clogging. The degree of clogging is expressed in terms of impregnation level (λ), which is calculated as a ratio of mass of soil particles in the geotextile voids and the mass of geotextile fibers (Palmeira et al. 1996). Upon the completion of 1-D filtration test, the filter cake was carefully removed from the geotextile and the cylindrical reservoir. To attain the degree of clogging, the wet and clogged geotextiles were collected carefully and weighted with a scale, A&D EW-12KI. Clogged geotextiles were allowed to dry for 24 hours at room temperature before taking the dry weight. Care was taken not to disturb the soil particles sticking on the surface of the geotextile.



$$w\% = 232.56\%$$

Figure 4.11: Clogged and Wet Non-Woven Geotextiles (E-19) after 1-D Filtration Test

The impregnation level or clogging level of geotextiles was calculated using the following equation.

$$\lambda = \frac{M_s}{M_f}$$

4.6

Where,

λ = impregnation level of geotextile

M_s = Mass of soil particles in the geotextile voids, gm

M_f = Mass of geotextile fibers, gm

Table 4.8: Impregnation Level of Clogged Geotextiles Obtained from the Test

Nonwoven	M_s (gm)	M_f (gm)	λ (M_s/M_f)	Woven	M_s (gm)	M_f (gm)	λ (M_s/M_f)
E-10	2.2 - 3.51	1.45	1.52 - 2.42	A-4	0.95 - 2.18	1.59	0.60 - 1.37
E-12	1.56 - 5.33	1.76	0.89 - 3.03	A-5	0.74 - 0.84	1.66	0.45 - 0.51
E-14	1.65 - 5.65	2.04	0.81 - 2.77	A-7	0.36 - 0.5	1.74	0.21 - 0.29
E-16	1.38 - 4.97	2.16	0.64 - 2.30	B-3	0.13 - 0.64	1.66	0.08 - 0.39
E-17	1.2 - 6.52	2.62	0.48 - 2.49	B-6	1.07 - 4.34	2.06	0.52 - 2.11
E-19	2.68 - 7.34	2.35	1.14 - 3.12	B-8	2.62 - 3.49	2.28	1.15 - 1.53

Results given in Table 4.8, it can be observed that the range of λ for non-woven geotextiles is higher (0.48 – 3.12) than the range (0.21 – 2.11) for woven geotextiles, which means more soil particles got trapped in the pores of non-woven geotextiles rather than woven geotextiles.

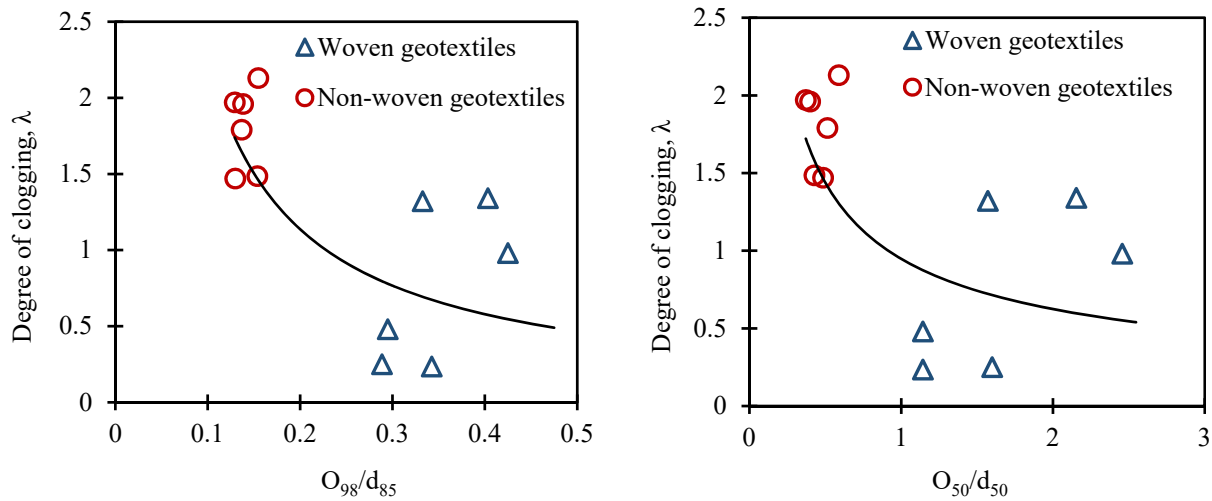


Figure 4.12: Relationship of Clogging to O_{95}/d_{85} and O_{50}/d_{50}

Two O_n/d_n criteria (O_{95}/d_{85} and O_{50}/d_{50}) were used to correlate the degree of clogging of all geotextiles. O_{98} was used instead of O_{95} in this study which is referred as bubble point obtained from the Capillary flow test. O_{50} was obtained from the Capillary flow test as well. Figure 4.12 shows that both O_{95}/d_{85} and O_{50}/d_{50} could be correlated with degree of clogging. A decreasing trend of degree of clogging was noticed with the increasing O_{50} and O_{98} . The ranges of O_{95}/d_{85} and O_{50}/d_{50} reported are 0.13 – 0.4 and 0.37 – 2.45 respectively. Non-woven geotextiles showed higher clogging than woven geotextiles, which indicates that soil sediments get stuck to the surface of non-woven geotextile and mixed with the fibers more easily than woven geotextiles. For woven geotextiles, because of their large pore sizes and shiny surface, not a lot of soil particles were trapped in the pores and got stuck to the surface of the geotextile.

4.4.2 Pressurized 2-D Test

In the last fifteen years, geotextile tubes have been used extensively for dewatering dredged sediments from a wide variety of water bodies. For this application, the selected geotextile properties (pore opening and permeability) should be compatible with the sediments. For a successful dewatering performance of geotextile tubes, three requirements must be addressed; the sediment slurry pumped into the tube should dewater efficiently, the retained sediments should have minimal water content, and the filtrate should have minimal turbidity. To increase the dewatering rate and to ensure the fine sediments retention in the tube, synthetic flocculants are often used (Satyamurthy and Bhatia 2009, Maurer 2011, Koerner and Koerner 2010, Yee et al. 2012, Khachan et al. 2013). Synthetic flocculants are used to enhance the formation of flocs. Generally, three kinds of flocculants are used, including cationic, anionic and nonionic polyacrylamide (PAM)-based flocculants. The cationic flocculants are the most commonly used as flocculants because of the negatively charged nature of soil (Bolto et al. 2001).

To evaluate the role of pore size distribution and permeability of the geotextiles on dewatering, pressurized 2-D tests were carried out. For this study, ten different geotextiles were tested with 900% water content slurry of Tully sand. Tully sand was obtained from the Clark Aggregate Co., a quarry located in Tully, New York. The properties and classification of the sediments are given in Table 4.9. The slurry was combined with two different types of polymers obtained from Watersolve LLC, an anionic polymer (Solve-426) used for coagulation and a cationic polymer (Solve-9330) used for flocculation. The jar tests were conducted to obtain the optimum dose of polymers. The optimum polymer dose used in the test for Tully sand slurry of water content 900%, were Coagulant (Solve-426) – 40 ppm and Flocculant (Solve-9330) – 30 ppm (Ratnayesuraj (2017)).

Table 4.9: Properties of Tully Sand Used in the Test, Ratnayesuraj (2017)

D ₁₀ (mm)	D ₃₀ (mm)	D ₆₀ (mm)	C _u	Liquid limit, LL	Plastic limit, PL	Plasticity index, PI (%)	USCS classification
0.0025	0.025	0.28	112	26	14	12	SP-SC

*C_u, coefficient of uniformity = d₆₀/d₁₀

The woven geotextiles selected are more open geotextiles with large pore sizes (O₉₈), the geo-composites are tight geotextiles and non-woven geotextiles ranged in their pore size distribution. (see Figure 4.13). The physical properties of these geotextiles are provided in Table 4.10.

Thickness and permittivity of geotextiles were obtained from the manufacturers, and permeability was calculated by multiplying permittivity and thickness. The permeability of the selected geotextiles ranged between 0.385 – 4.86 mm/sec.

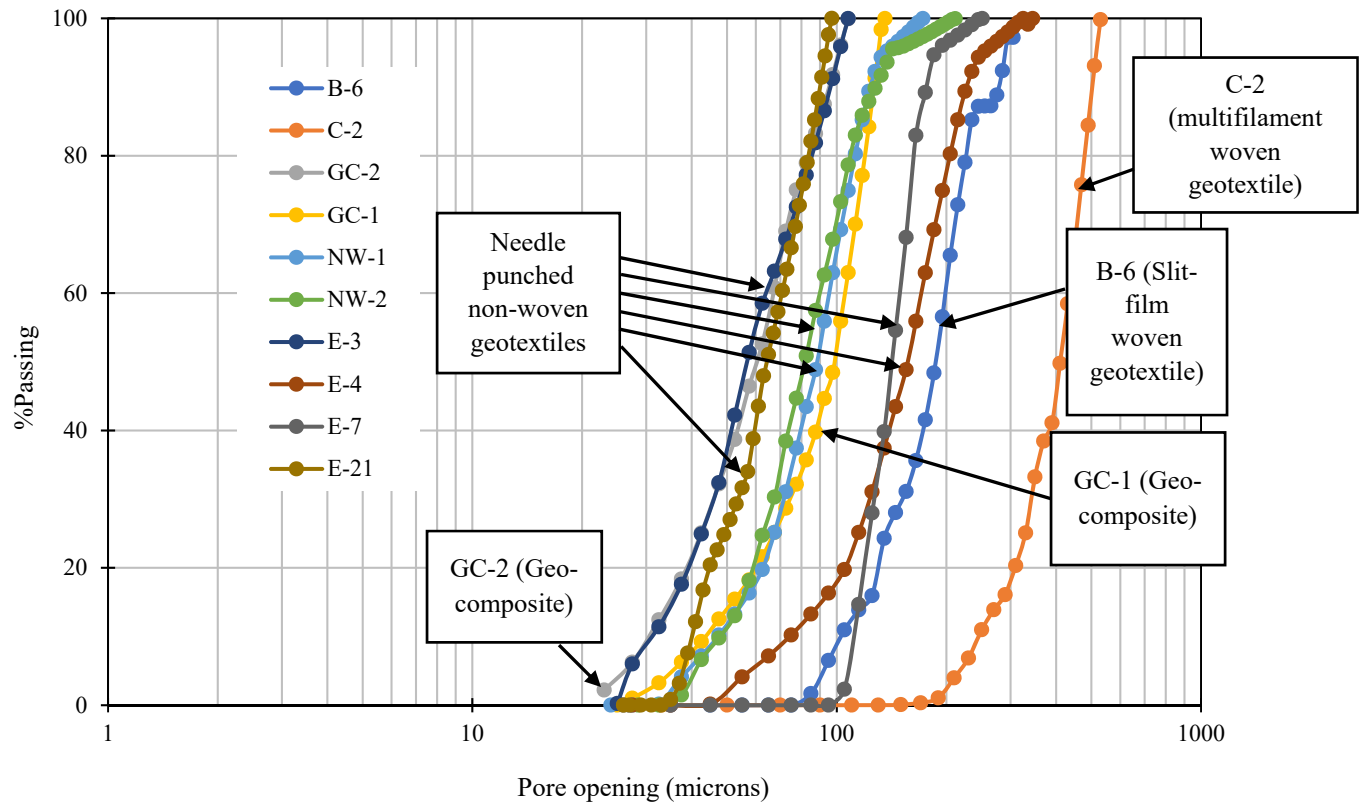


Figure 4.13: Pore Size Distribution of Geotextiles used in the P2DT

Table 4.10: Physical Properties of Geotextiles Used in the Pressurized 2-D Test

Geotextiles	Manufacturing process	Thickness* (mm)	Bubble point, O ₉₈ (microns)	Permittivity* (sec ⁻¹)	Permeability (mm/sec)
B-6	Slit film woven	1.04	265 – 331	0.37	0.385
C-2	Multifilament woven	1.76	421 – 630	0.35	0.616
GC-2	Geo-composite	2.23	88 – 122.5	0.39	0.869
GC-1	Geo-composite	2.84 – 3.37**	125 – 146	0.45	1.28 – 1.52
E-4	Needle punched non-woven	1.7	255 – 415	1.6	2.72
E-7	Needle punched non-woven	2.3	206 – 315	1.26	2.898
NW-2	Needle punched non-woven	0.69 – 0.99**	170.5 – 285	2.94	2.02 – 2.91
NW-1	Needle punched non-woven	1.88 – 2.52**	145 – 206	1.93	3.62 – 4.86
E-3	Needle punched non-woven	1.3	78 – 142.5	0.61	0.793
E-21	Needle punched non-woven	5.8	88 – 102.5	0.27	1.566

* Provided by the Manufacturers, ** Conducted at Syracuse University

A cylindrical frame with an internal diameter of 15 cm and an internal height of 30 cm was used in the test (see Figure 4.14). In 2-D test, two pieces of geotextiles, a 20-cm diameter geotextile used at the bottom of the equipment for axial flow and a 58-cm by-36 cm geotextile bolted inside the cylindrical frame, were used. To secure the bottom geotextile, a perforated steel plate was used under it. Before starting the test, the geotextiles were saturated properly with tap water to ensure a continuous flow during the test. For the test, 3599 ml of 900% water content slurry was mixed with 30 ml Solve-426 and 22.5 ml Solve-9330 properly and poured into the system and the valve was remained closed until the filling process was done. A high capacity (400 liters) balloon (Party Magic USA, L36-56729-3) was used to pressurize the slurry and promote the dewatering rate using 10kPa pressure. The further details of the experimental setup and test equipment can be found in Ratnayesuraj (2017). The dewatering was allowed to continue until no further axial or radial flow was measured. The axial and radial flows were measured using A&D EW-12KI and A&D FG-200KAL respectively, and flow ratio (a ratio of radial flow and axial flow) was measured for all geotextiles.

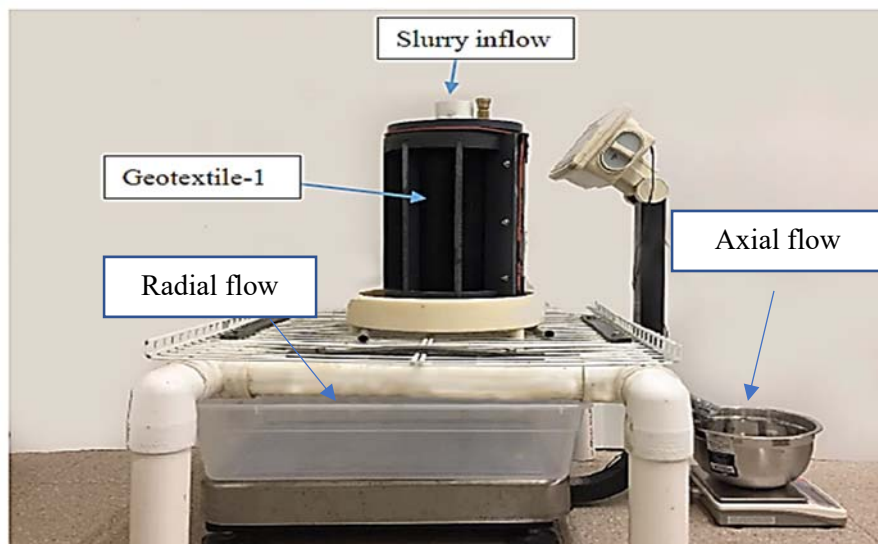


Figure 4.14: Pressurized 2-D Test Setup (Ratnayesuraj (2017))

Figure 4.16 (a and b) shows the results of Pressurized 2-D test as a plot of effluent volume (L) against dewatering time (minute) for all geotextiles. It was found that within 60 seconds most of the dewatering was completed for all geotextiles. As soon as the test started, a high radial flow was noticed for all woven, non-woven geotextiles and geo-composites. It was found that the radial flow was higher than the axial flow for all geotextiles. For GC-1 (geo-composite) and NW-1 (needle punched non-woven geotextile), the radial flow was higher than axial flow at the beginning of the test, however, after 1 – 1.5 minutes, the axial flow became slightly higher than the radial flow. Because after 1 minute of the test, a thin radial filter cake was formed along with a thick filter cake on the bottom geotextile, which reduced the permeability of geotextile and resisted the radial flow. For woven geotextiles, the radial flow rate within a minute was 2.6 – 2.7 liters, however, the axial flow rate was very low (0.2 – 0.25 L). No filter cake was formed on the radial surface of woven geotextiles, which led to a high radial flow, whereas, a filter cake was formed immediately on the bottom geotextile, which as a result decreased the axial flow. For geo-composites, filter cake was formed on the radial surface and bottom geotextile, which made the radial flow 1 – 1.3 L lower than woven geotextiles. Like geo-composites, for non-woven geotextiles, a thin radial filter cake was formed on the surface and a thick one on the bottom geotextile (see Figure 4.15). In the Pressurized 2-D test, since flocculated slurry was used for the test, the amount of soil piping and turbidity were very low (100 – 200 g/m² soil piping and 20 – 95 NTU turbidity). Most of the soil retained in the tube as a filter cake. Therefore, instead of soil piping flow rate is the issue in P2DT. To evaluate the flow rate of all geotextiles, flow ratio (radial flow/axial flow) was calculated and given in Table 4.11.

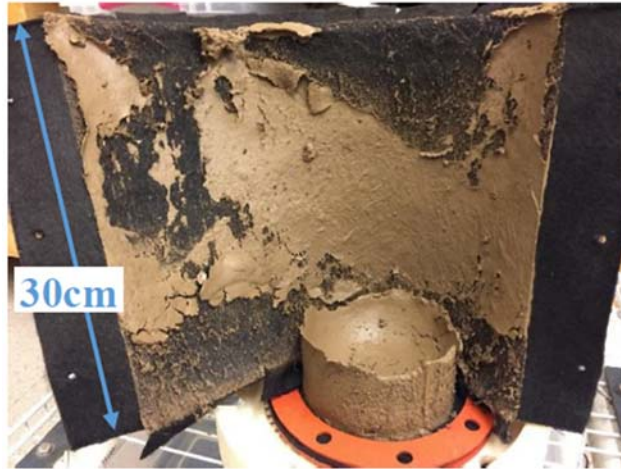
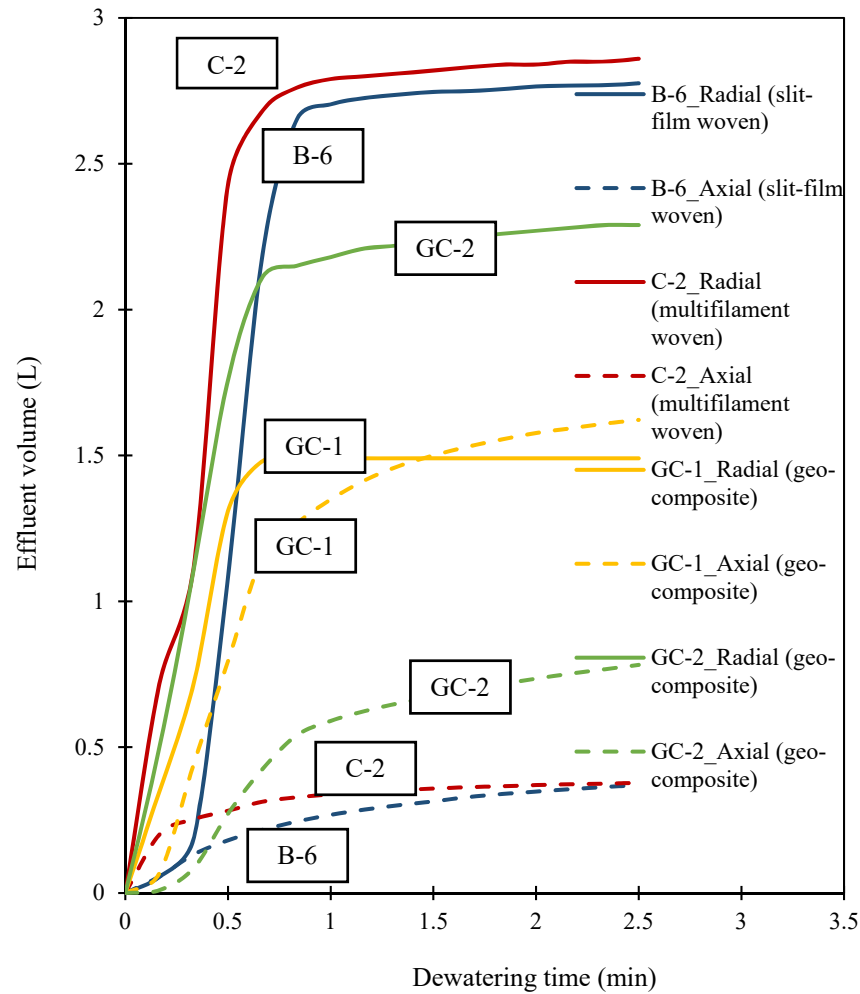
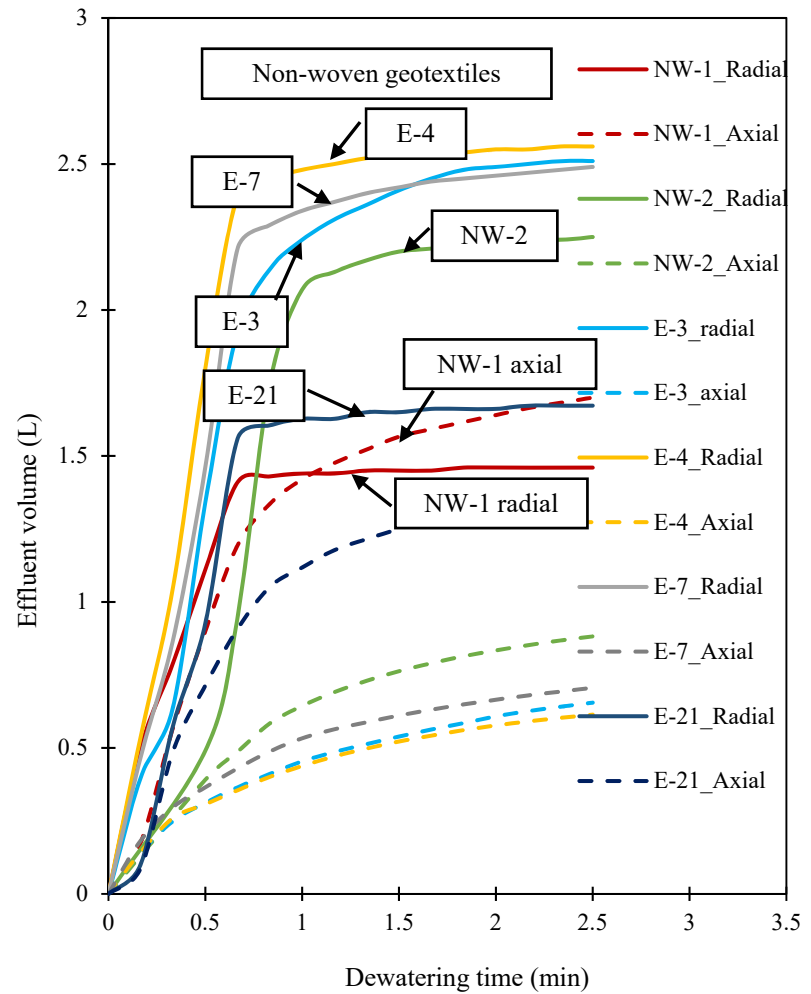


Figure 4.15: Filter Cake Formed for GC-1 (Ratnayesuraj (2017))



(a)



(b)

Figure 4.16: Pressurized 2-D Test Results of Geotextiles (a) Woven Geotextiles and Geo-composites (b) Non-Woven Geotextiles

No correlation was obtained between flow (radial or axial) and pore sizes of the geotextiles.

Upon completion of the test, the filter cakes formed on the surface and bottom geotextile were removed very carefully. The wet and clogged geotextile was saved and evaluated for degree of clogging. Since, flocs were used in the test, soil retention was not an issue in the P2D test and it was found that the degree of clogging is very low. Flow ratio was calculated for all geotextiles and plotted against a hydraulic property, permeability of geotextiles (see Figure 4.17).

Table 4.11: Pressurized 2-D Test Results (Ratnayesuraj (2017))

Geotextile	Manufacturing process	Permeability (mm/sec)	Flow ratio (Radial/axial)
B-6	Slit film woven	0.666*	6.10
C-2	Multifilament woven	0.595*	7.00
GC-2	Geo-composite	0.869*	2.50
GC-1	Geo-composite	1.28 – 1.52**	0.80
NW-1	Needle punched non-	5.24*	0.83
NW-2	Needle punched non-	3.62*	2.31
E-3	Needle punched non-	1.2*	3.35
E-4	Needle punched non-	2.72*	3.95
E-7	Needle punched non-	2.898*	3.18
E-21	Needle punched non-	1.7*	1.2

* Provided by the Manufacturers, ** Conducted at Syracuse University

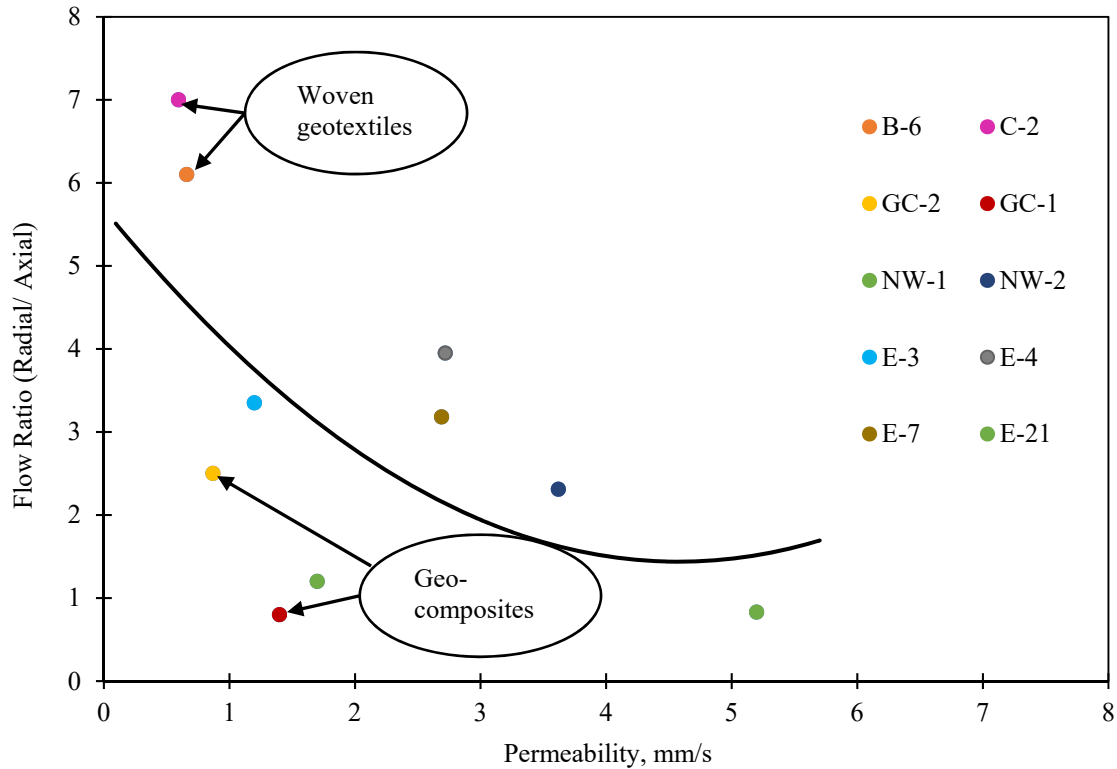


Figure 4.17: Flow ratio vs. Permeability

In Figure 4.17, a decreasing trend of flow ratio with the increasing permeability could be observed. The permeability used in the Figure 4.17 are the permeability of clean geotextiles. After the test, filter cake reduced the permeability. However, no radial filter cake was formed on the smooth surface of woven geotextiles, which resulted in the high radial flow. It was found that for woven geotextile with the smallest permeability, the flow ratio was higher than other geotextiles. For geo-composites and non-woven geotextiles, a thin radial filter cake was formed with time which decreased the permeability of geotextile and radial flow, and a thick filter cake was formed on the bottom geotextile. Therefore, the flow ratio of non-woven geotextiles is much lower than woven geotextiles, even with high permeability. In terms of non-woven geotextiles, some trend was found between flow ratio and permeability. Flow ratio decreased with the increasing permeability for non-woven geotextiles. However, the range of permeability is very narrow to draw any conclusion.

4.5 Summary:

- Twenty woven, twenty-nine non-woven geotextiles, and two geo-composites were used to develop a correlation factor between capillary flow test and dry sieving test. For all types of geotextiles, an increasing trend of AOS was found with the increasing BBP values. A better correlation was found for woven and non-woven geotextiles together rather than a correlation interpreted separately. Almost 78% AOS values could be predicted from the bubble point values in the correlation. Bhatia and Smith (1996) and TENCATE (2014) found that the measured bubble point, O_{98} obtained by the capillary flow test is consistently smaller than the AOS (O_{95}) obtained by the dry sieving test. However, Aydilek, et al., 2006 could not find any consistent relationship between capillary flow and dry sieving test. The results obtained from the previous studies were plotted as AOS vs. BBP, however, no strong correlation was noticed from the plot.
- Giroud (1996) equation was used to calculate the filtration pore opening of needle punched non-woven geotextiles and compared with the measured pore sizes obtained from the Capillary flow test. The theoretical values were found to be under-predictive compared to the Capillary flow test results.
- Performance test: 1-D filtration test (falling-head test) and Pressurized 2-D tests were performed to evaluate the influence of smaller to larger pores on the performance of soil retention and dewatering of geotextiles. It was found that in 1-D filtration test, soil piping rate of both woven and non-woven geotextiles increased with the decreasing water content (increasing solid content). Capillary flow test was performed with the clogged geotextiles preserved from the 1-D test. It was found that the degree of clogging decreases with the increasing pore sizes.

In pressurized 2-D test, no significant filter cake was formed on the surface of woven geotextiles. Therefore, the radial flow was much higher than other geotextiles. For non-woven geotextiles and geo-composites, filter cake was formed on the surface and bottom geotextiles, which resulted into lower radial and axial flow rate. From the figure plotted for flow ratio against permeability, it was found that flow ratio decreases with the increasing permeability of geotextiles.

4.6 References:

- ASTM D6767-16 Standard Test Method for Pore Size Characteristics of Geotextiles by Capillary Flow Test, ASTM International, West Conshohocken, PA, 2014.
- ASTM D4751-16 Standard Test Methods for Determining Apparent Opening Size of a Geotextile, ASTM International, West Conshohocken, PA, 2016.
- ASTM F316, “Standard Test Method for Pore Size Characteristics of Membrane Filters by Bubble Point and Mean Flow Pore Test”, American Society for Testing and Materials, West Conshohocken, Pennsylvania, USA.
- Aydilek, A.H. and Edil, T.B., (2002). Filtration performance of woven geotextiles with wastewater treatment sludge, *Geosynthetics International*, 9(1):41-69.
- Aydilek, A.H. and Edil, T.B. (2003). Long-term filtration performance of nonwoven geotextile-sludge systems, *Geosynthetics International*, 10(4):110-123.
- Aydilek, A. H., & Edil, T. B. (2003). Evaluation of woven geotextile pore structure parameters using image analysis. (2003): 1-12.
- Aydilek, A. H. (2006). A semi-analytical methodology for development of woven geotextile filter selection criteria. *Geosynthetics International*, 13(2), 59-72.

- Aydilek, Ahmet H., and Tuncer B. Edil. "Remediation of high water content geomaterials: a review of geotextile filter performance." First Panamerican Conference on Geosynthetics, GeoAmericas. 2008. (902-910)
- Baker, K. B., J. P. Chastain, and R. B. Dodd. (2002). Treatment of lagoon sludge and liquid animal manure utilizing geotextile filtration, ASABE Paper No. 024128, St. Joseph, MI.
- Barrington, S. F., El Moueddeb, K., Jazestani, J. & Dussault, M. (1998). The clogging of nonwoven geotextiles with cattle manure slurries. *Geosynthetics International*, 5, No. 3, 309–325.
- Bhatia, S. K., & Smith, J. L. (1996). Geotextile characterization and pore-size distribution: Part II. A review of test methods and results. *Geosynthetics International*, 3(2), 155-180.
- Bhatia, S. K., & Smith, J. L. (1994). Comparative study of bubble point method and mercury intrusion porosimetry techniques for characterizing the pore-size distribution of geotextiles. *Geotextiles and Geomembranes*, 13(10), 679-702.
- Blond, Eric; Vermeersch, O. G.; and Diederich, Romain (2015). A Comprehensive Analysis of the Measurement Techniques used to Determine Geotextile Opening Size: AOS, FOS, O90, and ‘Bubble Point’. *Geosynthetics 2015*, February 15-18, Portland, Oregon.
- Bolto, B., Dixon, D., Eldridge, R., and King, S. (2001). Cationic polymer and clay or metal oxide combinations for natural organic matter removal. *Water Research*, 35(11): 2669-2676.
- Christopher, B.R. and Holtz, R.D., 1985, “Geotextile Engineering Manual”, U.S. Department of Transportation, Federal Highway Administration, Washington, DC, USA, Report No. FHWA-TS-86/203, March 1985, 1044.

- CR., Ratnayesuraj. (2017). Analytical Modelling, Testing and Comparison of 1-D, 2-D and 3-D Dewatering Process. MS Thesis. Syracuse University, NY, USA.
- Elton, D. J., Hayes, D. W., & Adanur, S. (2006). Bubble point testing of geotextiles: apparatus and operation. 1-8.
- Fischer, G. R., Christopher, B. R., & Holtz, R. D. (1990, May). Filter criteria based on pore size distribution. In Proceedings of the Fourth International Conference on Geotextiles (Vol. 1, 289-294). The Hague The Netherlands.
- Fowler, J., Duke, M., Schmidt, M. L., Crabtree, B., Bagby, R. M. & Trainer, E. (2002). Dewatering sewage sludge and hazardous sludge with geotextile tubes. Proceedings of the 7th International Conference on Geosynthetics, Delmas, Gourc and Girard, Editors, Swets & Zeitlinger, Lisse, 1007 – 1012.
- Giroud, J.P., 1982, “Filter Criteria for Geotextiles”, Proceedings of the Second International Conference on Geotextiles, IFAI, Vol. 1, Las Vegas, Nevada, USA, August 1982, 103-108.
- Giroud, J. P. (2010, May). Development of criteria for geotextile and granular filters. In Proceedings of the 9th International Conference on Geosynthetics, Guarujá, Brazil (Vol. 2327, 4564).
- Henry, K. S., Walsh, M. R. & Morin, S. H. (1999). Selection of silt fence to retain suspended toxic particles. Geotextiles and Geomembranes, 17, No. 5–6, 371–387.
- Holtz, R. D., Christopher, B. R. & Berg, R. R. (1997). Geosynthetic Engineering, BiTech Publishers, Richmond, BC, Canada, 29–68.
- <https://en.wikipedia.org/wiki/Polypropylene>

- Huang, C. C., & Luo, S. Y. (2007). Dewatering of reservoir sediment slurry using woven geotextiles. Part I: Experimental results. *Geosynthetics International*, 14(5), 253-263.
- Khachan, M. M., Bhatia, S. K. & Smith, J. L. (2012). Retention performance of woven geotextiles subjected to cyclic-flow conditions. *Geosynthetics International*, 19, No. 3, 200–211.
- Khachan, M. M., Bhatia, S. K., Bader, R. A., Cetin, D. & Ramarao, B. V. (2014). Cationic starch flocculants as an alternative to synthetic polymers in geotextile tube dewatering. *Geosynthetics International*, 21, No. 2, 119–136.
- Khachan, M. M. (2016). Sustainable and innovative approaches for geotextile tube dewatering technology. PhD Dissertation. Syracuse University, NY, USA.
- Koerner, R.M., and Koerner, G.R. (2010). Performance tests for the selection of fabrics and additives when used as geotextile bags, containers, and tubes, *Geotechnical Testing Journal*, 33(3):1-7.
- Kiffle, Z. B., Bhatia, S. K., Khachan, M. M., & Jackson, E. K. (2014). Effect of pore size distribution on sediment retention and passing. In 10th International Conference on Geosynthetics, ICG 2014 Deutsche Gesellschaft fur Geotechnik e. V., 2014.
- Kutay, M. E., & Aydilek, A. H. (2004). Retention performance of geotextile containers confining geomaterials. *Geosynthetics International*, 11(2), 100-113.
- LaFleur, J., Mlynarek, J., Rollin, A.L., 1989. Filtration of broadly graded cohesionless soils. *Journal of Geotechnical Engineering* 115 (12), 1747–1768.
- Lawson, C. R. (2008). Geotextile containment for hydraulic and environmental engineering. *Geosynthetics International*, 15(6), 384-427.

- Liao, K., & Bhatia, S. K. (2005). Geotextile tube: filtration performance of woven geotextiles under pressure. Proceedings of NAGS, 1-15.
- Liao, K., & Bhatia, S. K. (2005). Geotextile tube: filtration performance of woven geotextiles under pressure. Proceedings of NAGS, 1-15.
- Lombard, G. and Rollin, A., 1987, "Filtration Behavior Analysis of Thin Heat Bonded Geotextiles", Proceedings of Geosynthetics '87, IFAI, Vol. 2, New Orleans, Louisiana, USA, February 1987, 482-492.
- Maurer, B.W. (2011) Flocculation and Filtration in the Geotextile Tube Environment. Department of Civil and Environmental Engineering, MS Thesis. Syracuse University, Syracuse, NY, USA.
- Montero, C.M. and Overmann, L.K. (1990). Geotextile filtration performance test, Geosynthetic Testing for Waste Containment Applications, ASTM STP 1081:273-284.
- Moo-Young, H. K., Gaffney, D. A. & Mo, X. (2002). Testing procedures to assess the viability of dewatering with geotextile tubes. Geotextiles and Geomembranes, 20, No. 5, 289–303.
- Moraci, N., Mandaglio, M.C., and Salmi, M. (2016). Long term behavior of woven and nonwoven geotextile filters. GeoAmericas 2016, vol. 1, 740-749.
- Mori, H., Miki, H., & Tsuneoka, N. (2002). The geo-tube method for dioxin-contaminated soil. Geotextiles and Geomembranes, 20(5), 281-288.
- Muthukumaran, A. E., & Ilamparuthi, K. (2006). Laboratory studies on geotextile filters as used in geotextile tube dewatering. Geotextiles and Geomembranes, 24(4), 210-219.
- Palmeira, E. M., Fannin, R. J., & Vaid, Y. P. (1996). A study on the behavior of soil geotextile systems in filtration tests. Canadian Geotechnical Journal, 33(4), 899-912.

- Palmeira, E. M., & Gardoni, M. G. (2000). The influence of partial clogging and pressure on the behaviour of geotextiles in drainage systems. *Geosynthetics International*, 7(4-6), 403-431.
- Palmeira, E. M., & Trejos Galvis, H. L. (2016). Opening sizes and filtration behaviour of nonwoven geotextiles under confined and partial clogging conditions. *Geosynthetics International*, 1-14.
- Pilarczyk, K. W. (2000). *Geosynthetics and Geosystems in Hydraulic and Coastal Engineering*, A.A. Balkema, Rotterdam, Netherlands.
- Rankilior, P.R., 1981, “Membranes in Ground Engineering”, John Wiley, Chichester, United Kingdom, 377.
- Satyamurthy, R., & Bhatia, S. K. (2009). Effect of polymer conditioning on dewatering characteristics of fine sediment slurry using geotextiles. *Geosynthetics International*, 16(2), 83-96.
- Schiereck, G. J. (2003). *Introduction to Bed, Bank and Shore Protection*, Spon Press, New York, NY, USA, pp. 135–140.
- Smith, J.L. (1996). The pore size distribution of geotextiles. MS Thesis. Syracuse University, Syracuse, NY, USA.
- Yee, T.W., Lawson, C.R., Wang, Z.Y., Ding, L., and Liu, Y. (2012). Geotextile tube dewatering of contaminated sediments, Tianjin Eco-City, China, *Geotextiles and Geomembranes*, 31:39-50.
- Yee, T.W., Lawson, C.R., (2012). Modelling of Geotextile Tube Dewatering Process, *Geosynthetics International*, 19(5), 339-353.

Chapter 5 Conclusion

5.1 Major Conclusion

Geotextile filters have been generally used to prevent soil erosion and provide maximum safety to a structure without the threat of leakage. Basically, two types of filters are used widely in geotechnical engineering, including granular filters composed of gravel or sand and filters composed of woven and non-woven geotextiles. For the last two decades, geotextiles have been extensively used for filtration performance. The rapidly growing geotextile industries have led to a diversity in the manufacturing process and characteristics of geotextiles. Filtration performance of a geotextile predominantly depends on the pore structure of a geotextile, permeability, soil retention criteria and clogging parameters. A properly designed geotextile filter is required to be free from clogging and to ensure the retention of filtered materials. The ability of a geotextile filter to fulfill these requirements basically depends on the pore sizes of a geotextile. In the USA, two standard methods of measuring the largest pore size of a geotextile have been accepted including dry sieving test (ASTM D4751) and capillary flow test (ASTM D676). Despite of the several drawbacks of dry sieving test including trapping of glass beads with the geotextiles and electrostatic effects, many filtration criteria are designed depending on the apparent opening size (AOS, O_{95}) of a geotextile obtained by the dry sieving test. On the contrary, the capillary flow test provides a complete pore size distribution along with the largest pore size (bubble point, O_{98}) of a geotextile. Regardless of providing both larger and finer pore sizes (O_{95} , O_{90} , O_{50} and O_{15}) that impact the existing geotextile retention criteria, this test is not widely accepted yet due to the variation in devices and liquids used in the test. Therefore, a study was carried out at Syracuse University to analyze the evolution of capillary flow test following ASTM D6767.

The objectives of this study were: 1) performing calibration of the Geo Pore Pro (GPP-1001A) with several materials of known sizes; 2) comparing the capillary flow test devices used by others with different ASTM standards and limitations; 3) comparing the results obtained by the capillary flow test with dry sieving test results; 4) establishing correlations between bubble point, O_{98} and AOS, O_{95} for woven and non-woven geotextiles. Evaluating the role of pore size distribution in the performance of geotextiles using 1-D filtration test and Pressurized 2-D test. For this study, more than 700 capillary flow tests were performed using Geo Pore Pro (GPP-1001A) manufactured by Porous Materials, Inc., for woven, non-woven, and composite (a combination of woven and non-woven geotextile) geotextiles. ASTM D 6767 was followed in this study. Mineral oil with a surface tension of 31.69 dynes/cm was used as a wetting liquid in the test. Comparisons were made between the capillary flow test device used in the current study and the devices used by others. Four thin metallic plates with uniform circular and cylindrical holes and two membranes with irregular holes were used to calibrate the Geo Pore Pro (GPP-1001A). The dynamic contact angle was tested for a thin metallic plate with mineral oil and it was found that the receding contact angle is zero degrees. Cleaning of the calibration materials and the testing equipment with Methanol significantly altered the results, which was not mentioned in the ASTM D 6767. It was found that the results (O_{100}) measured from the calibration test were larger than the actual pore sizes obtained by the manufacturers and the Scanning Electron Microscope. The calibration results obtained in the current study were compared with the results obtained by Przybylo (2007) and a similar trend in larger test results was found. However, ASTM D 6767 was not followed in the test performed by Przybylo (2007). Twenty woven geotextiles (7 monofilament, 11 slit film and 2 multifilament woven geotextiles), twenty-nine non-woven geotextiles (21 needle punched non-woven and 8 heat bonded non-

woven geotextiles), and two geo-composites were used in the capillary flow test to measure the pore size distribution. Nine to ten tests were performed with individual specimens to achieve a range of consistent bubble point, O_{98} . O_{50} and O_{10} were also measured from the pore size distribution along with O_{98} . It was found that the systematic error in the test and deviation in the pressure transducer influenced the test results crucially. Box plot and whisker diagrams were used in the study to find out the maximum and minimum outliers for all geotextiles. It was found that 2 monofilament, 2 slit film and 1 multifilament woven geotextiles, and 9 needle punched non-woven geotextiles provided outliers in the box plot and whisker diagram.

The smaller and larger pore sizes (O_{10} , O_{50} , and O_{98}) were plotted as a function of mass per unit area for woven and non-woven geotextiles. It was found that for both needle punched and heat bonded non-woven geotextiles, pore sizes (O_{10} , O_{50} , and O_{98}) decrease with the increasing mass per unit area. However, no such trend was found for woven geotextiles. The previous analysis conducted by Bhatia (1996), Vermeersch et al. (1996), Aydilek (2006), Elton et al (2007), and Przybylo (2007) were investigated as well and it was found that the bubble points of non-woven geotextiles decrease with the increasing mass per unit area, which validates the current study.

A correlation factor was established for all woven and non-woven geotextiles between the capillary flow test and the dry sieving test. The dry sieving test results were obtained from the manufacturers for most of the geotextiles and those geotextiles without available results were tested using the dry sieving test method. For all types of geotextiles, an increasing trend of AOS was found with the increasing BBP values. A better correlation with a straight-line equation: $y = 1.04x$ and $R^2 = 0.78$, was found for woven and non-woven geotextiles together rather than a correlation interpreted separately. Almost 78% AOS values could be predicted from the bubble point values in the correlation. However, beyond a limit of AOS and bubble point values, the

correlation is not valid for any geotextile with smaller pore sizes. The straight-line equation, $y = 1.04x$, obtained from the correlation for all geotextiles provides comparable AOS values corresponding to the bubble point values. However, theoretically, some woven and non-woven geotextiles provided much higher AOS values compared to bubble point values. Bhatia and Smith (1996) and TENCATE (2014) found that the measured bubble point, O98 obtained by the capillary flow test is consistently smaller than the AOS (O95) obtained by the dry sieving test. However, Aydilek, et al., 2006 could not find any consistent relationship between capillary flow and dry sieving tests. The results obtained from the previous studies were plotted as AOS vs. BBP, however the plot revealed no strong correlation.

To evaluate the role of pore size distribution in the performance test of geotextiles, 1-D filtration test (falling-head test) and pressurized 2-D tests were conducted and the influence of pore sizes on the performance of soil retention and dewatering of geotextiles were investigated. 6 pairs of geotextiles (3 pairs of woven and 3 pairs of non-woven geotextiles) were used to perform 1-D filtration test using 3 different water content (882.35%, 400% and 232.56%) and it was found that piping rate of both woven and non-woven geotextiles increases with the decreasing water content. After the filtration test, the partially clogged geotextiles were evaluated to measure the degree of clogging. It was found that the level of impregnation (degree of clogging) was higher than woven geotextiles, which means more soil particles were trapped in the non-woven geotextiles. In the pressurized 2-D test, 2 woven, 2 geo-composites, and 6 non-woven geotextiles were used. Tully sand combined with two different types of polymers were used in the test as a slurry. 10 kPa pressure was applied to promote the dewatering rate. It was found that no significant filter cake was formed on the surface of woven geotextiles. Therefore, the radial flow was much higher than with other geotextiles. For non-woven geotextiles and geo-composites, a

filter cake formed on the surface and bottom geotextiles, which resulted into lower radial and axial flow rates. From the figure plotted for flow ratio against permeability, it was found that flow ratio decreases with the increasing permeability of geotextiles.

5.2 Future Work

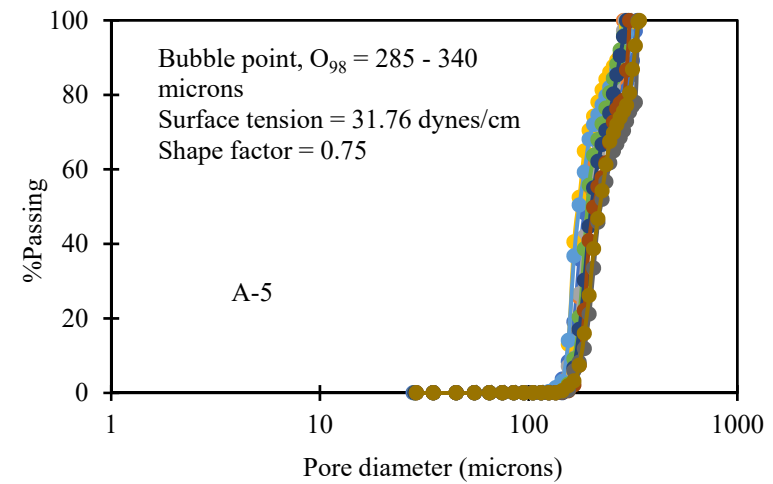
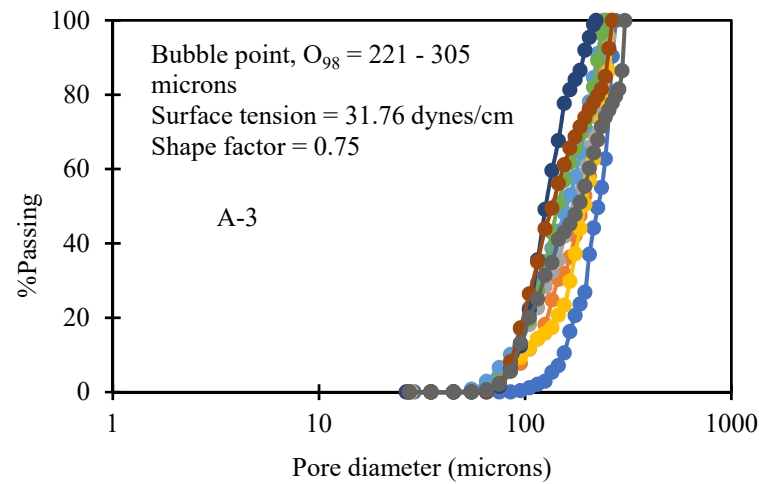
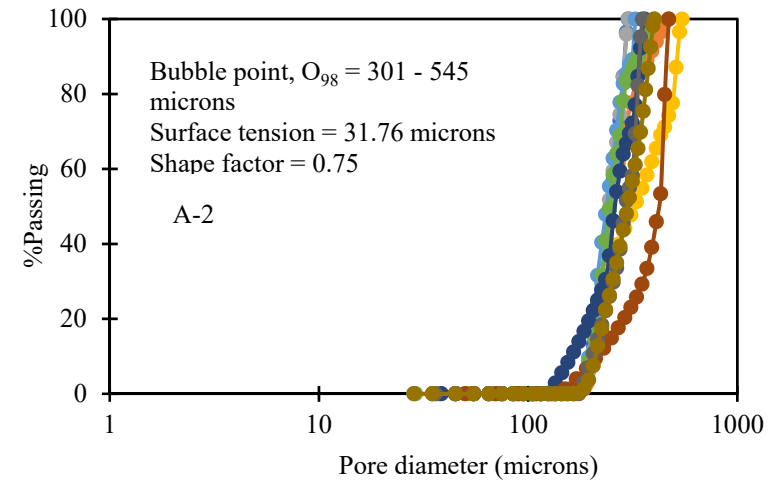
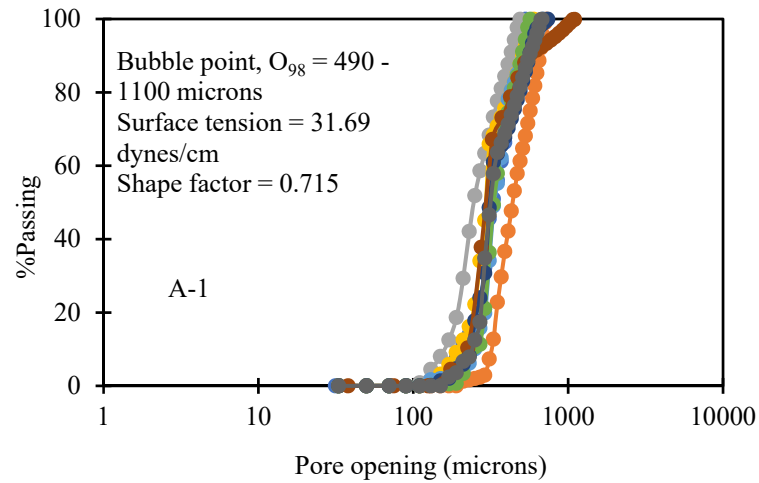
The device used in the capillary flow test is not a standard device. The pressure transducer attached inside the equipment fluctuates very frequently, which may not affect the results of largest pore sizes, however, it may affect the smaller pore sizes. Therefore, the pressure transducer should be stable throughout the test. Before doing the test, the operator should acknowledge the particularities of the equipment as well.

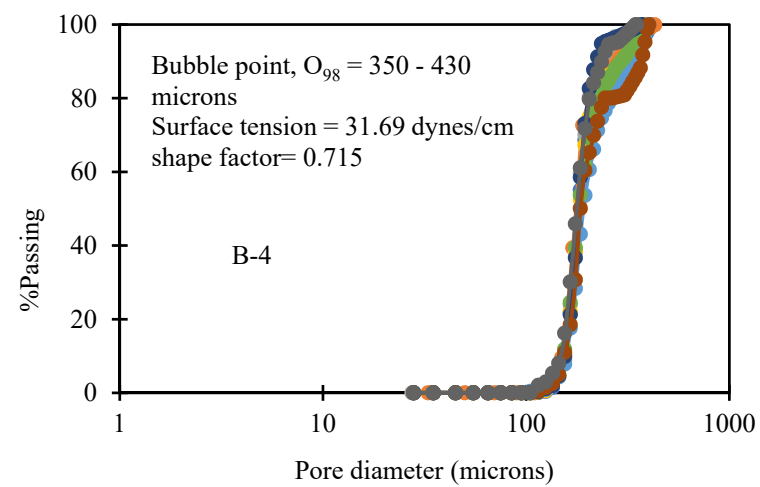
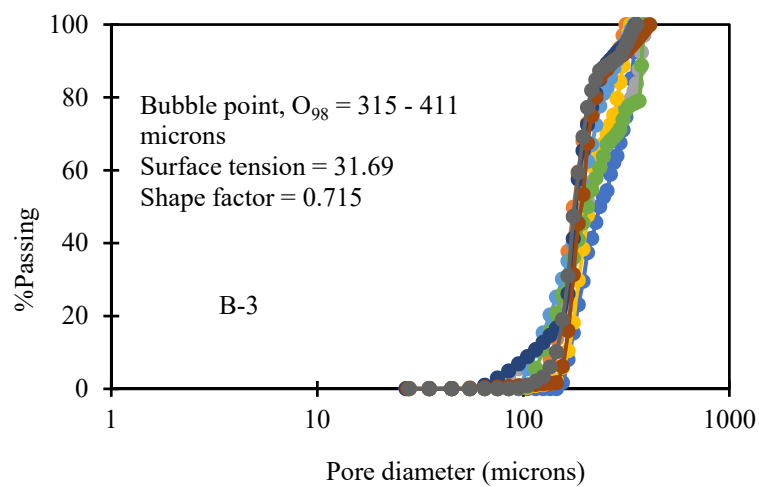
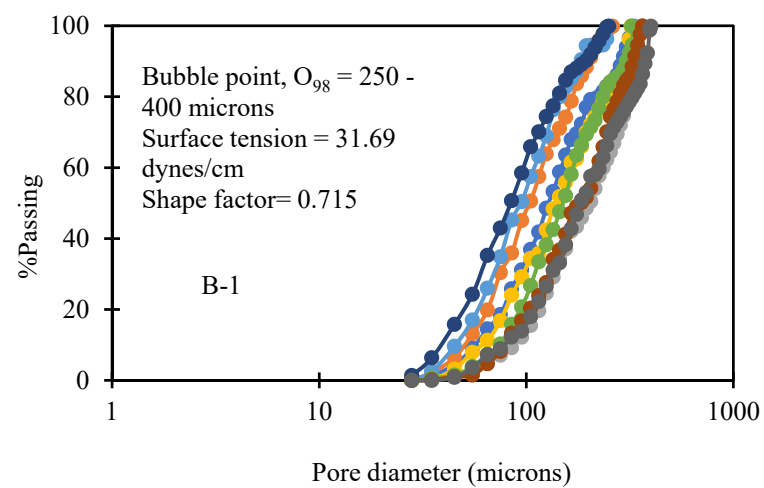
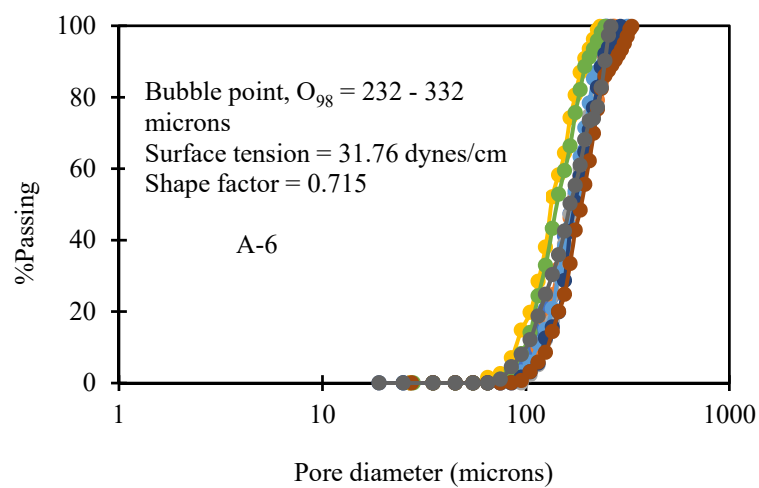
Cleaning of calibration materials play an important role in the results that should be mentioned in the ASTM standard. The standard liquid, mineral oil, provided larger pore sizes of the calibration materials than manufacturers and SEM pore sizes, however, the dynamic contact angle was reported as zero degrees. Therefore, the role of wetting liquid should be examined properly before doing any test.

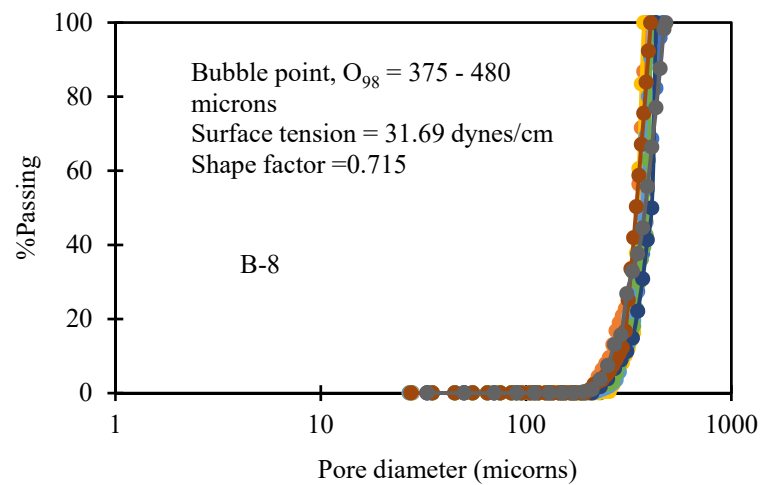
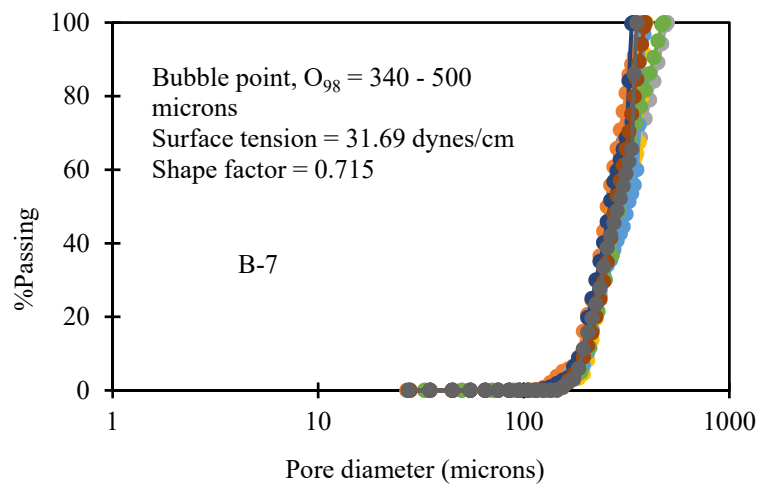
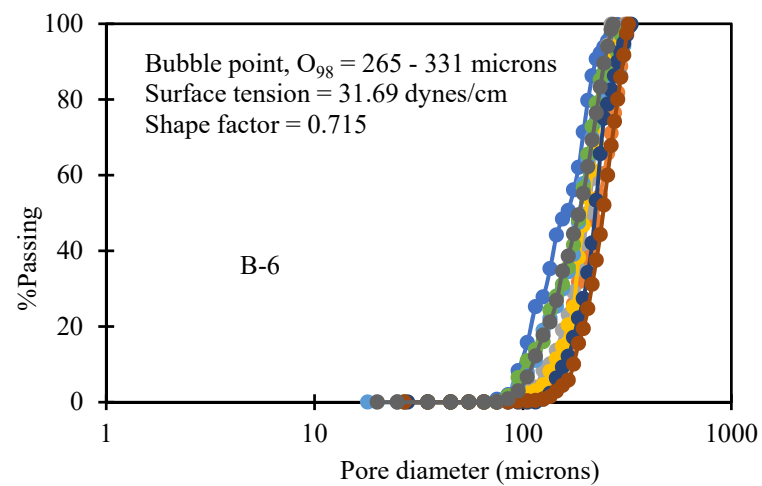
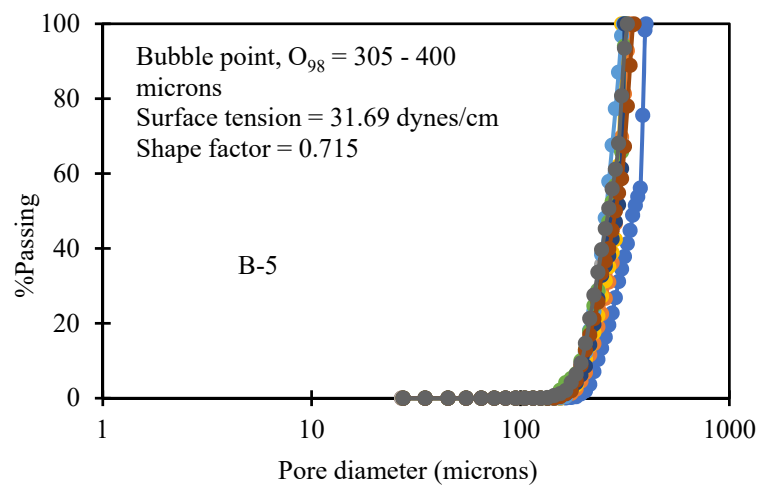
Only two multifilament woven geotextiles and two geo-composites were used in the capillary flow test. Therefore, no correlation was developed for them separately between bubble point and AOS results. More multifilament woven and composite geotextiles should be included in the study in future to evaluate the pore size distribution.

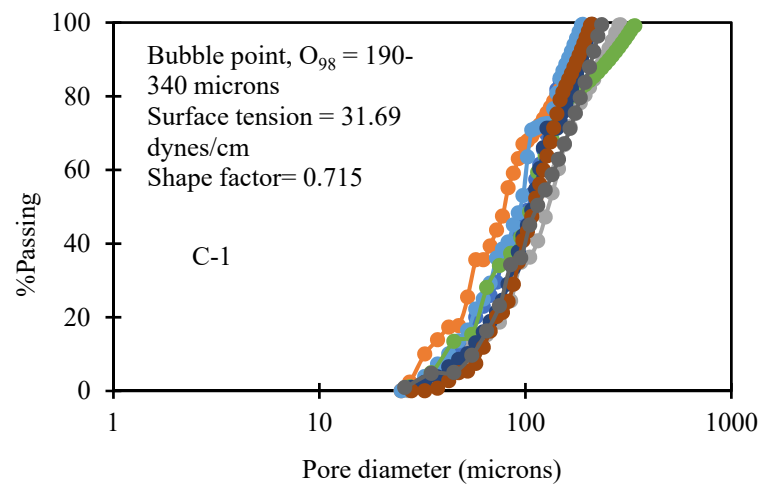
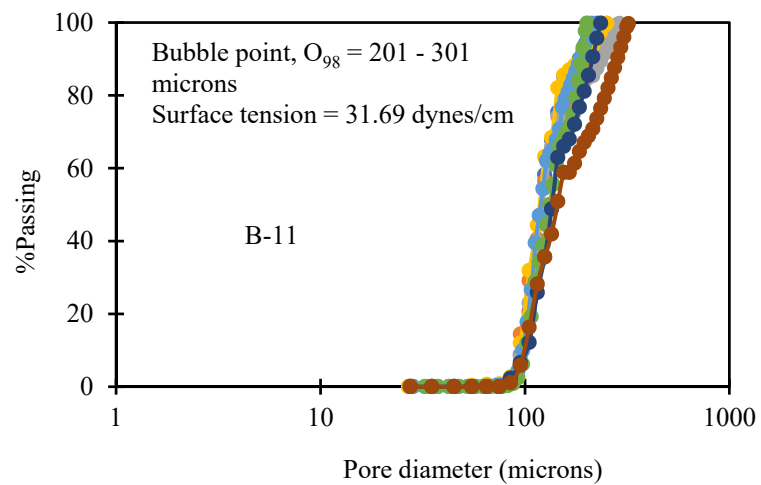
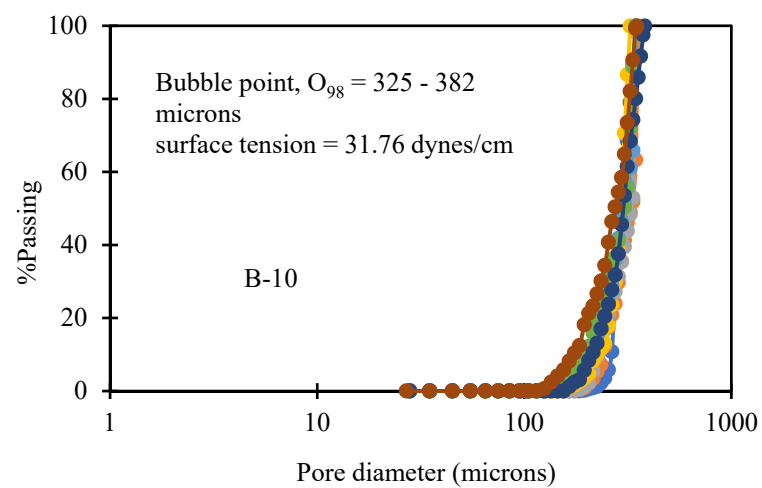
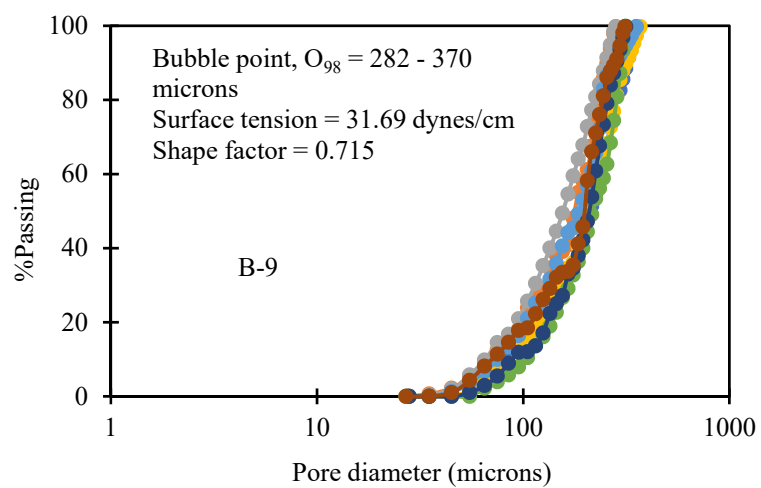
APPENDIX A

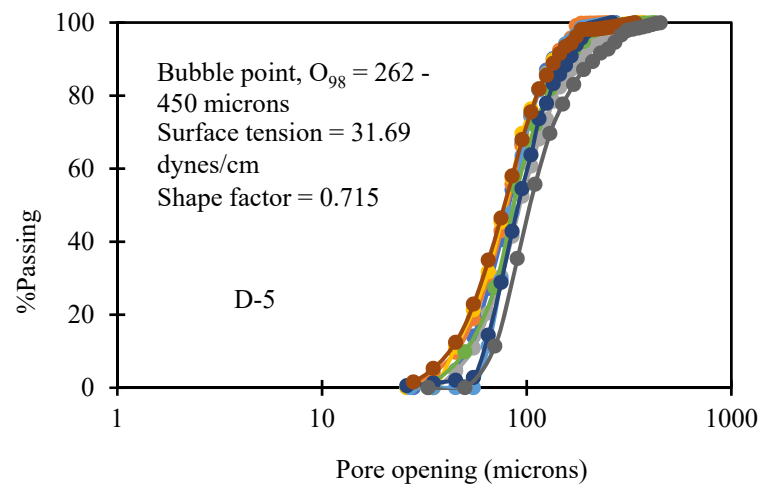
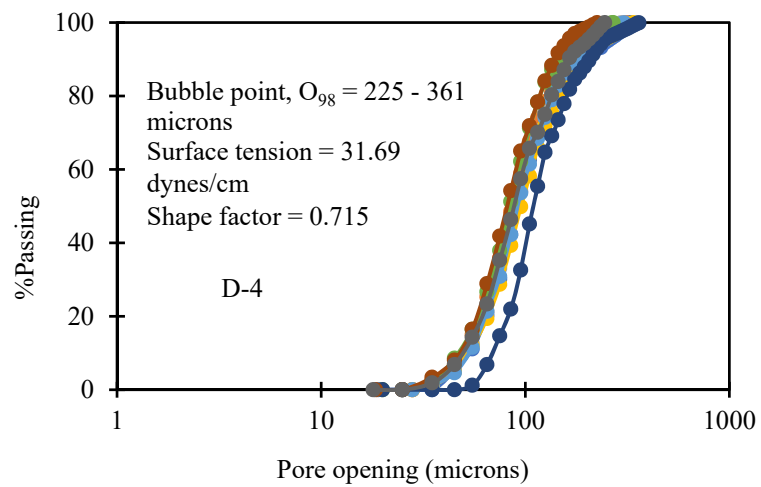
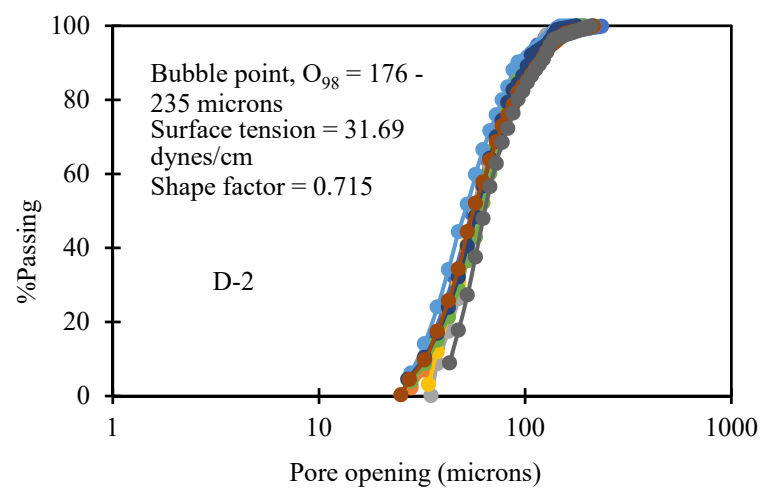
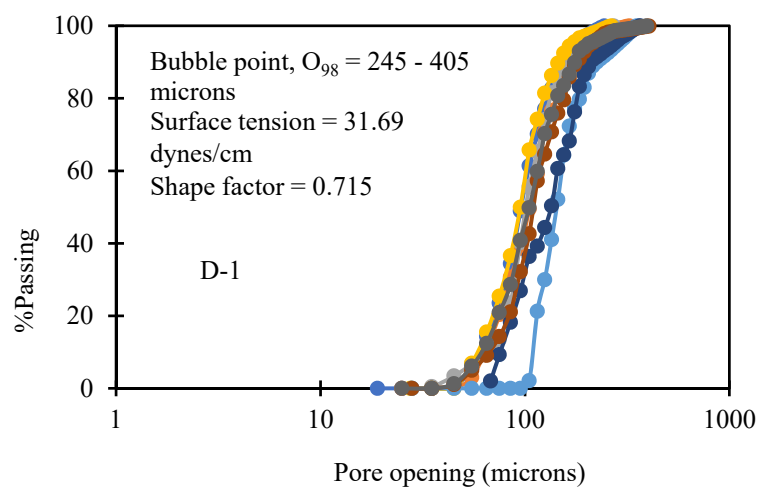
Capillary Flow Test – Pore Size Distribution

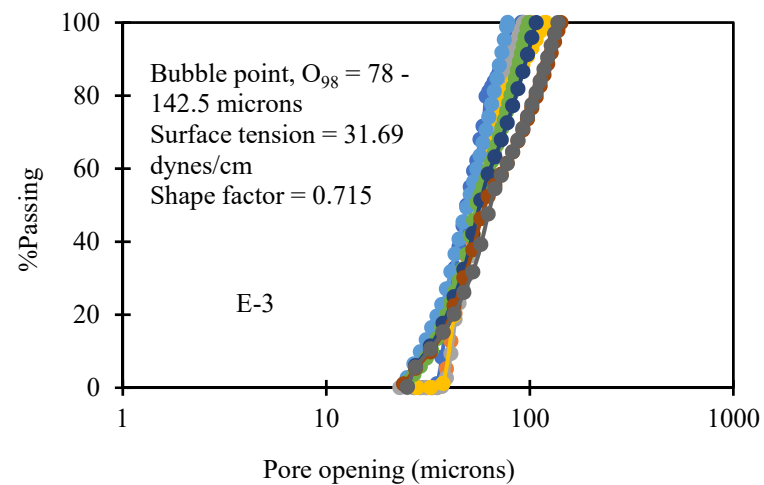
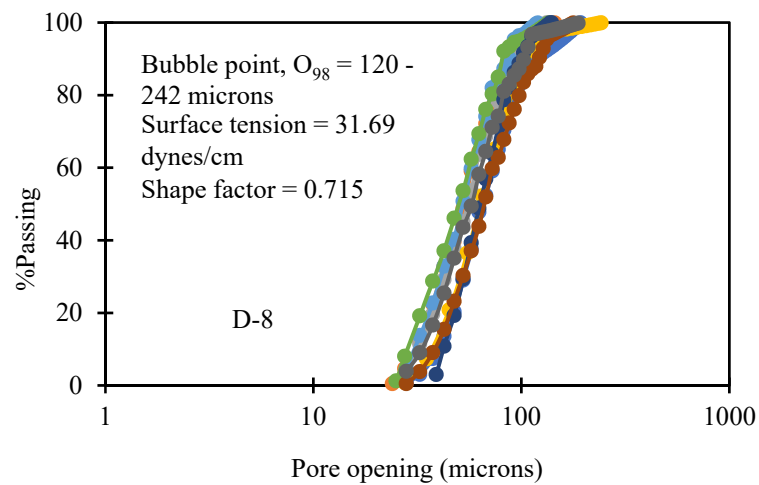
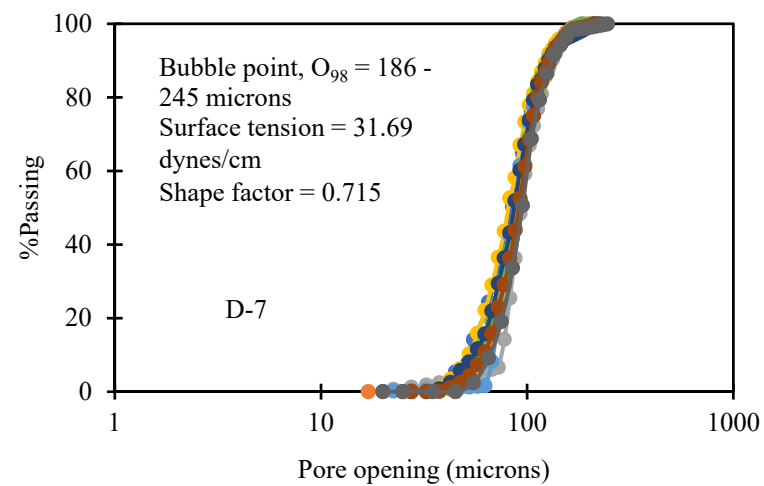
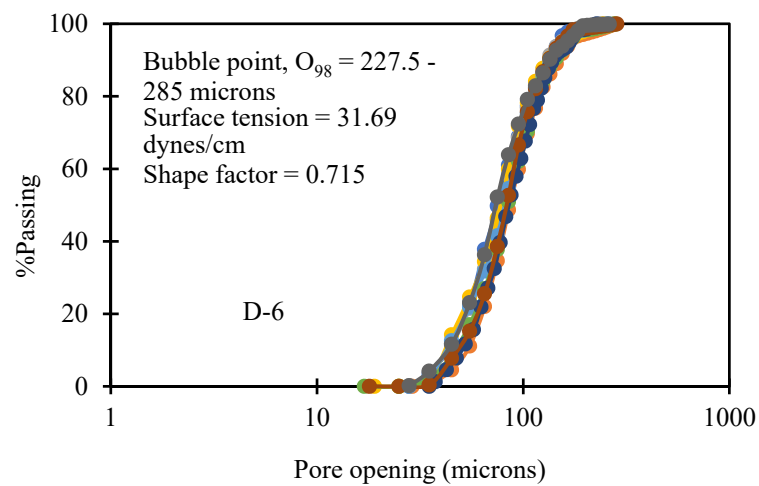


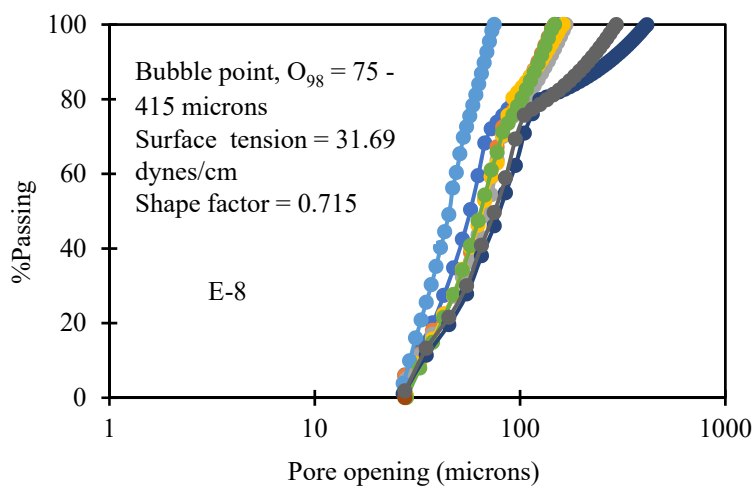
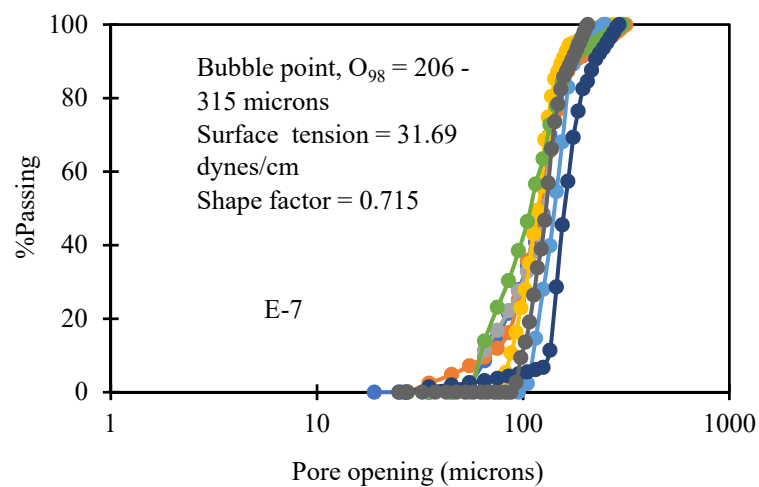
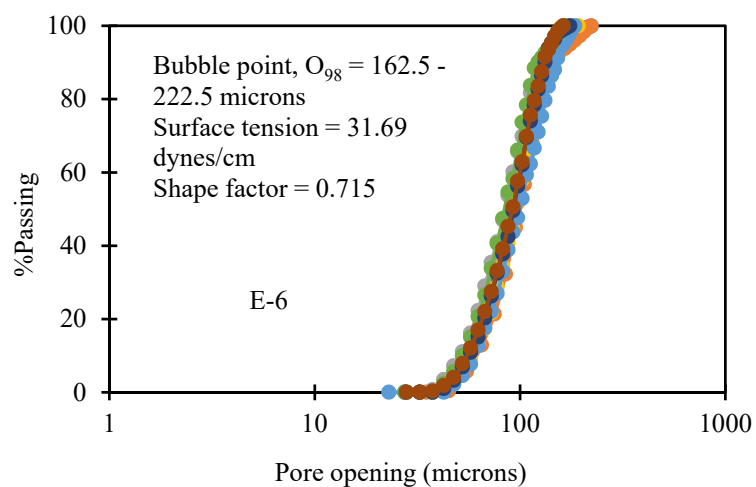
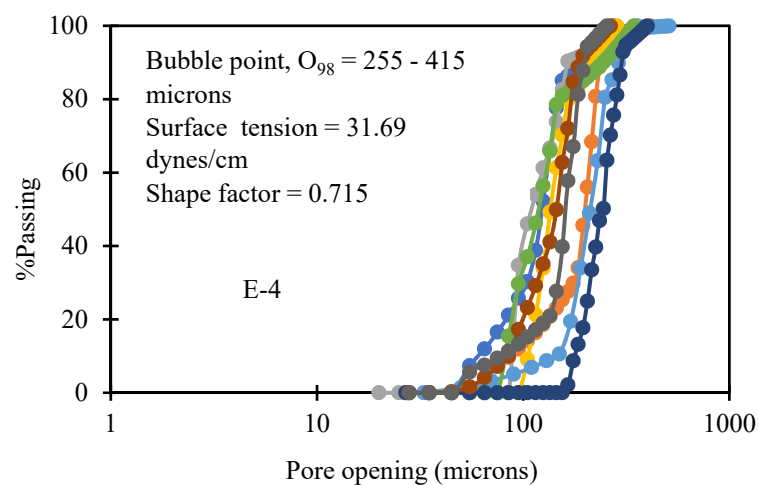


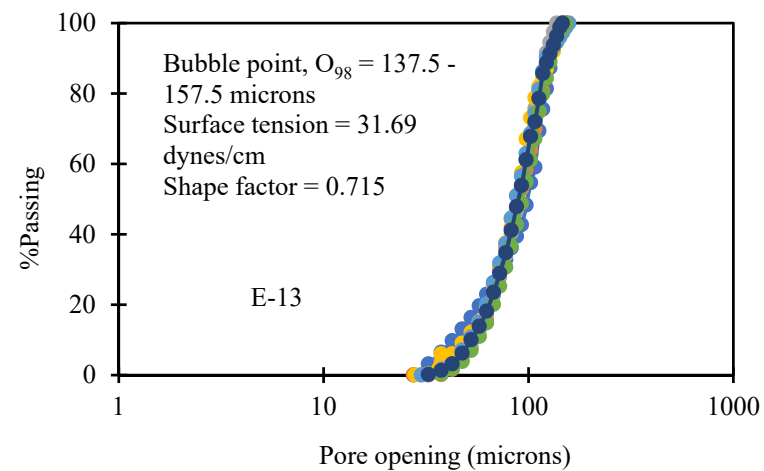
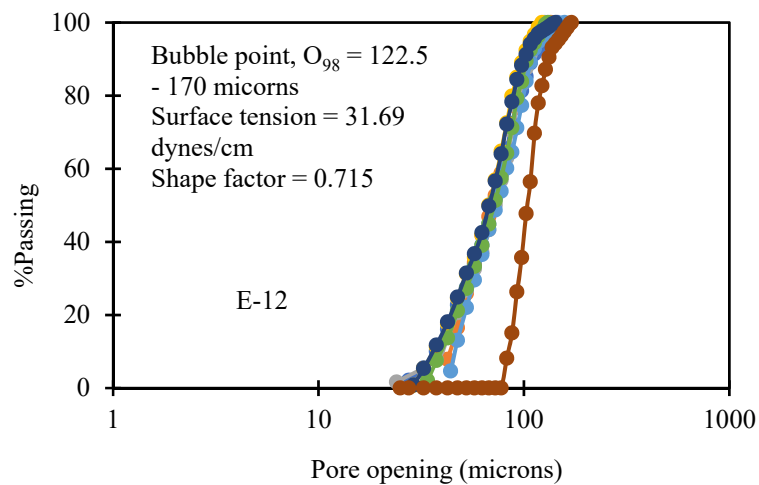
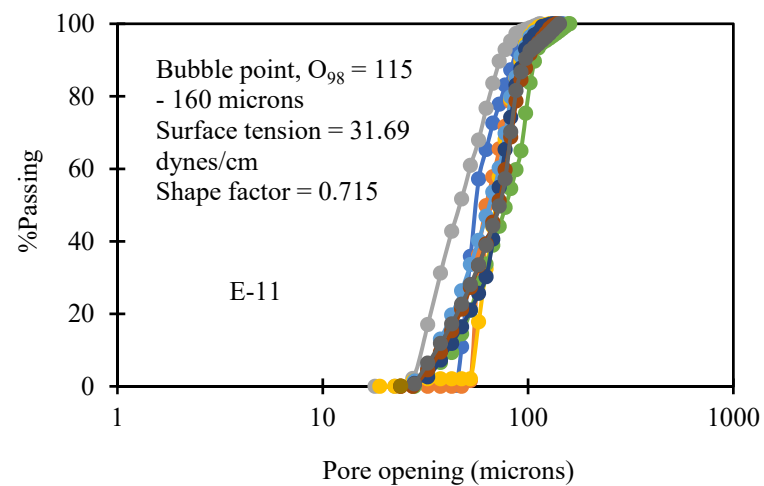
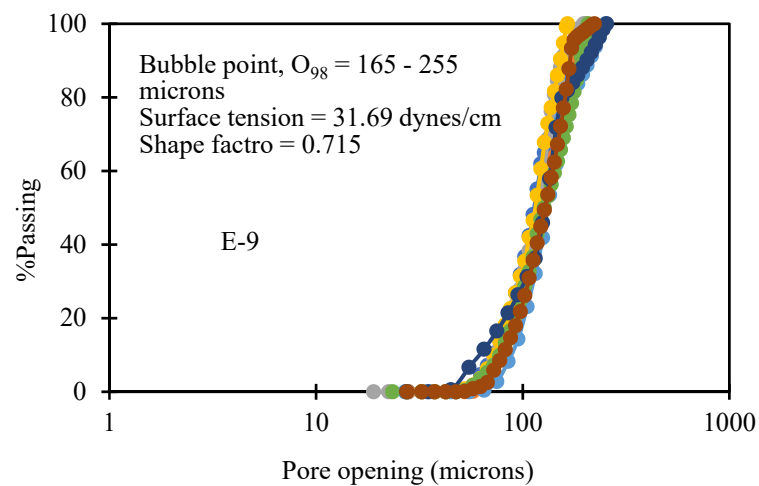


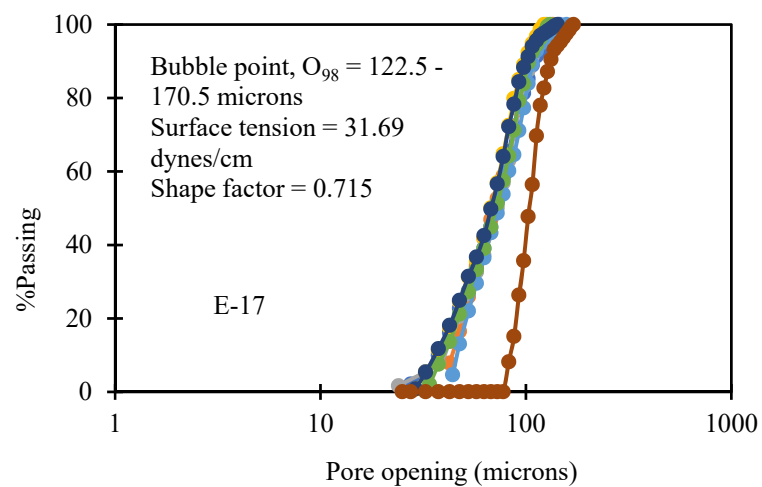
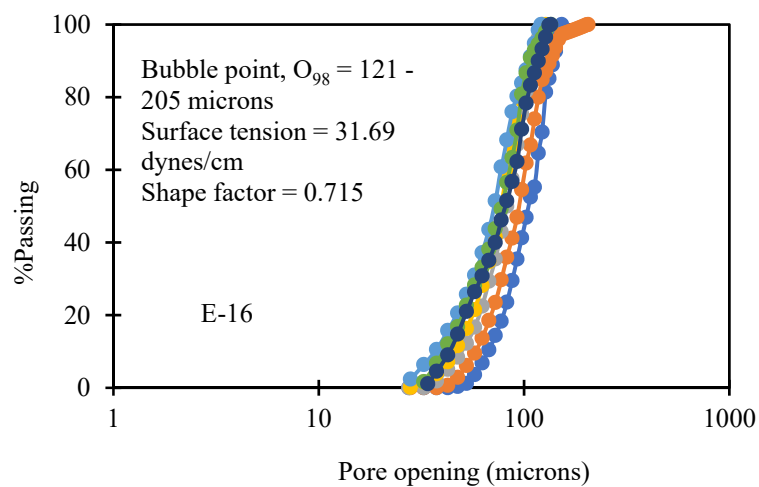
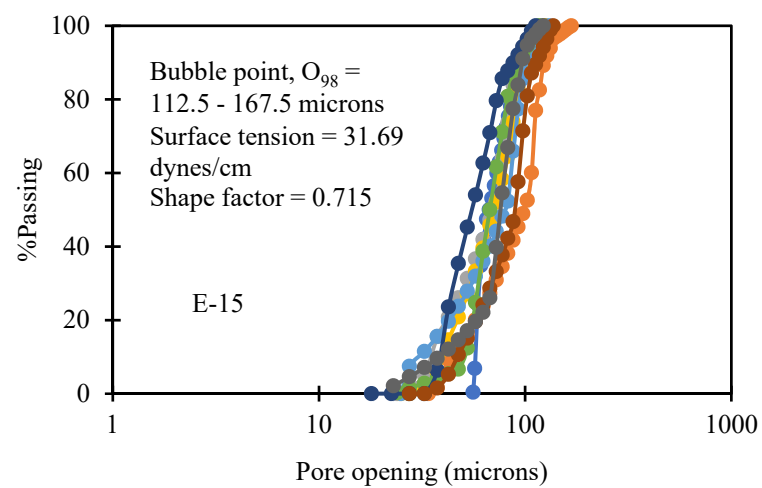
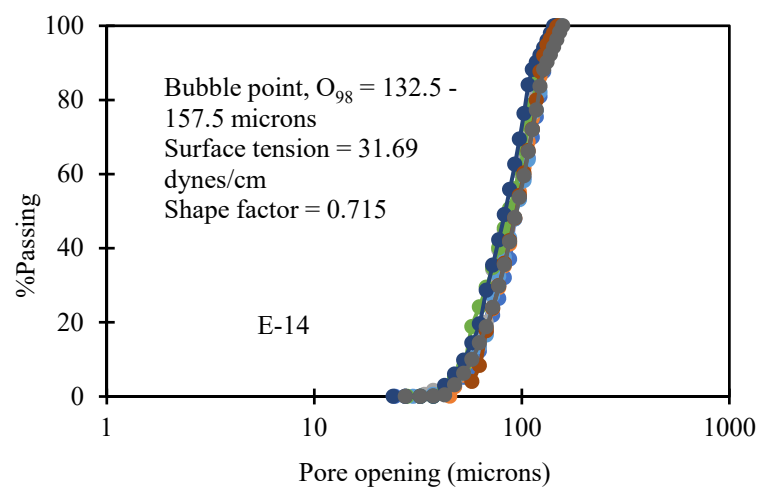


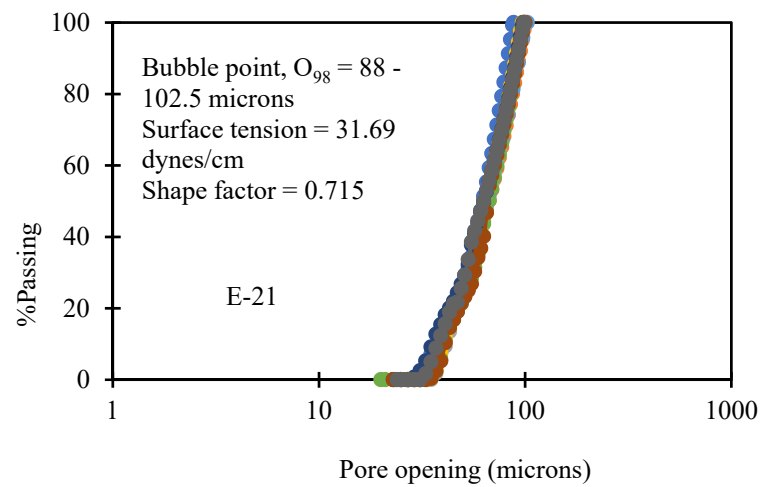
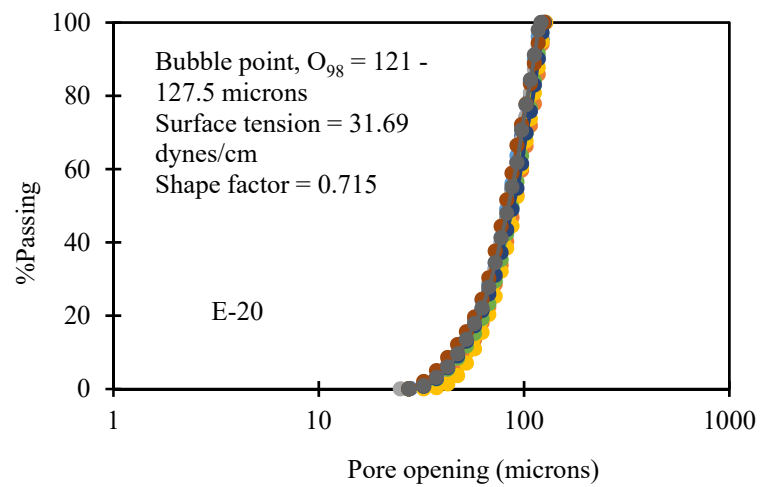
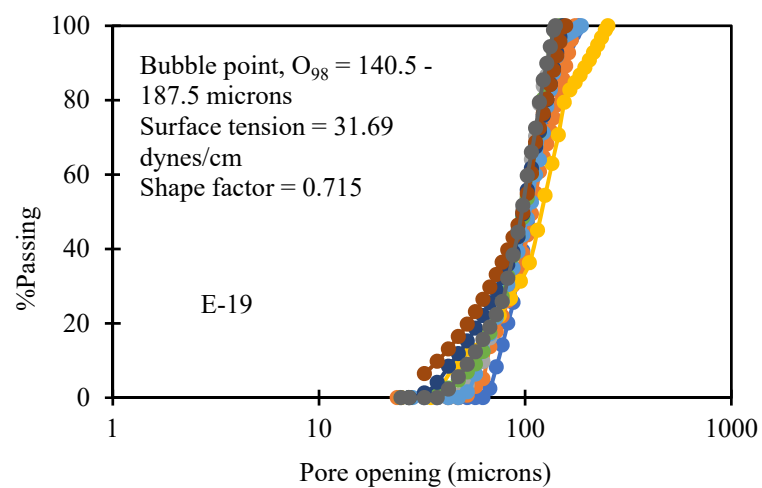
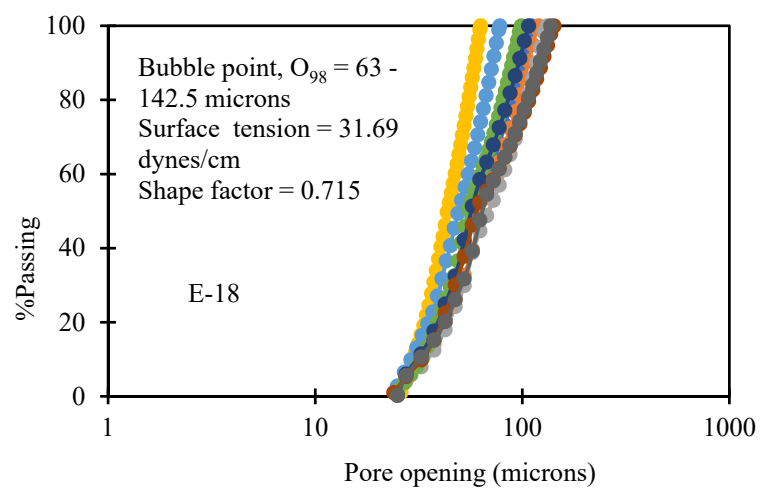


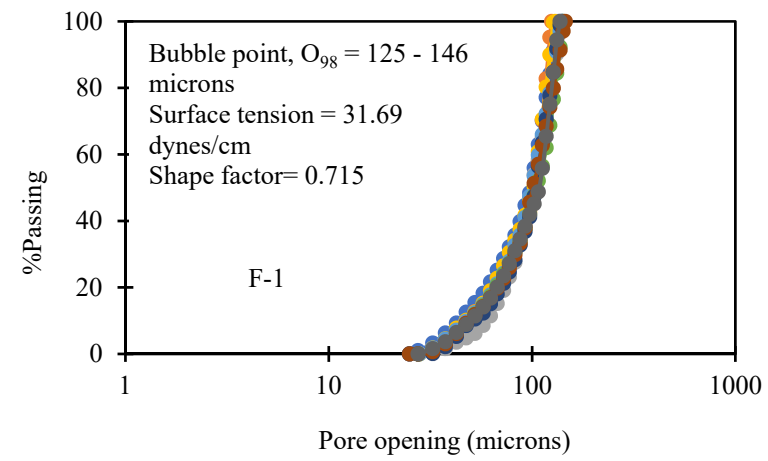












Vita

Name of Author: Nuzhath Fatema

Place of Birth: Bangladesh

Date of Birth: March 1, 1989

Graduate and Undergraduate Schools Attended:

Bangladesh University of Engineering and Technology (BUET), Bangladesh

Syracuse University, Syracuse, New York

Degrees Awarded:

Bachelor of Science, Civil Engineering, 2013, BUET

Master of Science, Civil Engineering, 2017, Syracuse University

Professional Experience:

Research Assistant, Department of Civil and Environmental Engineering, Syracuse University, Spring 2016, Summer 2016, Summer 2017

Teaching Assistant, Department of Civil and Environmental Engineering, Syracuse University, Fall 2016, Fall and Spring 2017.